THE TRANSIENT PERFORMANCE OF POWER SYSTEMS

ProQuest LLC.
789 East Eisenhower Parkway
P.O. Box 1346
Ann Arbor, MI 48106 – 1346

SUMMARY

This thesis is divided into two parts. In Part 1, an account is given of some measurements of the frequency and transient response of the elements of a 132 kV. power system, and a 440 V., 625 k.V.A. generator, with particular reference to their behaviour under recovery voltage and impulse conditions. In each case comparisons are made between the measured data and that calculated from the physical dimensions. These comparisons show that the equivalent circuits, used in recovery voltage analysis, are not valid when current chopping and impulse conditions are considered. It appears necessary then to include the distributed nature of the parameters in the evaluation of the response.

The difficulties in the selection of system parameters, and the uncertainty concerning the nature of the wave propagation led to the theoretical investigation described in Part 2. In this, the effects of dispersion of the magnetic field at low frequencies, and the necessity of including the finite velocity of propagation at high frequencies, are examined for a cable with individual

sheaths, a generator, and a transformer. The present theories are discussed, and, in each case, ideal structures representing the particular element are analysed as rigorously as possible, and the results compared with the experimental data. The propagation of waves along the cable is examined almost completely, and the results obtained compare favourably with the experimental data. The generator is studied by separating the various structural influences on the propagation and studying each in turn. A similar procedure is used when dealing with the transformer: first the effects of the laminated core on the low frequency behaviour are determined, and then the high frequency behaviour is examined, considering the periodic nature of the coil and the effect of the source. The use of a sheath representing the coil is justified, and it is suggested that further analysis using this model would yield valuable results.

In an appendix a description is given of Bergeron's graphical solution of one dimensional wave problems. It is indicated how this method may be extended to the solution of the three dimensional problem of a transient in a waveguide.

Page

PART 2.

A Theoretical Investigation of the Propagation of Electromagnetic Waves through the Elements of a Power System.

Page

APPENDICES

PART 3.

Diagrams, Oscillograms and Graphs

INTRODUCTION

The problems associated with the transient behaviour of power systems are mainly of two types, although in both the same physical phenomena of wave propagation occur. The insulation problem has given rise to investigations of the voltage distribution along the system on the impact of steep fronted waves due to lightning, whereas the determination of recovery voltage for circuit-breaker design has led to investigations of possible equivalent circuits for the system.

The difference of approach in these separate problems is due to the approximations which are made possible by the different types of surges. In recovery voltage analysis, if no current chopping takes place, the surge has a relatively slow rising front, and it is therefore often possible to neglect the finite velocity of wave propagation, and to replace the network by a circuit of lumped parameters. On the other hand, when chopping takes place, or when a lightning surge is applied, the physical size of the system may have to be considered.

This thesis is concerned with a general investigation of the behaviour of the elements of a system under

the transient conditions described above, the object being to gain a better understanding of the nature of wave propagation in these elements, and to examine the validity of the equivalent circuit approach.

It is divided into two parts. Part I is concerned with the measurement of the transient and frequency response of the various elements of a power system, in this case:-

a 132 kV. 3-phase underground cable,
a 60 M.V.A. 132 kV transformer,
a double circuit 132 kV. overhead line, and
a 440 volt 625 kVA. generator.

The measuring techniques used were, in general, of a standard type, a recovery voltage indicator (R.V.I.) with chopping facilities and a recurrent surge oscillograph (R.S.O.) being used in the transient response measurements, and simple bridge networks in the frequency response measurements. Short descriptions of the R.V.I. and R.S.O. are given in Appendices 1 and 2 respectively.

This experimental work formed the basis for Part 2 of the thesis which is a theoretical examination of the behaviour of each component of the system. It was found that the present theories did not account sufficiently

well for the experimental results, and in each case the relevant theories are examined and more rigorous analyses attempted. In its present form the work, particularly on the generator and transformer, is by no means complete. However, some of the results obtained do indicate that the method, which is to examine rigorously the behaviour of simplified representations of the elements, may help towards a solution of these complex problems.

A SHORT HISTORICAL REVIEW OF THE LITERATURE

The first signs of interest in recovery voltage appeared in the 1920's in the form of short additional notes in other papers. Experience was showing then that duplicate breakers, when installed in different circuits, were giving a wide variation of performance, and to account for this Hilliard[1] seems to have been the first to suggest that the cause might be the high frequency oscillation. J. Slepian[2] in 1928 was the first to present a complete paper on the problem, analysing the connection between the transient recovery voltage and the dielectric recovery.

In the years following 1930 a large number of papers appeared, one of the most notable in this period being presented by Park and Skeats[3] in 1931. This deals mainly with the fundamental frequency component, and gives a mathematical analysis to include different types of fault and apparatus. A good review of the work up to 1932 is given by Kopeleowitsch and Brown[4].

The investigators, so far, had considered the whole problem, including the nature of arc extinction and the effects of the network. The logical development was the separation of the uncertain physical aspects of

arc extinction and the determinable effects of the system. Boehne in 1935 was the first to accomplish this when he introduced a factor 'recovery impedance'. Although this network parameter has, in general, no simple physical meaning in terms of the network constants, it is a convenient method of stating the 'severity' of the circuit. Its use is, of course, limited to surges with slow linear fronts. The division is also made clear in a paper by Cassie[6] in 1935, when he introduces the concept of the 'α' or perfect switch, thus ignoring the uncertain effects of the arc behaviour. These two papers therefore represented a real advance in the approach to the problem.

Although, even now, the physical aspects of arc extinction are still largely uncertain, the problems associated with the response of the circuit have been more satisfactorily solved. The difficulties associated with the latter are mainly in the complexities of the circuits and the choice of parameters. Various methods of solution have been suggested. Evans and Witzke[7], for example, in a paper in 1943, showed how transients of complicated networks can be most conveniently determined by the miniature system introduced by Evans and Monteith[8] in 1937, using the classical method with the aid of differential equations. Mortlock[9] in 1946, proposed a

scheme for the reduction of complicated networks, and also showed the evaluation of standard circuits. A very comprehensive work on transient recovery voltage, with particular reference to Swedish power systems, was written by Hammarlund[10]. In it the transient oscillations of different network elements and apparatus are treated analytically, practical methods for calculation are given, and values for the capacitances and inductances of network components are compiled. He also analyses the most important inadequacies previously mentioned in other papers.

On the other hand, the destructive effects of lightning surges resulted in a development of interest in surge propagation. This was, at first, mainly centred round the behaviour of transformer windings, because they were the most readily damaged elements of the system. The first papers were published at the beginning of the century by Wagner[19] in Germany and Blume and Boyajian[25] in America, and these two papers have formed the basis of all that has followed.

The development of cathode ray tube techniques stimulated the interest in these surge phenomena, and the investigations broadened to consider the behaviour of the other elements of the system. The transmission line problem has been tackled by many investigators , the most

comprehensive treatment being given in Surge Phenomena[33] and in a paper by Pelisser[35]. It should be noted that most of the theoretical analysis in this field is based on the work of Carson[34].

The propagation of surges along power cables has been considered, with reference to recovery voltage by Gosland[11], and, of course, this fundamental problem has been tackled rigorously by many investigators, mainly, however, with high frequency transmission systems in mind.

The analysis of the transient behaviour of the generator has lagged behind that of the other elements. This is mainly because the problem is difficult, and also because its situation in the system generally ensures that surges arriving at its terminals will not be dangerous. Recently, however, Robinson[38,39] has published two interesting papers on the problem. These are based to a large extent, on the original conception of the problem by Friedlander[37], who considered the winding in a similar way to a transformer coil.

A more detailed description of many of these papers is given later in the relevant chapters.

CHAPTER 1.

THREE PHASE 132 kV. S.L. CABLE

1.1 Introduction

An examination of the performance of two types of power cable, with reference to recovery voltage, has already been carried out. Gosland and Whitney[14] have considered a 3-core belted-type cable, and Gosland[11] a 3 single core paper insulated double lead sheathed cable laid in trefoil. In both cases, the cable resistance is shown to cause a variation of the surge impedance calculated in the usual way from $\sqrt{\frac{L}{C}}$

In this chapter, an account is given of measurements made on a 3-phase S.L. cable with the R.S.O. and R.V.I. to determine its surge impedance and propagation time. Comparisons are then made of these measured parameters, and those calculated from the cable dimensions. The graphical method of Bergeron[43] is used to show the effect of a lumped end capacitance on the wavefront of the recovery voltage transient. A description of this method is given in Appendix 3.

The cable consists of 4452 yards of 132 kV. pipe line compression cable, with 17.5 yards of single

core cables at each end from the trifurcating joints to the sealing bells. It has oval conductors and individual sheaths, which are bound with non-ferrous tapes, and bonded together and to earth at intervals of 300 yards.

The instruments were placed in a switch house about 30 yards from the sealing bells, to which the connections were made with coaxial cables in order to reduce the high frequency pick-up. Tests were made to represent the conditions encountered by a switch opening on the following short circuits at the end of the line.

(1) Phase to earth
(2) Phase to phase
(3) Phase to phase to earth
(4) Three phase fault
(5) Three phase to earth fault.

1.2 Measuring techniques

(1) R.V.I.

The surge impedance and propagation time can be found, using the R.V.I., by oscillographic measurement of the voltage response to the half sine current wave. For zero chop, the surge impedance is derived from the approximate equation

$$e = 2\pi f \chi . \hat{i} Z_c t \quad \ldots\ldots\ldots\ldots (1)$$

where e = wavefront of voltage response

$\hat{i}$ = maximum value of half sine wave of current

f = frequency of current wave (50 c/s)

Z_c = surge impedance.

This formula is valid only when the propagation time of the cable is small enough to be able to approximate the sine wave, near the current zero, to a linear front (i.e. less than approximately 1 m.s.).

For a chopped current wave the surge impedance is found from the equation

$$\hat{e} = i_c Z_c \quad \ldots\ldots\ldots\ldots (2)$$

where i_c = the value of current at the chop

$\hat{e}$ = the voltage peak

This formula is also dependent on the assumption that the propagation time is small.

In both cases, the propagation time can be obtained from a measurement of the distance between the voltage peaks of the oscillation as shown in Fig. 1.

(2) R.S.O.

By applying an impulse generated by the R.S.O. to the cable, and recording this wave and its reflection from an impedance connected at the far end, the surge

impedance and propagation time can be determined. According to the well known law, the reflected wave from a line termination is given by

$$e_R = e_T \frac{Z_c - Z_R}{Z_c + Z_R} \qquad (3)$$

where Z_R = load impedance

e_R = reflected wave

e_R = applied wave

The surge impedance is found by adjusting Z_R till there is no reflected wave, when from equation (3) $Z_R = Z_C$.

The time for the wave to propagate along the line and back corresponds to the distance on the trace between the generated and reflected waves as shown in Fig. 2.

(3) The cable inductances and capacitances were measured using a 1,000 c/s impedance bridge.

(4) Cable waves

An attempt was made to obtain cable waves by applying a d.c. source (in this case an H.V. dry battery) to the open-circuited cable. Because of the difficulties of triggering the oscilloscope and of the beam brightness

for a single stroke, this was not successful. However, cable waves were obtained using the R.V.l. to inject a chopped wave (Fig. 1).

1.3 Calculations of cable parameters

The calculations were made with the following assumptions.

(1) That the cores and sheaths were circular. The radius taken was the mean of the minimum and maximum radii of the oval conductors.

(2) In calculating the core to sheath values of inductance, it was assumed that the sheath currents flowed along the inside surface.

(3) For the core to core inductance values the presence of the sheaths was ignored.

(4) Because of the bonding it was assumed that no electrostatic field could exist between the sheaths, and so the capacitance between cores was calculated from the appropriate connection of core to sheath capacitances.

(5) Proximity and skin effects were ignored, and the well known formulae for inductance and capacitance of co-axial cables used.

1.4 Results

TABLE I.

Cable surge impedance (ohms)

Connection	Z from R.V.I. records	Z from R.S.O. records	(a) $Z = \sqrt{\frac{L}{C}}$		Mean of (1) and (2)
			(1)	(2)	
Phase to Phase	71.6	60	78.4	58.2	69.4
Phase to Phase to earth	36.1	31.5	39.2	29.1	34.7
Phase to earth	36.1	31.5	39.2	39.1	34.7
Three Phase	51.2	46.5	58.8	43.6	51.2
Three Phase to earth	18.4	19.6	19.6	14.6	17.1

(a) Calculated from $\sqrt{\frac{L}{C}}$, using the power frequency constant

(1) taking the inductance as the star reactance x $\frac{1}{\omega}$

(2) taking it as the core to sheath inductance and neglecting losses.

TABLE II.

Time for wave to travel along cable (milliseconds)

(a) Obtained from R.V.1. records with

(1) zero chop 0.031

(2) chop 0.028

(b) Obtained from R.S.O. records 0.0275

(c) Calculated from $\sqrt{LC}$, using power frequency constants

(1) taking the inductance as star reactance x $\frac{1}{\omega}$ 0.0404

(2) taking the core to sheath inductance 0.0302

TABLE III.

Inductance values (mH.)

Connections	Calculated from dimensions	Measured at 1000 c/s	Given in Spec.
Core and sheath	0.875	0.876	-
Core and core	2.0	1.94	-
Three cores and sheath	0.293	0.23	-
Star inductance at 50 c/s	1.53	-	1.59

TABLE IV.

Capacitance values (μF.)

Connection	Calculated from dimensions	Measured at 1000 c/s	Given in Spec.
Core to sheath	1.07	1.03	1.035
Three core to sheath	3.21	3.07	-

TABLE V.

Resistance values for a cable length. (ohms).

Connection	Calculated d.c. resistance	Given in Spec.
Single core	0.39	0.368
Single sheath	4.14	-

1.5 Discussion of Results

It will be seen from Table I that there is agreement between the surge impedance values calculated using core to sheath inductances, and those measured using the R.S.O. impulse and the R.V.1. chopped wave. There is also agreement between the values derived using the R.V.1. wave with no chop, and those calculated as the mean of two values, using as inductance the core to sheath and core to core values. Similar conditions appear to exist in the values of propagation time given in Table II.

These relationships were recorded by Gosland[11] for the three single core cables which, of course, should follow since the only significant difference between the two types is that the spacing between the sheaths of the S.L. cable is smaller. Gosland showed how the relationships were due to induced currents in the sheath circuits, and, ignoring the skin and proximity effects, he indicated how the transient voltage wavefront may be derived. In Appendix 4 an extension to Gosland's analysis is made to facilitate the calculation of the surge impedance. Then in Chapter 6 a more rigorous investigation of the electromagnetic behaviour of the cable is carried out taking account of the skin and proximity effects. From this it appears that, at low frequencies, the magnetic fields of the currents in the cores penetrate the sheaths producing

a coupling effect, and as the frequency increases these fields become confined to the area between the core and the sheath. It follows that the inductance and surge impedance will vary, their values decreasing as the frequency increases to limits determined by the core to sheath inductances. The fast waveforms of the impulse and the chopped current wave should therefore encounter a lower surge impedance than the 50 c/s half sine wave injected by the R.V.l., which is in agreement with the results obtained.

It is noticed that the peaks and start of the transients for zerochop Fig. (la), and the front of the transient for a chopped current wave (Fig. lb), are curved. Gosland explained the former as being caused by waves of different velocities returning to the sending end at different instants. This is certainly true, but does not explain the curvature at the beginning, which appears to be caused by a lumped capacitance connected at the near end of the line. Figs. 81 and 82 show the response derived from surge diagrams of the line with a capacitance of 0.05 μF connected the input, and these agree well with the actual measured voltages. This capacitance represents approximately the total capacitance from the trifurcating joint to the instrument

plus the output capacitance of the instrument itself.

Fig. 2 shows examples of the records made using the R.S.O. in the measurement of the surge impedance. A variable resistance R was used as the line termination. Because of the losses in the cable the surge impedance for an impulse varies with time, so that a proper termination is not possible. The value of R taken as the surge impedance was that which gave the minimum reflection.

1.6 Conclusions

As Gosland suggested, this cable behaves in a similar way to the cable he examined. The effect of difference in sheath spacing is made clear in a comparison of the empirical formula for the effective surge impedance determining the recovery voltage wave-front.

For the 3-single core cable $Z = 0.75 \sqrt{\frac{L}{C}}$

For the S.L. cable $Z = 0.92 \sqrt{\frac{L}{C}}$

where L and C are power frequency constants, L being the star inductance. It should be noted that these empirical relationships are dependent to some extent on the length of the cable under test, and therefore should not be

considered as general formulae.

For chopping and impulse conditions the inductance and surge impedances are given by the core to sheath values.

CHAPTER 2.

60 M.V.A., 132 kV. TRANSFORMER

2.1 Introduction

The experimental data on the transient behaviour of transformers is very extensive.[21,33] It has been provided, in the first place, to support the theories of wave propagation along windings and to assist in the design of windings to limit inter-turn voltages, and also for the determination of equivalent circuits in recovery voltage problems.[10] In the former it is mainly oscillographic records of voltage at different points along a winding subject to a steep fronted surge, whereas in the latter it is records of the voltage response of the winding to half sine waves of current, and measured values of winding parameters.

This chapter is concerned only with the terminal behaviour of a 60 M.V.A., 132 kV., star-delta transformer with earthed neutral, since access to the winding itself was not possible. Measurements, using standard techniques[13], were made of its transient and frequency response with a view to gaining a better understanding of the nature of

wave propagation along transformer coils. The equivalent circuit for recovery voltage was examined under chopping conditions.

2.2 Measuring techniques

(1) Self-capacitance

Measurements were made of the transformer self-capacitance using (a) R.V.L., (b) Signal Generator.

(a) This consists essentially of injecting a current surge into the winding with a capacitance connected across it, and recording the resultant transient voltage.

(b) By adjusting the frequency of a signal generator connected with an oscilloscope to the same network as above, the resonant frequency could be found.

With an additional capacitance comparable in size with the self-capacitance of the winding, the self-capacitance is obtained from the equation

$$\frac{C_o + C_1}{C_o + C_2} = \left(\frac{f_2}{f_1}\right)^2 \qquad \ldots\ldots\ldots\ldots (1)$$

where C_o is the self-capacitance, C_1 and C_2 are the additional capacitances, and f_1 and f_2 the corresponding resonant frequencies. It is assumed that the transformer inductance has varied negligibly between the frequencies

f_1 and f_2.

(2) Transformer Inductance

The variation of the transformer inductance with frequency was obtained in a similar way. Larger values of capacitance were added so that the resonant frequency was altered considerably. The inductance is derived simply from the equation

$$f = \frac{1}{2\pi\sqrt{LC}} \qquad \ldots\ldots\ldots\ldots\ldots\ldots (2)$$

where C is the sum of the self and additional capacitances, and f is measured as before.

When considering an unearthed fault, measurements are made with the instrument isolated from earth. For this case it was found necessary to take account of the capacitance of the instrument to earth, since it produces a reduction in the measured value of the resonant frequency. This effect is examined in Appendix 5.

(3) Transformer Admittance

The modulus of the admittance of the transformer for different additional capacitances was derived from measurement of voltage and current using a valve voltmeter. The source was a signal generator with a frequency range

of 20 c/s to 50 kc/s.

(4) Measurements were made of winding capacitances and inductances using a 1000 c/s impedance bridge.

(5) R.V.1.

A value for the transformer inductance was obtained from a measurement of the voltage response to the half-sine wave of current generated by the R.V.1. The magnitude of the voltage transient is given by

$$\hat{e} = \hat{i}\, 2\pi f.L \quad \ldots\ldots\ldots\ldots\ldots\ldots (3)$$

where f is the frequency of the current wave (50 c/s), and L is the inductance.

The maximum value of the voltage response to the chopped current wave is given by

$$\hat{e} = i_c \sqrt{\frac{L}{C}} = i_c Z_c \quad \ldots\ldots\ldots\ldots (4)$$

where i_c is the current value at the chop, and C the self-capacitance of the transformer. Therefore, from a measurement of $\hat{e}$ and i_c the surge impedance of the transformer Z_c can be obtained, or alternatively by inserting the value for the self-capacitance already measured, the inductance.

The natural frequency of the winding can be

measured directly from oscillograms. Examples of oscillograms are shown in Fig. 3.

(6) R.S.O.

The transformer surge impedance can also be derived from measurements of the current response to the voltage impulse generated by the R.S.O. In this case the current oscillates and the impedance is determined by measuring the voltage and current before the current has reached the maximum value, i.e. before a reflection from the other end of the transformer has returned, as shown in Fig. 4.

2.3 Results

(1) Self-capacitance

Winding connected to represent the conditions of the first phase to clear a three-phase fault at the secondary terminals

Table shown overleaf

Capacitance added μF	Resonant Frequency Kc/s using		Self-capacitance μF using	
	Sig. Gen.	R.V.1.	Sig. Gen.	R.V.1.
0	7.05	6.5	0.0031	0.00338
0.00169	5.67	5.3	0.0032	0.00335
0.00448	4.55	4.26	0.0033	0.0034

(2) Ground capacitance of primary winding with secondary windings earthed. 0.0168μF.

(3) The variation of transformer inductance is shown in Fig. 5. In this graph all the values for the primary and secondary windings are included, expressed as a fraction of the inductance values at 1000 c/s, which were measured using the impedance bridge.

(4) Admittance-frequency curves are plotted in Fig. 6 for the transformer connected to represent the first phase to clear a three-phase fault at the secondary terminals. This also shows the effect of additional capacitance.

(5) A comparison of the transformer surge impedance

(a) obtained from $\sqrt{\frac{L}{C}}$ using as inductance the value measured at 1000 c/s, and the self-capacitance. 6840 ohms

(b) obtained from the response of the winding to a half sine wave, and using the self-capacitance. 6560 ohms

(c) derived from the response of the winding to a chopped current wave. 5040 ohms

(d) derived from response to the R.S.O. impulse. 3000 ohms

2.4 Discussion of results

From Table (1) it is observed how the different instrument capacities affect the resonant frequencies: the R.V.1. having the larger capacity to earth gives a lower value for the frequency. From the agreement between the two sets of results, it would appear that the approximate analysis given in Appendix 5 is adequate.

Fig. 5 shows clearly the frequency dependence of transformer inductance. This phenomenon is known to be due to eddy currents in the transformer. The only published attempt at a theoretical explanation is by Gosland and Dunne[12] who show that the main factor producing this variation is the displacement of the flux from the copper winding, and they consider that the variation of core flux will have a negligible effect. In Chapter 8 the author tries to show that Gosland's conclusions are not completely

justified, and develops a theory taking into account the finite thickness of the lamination. Because no data was available of the construction of the transformer core, the results of this analysis could not be compared in detail with experimental results.

It is interesting to note that the response of the winding to half sine waves of current, shown in Fig. 3a, is a single frequency oscillation, whereas the measured frequency response, Fig. 6, indicates the presence of other natural frequencies at 9.5, 32 and 39 kc/s. For such an input the components of these higher frequencies must be of too small an amplitude to be observed. When the input is a chopped wave, however, the response, Fig. 36, does appear to indicate the presence of other frequency components, although their amplitude must still be small.

In Fig. 6 the effect of additional capacitance on the winding admittance is also indicated. It appears that this capacitance only affects the first natural frequency, from which it may be concluded that the other frequencies are due largely to the presence of other windings. A further interesting factor is that, at these low frequencies, the winding does not exhibit any line characteristics, for resonant frequencies do not appear at multiples of the fundamental natural frequency; unless

perhaps the second resonant frequency is a harmonic, and the others beyond it have been damped out.

The values of the surge impedance shown in Table (5) are widely different. It should be said here that the parameter of surge impedance for a transformer does not have the same physical significance it has for a transmission line. This is because of the nature of the coupling between turns and the periodic nature of the coil, which introduces several arbitrary factors. This will be discussed in greater detail in Chapter 9. However for the purpose here, which is of a qualitative nature, it is a convenient concept. The main aspect of that table is that the steep fronted waves of the impulse and the chopped current surge encounter a much lower impedance than the slower waves of the 50 c/s current surge and that derived using the 1000 c/s inductance value. This appears to indicate a considerable decrease of the transformer inductance at frequencies much higher than 50 Kc/s., which is confirmed by the theoretical analysis.

2.5 Conclusions

The various measuring techniques seem adequate for the determination of an equivalent circuit in recovery voltage problems, when chopping conditions are not considered.

Such an equivalent circuit is not valid under chopping or impulse conditions and a more detailed examination of the nature of wave propagation in windings appears necessary.

The admittance measurements lead to some interesting conclusions regarding the effects of the other windings and the behaviour of the winding at the low frequencies, and a measurement of the phase as well as the amplitude of this admittance over a wide frequency range would be very valuable.

CHAPTER 3.

RECOVERY VOLTAGES OF A 132 kV. POWER SYSTEM

3.1 Introduction

After measurements had been made on the cable and transformer separately, the author was afforded the opportunity of taking records with the R.V.1. at the circuit-breaker terminals of the power system containing the elements already examined. A comparison could therefore be made between measured recovery voltages, and those determined analytically using the parameters already determined.

The system consists of a 132 kV. three-phase cable from the circuit-breaker at Braehead Power Station to a transformer at Govan Sub-Station, and then to an identical one at Hagg's Road.

The tests were made in three groups. The first was for faults on the secondary of the Govan transformer, with the Govan to Hagg's Road cable disconnected, while the second was for faults on the Hagg's Road transformer, with the Govan transformer disconnected. In the third group simultaneous faults were fixed on both transformer

secondaries. Although this is a rather hypothetical case, it did provide a more complicated circuit.

In each case, connections were made to represent the switching operations for the faults:-

(1) Phase to earth

(2) Phase to phase

(3) Three phase

(4) Three phase to earth

Recovery voltage transients were recorded for each of these faults. Because of the low natural frequencies of the system the duration of the transients was longer than the time between each current surge (1/100th sec.) This resulted in an overlapping of the transient oscillations, making their interpretation rather difficult. The method used to overcome this difficulty is described in Appendix 1. Examples of the oscillograms are shown in Fig. 7.

3.2 Results

Table 1

A comparison of the natural frequencies, and of the magnitude of the first peak of the recovery voltage transients

(a) obtained from R.V.l. records,

(b) calculated from system parameters

on the system.

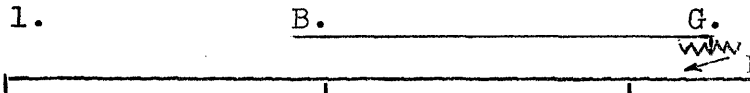

Fault	Natural Frequency c/s		Degrees of Chop	Amplitude of first peak, volts	
	Measured	Calculated		Measured	Calculated
Phase to earth	426	412	0	1.76	1.75
Phase to phase	434	457	0	3.61	3.5
Three phase	366	387	0	2.83	2.68
Three phase to earth	387	412	0	1.76	1.75
Phase to earth	426	412	52	2.6	2.49
Three phase to earth	387	412	57	2.68	2.78

2. On the system

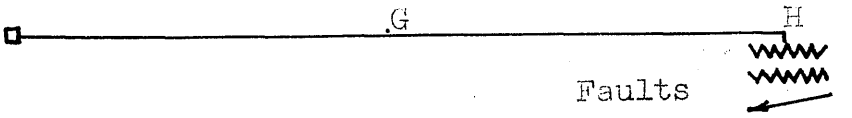

Fault	Natural Frequency c/s		Degrees of Chop	Amplitude of first peak, volts	
	Measured	Calculated		Measured	Calculated
Phase to earth	270	280	0	0.89	0.97
Phase to phase	284	310	0	2.0	1.94
Phase to phase to earth	303	294	0	0.90	1.0
Three phase	280	289	0	1.54	1.52

3. On the system

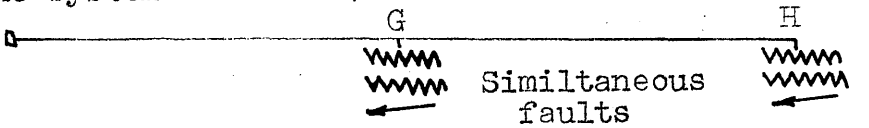

Phase to earth	407	403	0	0.77	0.73
Three phase	399	401	0	1.39	1.27
Phase to earth	407	403	34	2.27	2.22
Phase to phase	432	451	34	2.32	2.22

3.3 Calculation

In the calculation of the recovery voltage for zero chop, it was assumed that the cable and transformer were represented by lumped capacitance and inductance respectively. For chopping conditions, however, it was found necessary to take account of the propagation time along the cable. To include this factor analytically is obviously a tedious process, and so Bergeron's graphical method was used. A comparison of the derived and measured recovery voltage for the case of simultaneous faults on both transformers is shown in Fig. 83.

The parameters of the cable and transformer used in the calculation of the zero chop transients were those measured at 1000 c/s. In the construction of the Bergeron diagram illustrating the response to a chopped current wave, the high frequency values were used. For the cable these were the core to sheath values of surge impedance and propagation time, and for the transformer the inductance measured at its natural frequency.

3.4 Conclusions

This analysis shows clearly the value of Bergeron's graphical method in the solution of problems where the physical size of the network is important.

Under chopping conditions the representation of the transformer by a lumped inductance is justified with the cable situated between it and the circuit-breaker.

CHAPTER 4.

DOUBLE CIRCUIT 132 kV. OVERHEAD LINE

4.1 Introduction

The original and fundamental studies of propagation of waves along transmission lines were made, in general, from the point of view of the telegraphist. These led, as for example, in Carson's work[34], to approximations which were complex and not suitable for power transmission lines. They did, however, provide the basis of the theories later developed for power lines, as in the very comprehensive treatment given in Surge Phenomena[33] and two papers by Frenchmen worthy of note. The first, by Pelissier[35], gives a very interesting analysis of the problem, considering in a novel way, the factors of attenuation. In the other Fallou[36] confirms the use of Kirchoff's equation from the rigorous analysis of Carson; he employs symmetrical components in the analysis of three phase lines, and describes various techniques for the measurement of the frequency dependence of the various line parameters.

For representation in recovery voltage problems it has been the general procedure to set up substitute

circuits of lumped capacitance and inductance. Hammarlund[10] deals fairly thoroughly with this, giving details of many equivalent circuits. The problem can also be tackled assuming that the parameters do not vary, by time-lattice diagrams or by Bergeron's method.

In this chapter measurements of the frequency and transient response of a 3-mile length of double circuit 132 kV. line with earth wire protection, are described.

4.2 Measuring Techniques

(1) The surge impedance

The modulus of the surge impedance can be found from a measurement of the input impedance of the line with the end open and short circuited. If the modulus of the short circuited impedance is Z_1, and the modulus of the open circuited impedance Z_2, then the surge impedance is given by

$$|Z_c| = \sqrt{Z_1 Z_2}$$

The input impedances were measured in two ways:

(a) In the first method a variable frequency source supplied either the line or a variable resistance, and a thermocouple milliammeter and value voltmeter were connected as shown in Fig. 8. The power source was an audio frequency

power amplifier having a maximum output of 15 watts, and supplied by a signal generator. By setting the output voltage of the source the same for both line and resistance measurements, and measuring the current, the inherent error due to the valve voltmeter was reduced. If I_L and I_R are the measured line and resistance currents for a particular frequency, the modulus of the input impedance of the line is given by

$$|Z_{in}| = R \cdot \frac{I_R}{I_L}$$

(b) The circuit for the second method is shown in Fig. 9. This is the same as for (a) but instead of the power amplifier a voltage amplifier with a high output impedance was used, and the current determined by a measurement of the voltage across the resistance R_1. In this case also the resistance R was adjusted till it equalled the line input impedance, thereby reducing instrument errors.

The methods so far described enable a determination of the surge impedance as a function of frequency. Its value under transient conditions was measured in two ways using the R.V.1.

(c) This consists essentially of injecting a half sine wave with or without chop into the line short circuited

at the far end, and recording the resulting transient voltage on a cathode ray oscilloscope. For a current input with no chop the surge impedance is found from the equation

$$e = Z_c \hat{i}\, 2\pi f\, t. \qquad \ldots\ldots\ldots\ldots\ldots (1)$$

where e = the wavefront of the voltage transient,

$\hat{i}$ = the maximum value of the current,

and f = the frequency of the half sine wave.

For a chopped wave the voltage peak is given by

$$\hat{e} = Z_c\, i_c \qquad \ldots\ldots\ldots\ldots\ldots\ldots\ldots (2)$$

where i_c = the current magnitude at the chop.

As stated previously these formulae are only valid if the propagation time of the line is less than 1 ms. Examples of records of these voltage transients are shown in Fig. 11.

With zero chop the voltage transients were comparable in magnitude to radio frequency pick-up, and to reduce this, it was necessary to connect a small capacitance of 400 μμF across the end of the line. Oscillograms, Fig. 11(c,d) show the recovery voltage transient with and without the capacitance connected.

(d) In this method the R.V.1. is connected to the line and a variable resistance, as shown in Fig. 10. A

chopped current wave is injected into the line, and the voltage across the resistance displayed on an oscilloscope. When the resistance equals the surge impedance of the line, the current divides; one half flows through the resistance, and the other half travels to the short circuited end where it is reflected with the same polarity and returns at a time 2T later to add to the current already flowing in the resistance. Some examples of the oscillograms taken are shown in Fig. 12.

(2) Propagation time

The propagation time can be determined from the natural frequencies of the line, using methods (a) or (b). It can be determined from the frequency of the transient voltage response to current surges (c), or it can be measured as described in (d) above.

(3) Attenuation

This can be estimated from the decrement of the transient voltage response to the current surges.

Fallou, using measuring techniques similar to those described under (a) and (b) above, showed how the attenuation could be related to the value of the line impedance at resonance. However, the line on which Fallou's measurements were carried out was much longer,

having a natural frequency of 540 c/s. In this case the natural frequency was 20 Kc/s, and so using his method the attenuation could only be evaluated at the frequencies 20, 40 ... Kc/s.

4.2 Discussion of measuring techniques

The main difficulty about the measurement of the input impedance of a line over a wide frequency range is the wide variation of its value. In this case it varied from about 10 ohms to 10,000 ohms. Method (a) was therefore used most successfully, because of the low output impedance of the source, in the measurements of low impedance, e.g. low frequencies for the short circuited line, near resonance for the open circuited line. When the impedance was high, e.g. low frequencies for the open circuited line, the method (b) was used.

It has been shown how the surge impedance can be calculated from the voltage response of the line to current surges generated by the R.V.l. This method involves measurement from oscillograms of the voltage and current waves, and is therefore not as convenient as method (d) in which the surge impedance is compared directly with a resistance. However, this method, as with that using the R.S.O. described in Chapter I, will only give the high frequency value of surge impedance.

Compared with the technique using the R.S.O., this has the advantage that no operator is required at the far end of the line.

4.3 Calculation of parameters

The various surge impedances were calculated assuming that the earth and the conductors were of infinite conductivity. Their evaluation, developed from the analysis given in Surge Phenomena, is shown in Appendix 6.

4.4 Results

TABLE 1.

A comparison of surge impedance values (ohms)

Connection	Z_1	Z_2	Z_3	Z_4	Z_5
Phase to earth	739	720	710	726	660
Phase to phase	465	450	445	490	470
Phase to phase to earth	419	410	410	395	396
Three phase	500	540	535	510	518
Three phase to earth		280	280	295	307

Z_1 is the calculated surge impedance.

Z_2 is the surge impedance derived from measurements of the inductance and capacitance at 1,000 c/s.

Z_3 is the value measured directly using the R.V.1.

Z_4 is the surge impedance derived from the voltage response to a half sine wave.

Z_5 is the value derived from the response to a chopped half sine wave.

TABLE II.

The propagation time (milliseconds)

(i)	With earth return	
	(a) Derived from frequency response to half sine wave.	0.0253
	(b) Calculated from constants measured at 1,000 c/s.	0.026
	(c) Obtained from R.S.O. records.	0.0235
(ii)	No earth return	
	(a) Derived from frequency of response to half sine wave.	0.025
	(b) Derived from frequency of response to chopped wave.	0.0234
	(c) Calculated from constants measured at 1,000 c/s.	0.0254
	(d) Obtained from R.S.O. records.	0.0236

TABLE III.

Attenuation

Ratio of successive peaks of transient response to half sine wave

(i)	With earth return	0.8
(ii)	Without earth return	0.86

4.5 Discussion of results

It appears from the oscillograms of the voltage response to a chopped current wave, (Fig. 11(b), as in the cable measurements (Chapter 1), that a lumped capacitance is connected across the ends of the line. In this case the capacitance probably comprises several factors, instrument capacity, the capacity of the connecting leads, the insulator capacity, and the non linearity of the distributed capacitance at the end of the line as described by Pelissier[35]. No attempt has been made to evaluate it, since this would have involved a careful arrangement of the instruments, and when the tests were made this was not realized.

From the same oscillogram, Fig. 11(b), it is noticed that the first peak is smaller than the second. This is because the end capacitance has not been completely

charged by the time the reflected wave returns. As a result, the successive peaks are distorted in such a way that one might imagine that there are two waves of slightly different velocities travelling along the line. In the case of propagation between a line and earth, Fig. 11(e), this distortion is not evident, probably because the attenuation is much greater than for propagation between lines.

Fig. 13 shows the relationship between the surge impedance and the frequency. The greater decrease of impedance for earth connections is due to the considerable dispersion of the field in the earth, which occurs at the low frequencies. As the frequency increases, the earth currents tend to flow near the surface. For propagation without an earth return the change is due mainly to a displacement of the field from the conductors.

Because of the frequency dependence of surge impedance it follows that the value under surge conditions will alter with the shape of the surge. Further, since the impedance approaches a minimum at the high frequencies, then its value, when the steep fronted waves of the impulse and chopped current wave are applied, should be smaller than that to the half sine wave. This is in agreement with the results shown in Table I.

The dispersion of a field, in this case into the earth, only affects the values of the inductance and resistance, and so it follows that the propagation time ($\sim\sqrt{LC}$) will vary in the same way as the surge impedance ($\sqrt{\frac{L}{C}}$). This is indicated in the measurements under surge conditions as shown in Table II.

4.6 Conclusions

1. For representation in recovery voltage problems, and for approximate investigations of the transient response to impulse waves, it is sufficient to consider the surge impedance and propagation time as constant. When a more exact evaluation is necessary, including attenuation, etc., the more rigorous methods given in reference 33 would have to be considered.

2. The evaluation of the end capacitance would be necessary for an exact evaluation of the response of a line to surges.

CHAPTER 5.

440 V., 625 k.V.A. GENERATOR

5.1 Introduction

As with the transformer, the experimental data on generators is concerned with the measurement of the voltage distribution along windings subject to steep fronted surges, and with the determination of equivalent circuits in recovery voltage problems. Robinson[38,39] has dealt fairly thoroughly with the former, and Hammarlund[10] with the latter.

This chapter is devoted to an account of measurements made on a generator of the frequency and transient response. In this case a Q meter was used for frequencies greater than 50 Kc/s. The voltage distribution along the winding subject to a surge was measured, and the effect of rotor position and excitation examined.

The main object of the investigation was to obtain a better understanding of the nature of wave propagation through a generator. Recovery voltage conditions could not be examined because of the very low inductance of the winding.

The generator was an 8-pole, 3-phase, 625 kVA., 440 volt machine, with 48 slots, and 2 conductors per slot, and having a salient pole rotor. The winding diagram and slot dimensions are shown in Fig. 14. Both ends of each phase were brought out, so that the generator could be connected star or delta. This meant that measurements could be made on one phase, with the other two isolated or earthed. Since there was no insulation at the end of each conductor, tappings along the winding could be taken from direct connections.

5.2 Tests carried out

(1) Tests were carried out to determine the voltage distribution along the winding on the application of impulse waves. An R.S.O. was used to generate the surges and measure the voltage at different points along the winding.

(2) To determine the surge impedance of the winding, measurements were made of the current response to various impulse waves.

(3) The input impedances of the winding, with the remote end open and short circuited, were measured using (a) bridge at 1 and 10 kc/s.

(b) 'Q' meter between 50 kc/s and 2 mc/s.

(4) The effects of the rotor position, and field, on the input impedances of the winding, were investigated.

5.3 Results

(1) Surge Impedance (ohms)

TABLE I.

Connection	Z_1	Z_2	Z_3
One phase to earth, other phases insulated.	24.5	27	19
As above, but with one other phase earthed at both ends.	65	56	-
As above, but with the other two phases earthed at both ends.	69	60	49

Z_1 is the surge impedance derived from oscillograms of the input voltage and current through the winding.

Z_2 is the surge impedance derived from measurements made using the Q meter. It is the minimum value which occurs at high frequencies. (See Fig. 15).

Z_3 is the surge impedance calculated assuming the iron and copper to be infinitely conducting planes.

(2) Propagation time

(a) Derived from the measurement of the natural frequency - 0.52 μs.

(b) Measured from oscillograms - 0.5 μs.

(3) The effect of the rotor position, with no excitation, on the winding impedances is shown on Fig.17.

(4) The effect of field excitation on the winding impedances.

It was found that beyond 50 kc/s the field excitation had no effect on the Q meter measurements for any position of the stationary rotor.

5.4 The determination of the values of the surge impedance

(1) Z_1

When a voltage surge is applied to a distributed line, the parameters which determine the current response are the surge impedance, the propagation time, and the attenuation. However, between the times $t = 0$ and $t = 2T$ (i.e. until the wave reflected from the far end returns), the current and voltage are related simply to the surge impedance by Ohm's Law, and the response is not

affected by the attenuation of the line. Z_1 is the value calculated during that time interval. (Fig. 18).

(2) Z_2

The input impedance of the winding with the end open or short circuited was found using a 'Q' meter and an impedance bridge. If Z_o and Z_s are the complex open and short circuit impedances at the same frequency f, then the surge impedance is

$$Z_c = \sqrt{Z_o \; Z_s}$$

and the propagation time is

$$T = \text{Imaginary Part} \left[\frac{1}{\omega} \tanh^{-1} \sqrt{\frac{Z_s}{Z_o}} \right]$$

$$= \frac{1}{2\omega} \arg \left[\frac{\sqrt{\frac{Z_o}{Z_s}} + 1}{\sqrt{\frac{Z_o}{Z_s}} - 1} \right].$$

Because the winding had a large capacitance to earth, all measurements using the Q meter had to be made on its capacitance arm, one end of which was earthed to the chassis. This meant that inductances were determined as negative capacitances.

The measuring circuit is shown in Fig. 19. At each frequency, measurements were made with and without the generator connected. In each case C^1 was adjusted until the resonance point was reached. The

input series resistance and capacitance is then given by

$$C_0 = \frac{C(C + C_1' - C_2')}{C_2' - C_1'}$$

$$R_1 = \frac{C_2(Q_1 - Q_2)}{\omega K_1 K_2 Q_1 Q_2}$$

where

$$K_1 = \frac{CC_0}{C + C_0} \quad ; \quad K_2 = \frac{CC_0C_2'}{CC_0 + C_0C_2' + C_2'C}$$

The subscripts 1 and 2 refer respectively to measurements taken without and with the generator connected. The derivation of the formula is given in Appendix 7

(3) Z_3

At high frequencies it appeared that the electromagnetic field was confined to the dielectric, and that the currents travelled along the surface of the iron and copper. For the case of propagation between one phase and earth, with the other two isolated, the distribution of current is assumed to be that shown in Fig. 20(a). Since there will only be small interaction between the field of the currents flowing in different sides, the system will have the same characteristics as that of three parallel plane wave guides. Hence the surge impedance is given by the well-known formula

$$Z_c = \sqrt{\frac{\mu}{\epsilon}} \cdot \frac{a}{b}$$

where a is the thickness of the dielectric and b the width of the guide.

When the other two windings are earthed, because of the lower resistance of the copper, the current would tend to return through the other two phases. The current distribution would then be that shown in Fig. 20(b), and again the surge impedance would be given by the formula above.

5.5 Discussion of Results

As shown by the winding diagram, Fig. 14, no two turns of a phase are in the same slot. There will therefore be little interturn capacity, and, as a result, the winding should behave like a transmission line. This is borne out by oscillograms and measurements, and is shown by the Bergeron diagram of Fig.84. In this diagram a comparison is made between the voltage at the open circuited end of the generator winding and of a simple distributed line, when the same impulse wave is applied to the other end. Since the purpose of this diagram was merely to examine the general behaviour of the winding, it was not necessary to compute the values of the surge impedance and damping factor to be used. These were selected to give the best agreement, and so

to indicate most clearly the response of the winding.

Figures 15 and 16 show the change of surge impedance and propagation time with frequency. These curves give an indication of the distribution of the electromagnetic field. At low frequencies the field is distributed throughout the cross section of the iron, dielectric, and copper, and the velocity of the electromagnetic waves is reduced considerably by dispersion. As the frequency increases, the field gradually becomes confined to the dielectric area between the iron and the conductors, producing a reduction in the surge impedance and an increase in the wave velocity. The slot and conductor now act somewhat like a conventional wave guide, and it is interesting to note that the surge impedance calculated from that assumption is remarkably close to the high frequency value (cf. Z_3 and Z_1 in Table I).

When the other two phases are earthed, it is seen (Table I) that the calculated value is considerably smaller than the other two values. This may be partly due to the fact that these phases were earthed only at the ends.

These deductions on the distribution of the fields at high frequencies are confined by the tests on the effects of the rotor position (Fig. 17), and the

magnitude of the field, on the input impedances.

5.6 Conclusions

This particular winding behaves, under all transient conditions, like a distributed line (i.e. there is no critical frequency).

For representation in recovery voltage problems the considerable variation of zero sequence inductance over the frequency range 1,000 c/s to 3 Mc/s would produce difficulties in the selection of the appropriate inductance valve.

There appears to be a considerable need for a theoretical investigation into the nature of wave propagation through the generator, and, in particular, to account for the frequency variation of the winding surge impedance. An attempt is made to solve this complex problem in Chapter 7.

GENERAL CONCLUSIONS TO PART I.

For representation of a power system in recovery voltage problems when chopping conditions are not considered, it has been the practice to attempt to relate the parameters to the power frequency constants. This is a justifiable procedure, but care has to be taken when applying what appears to be a general rule, e.g. Gosland's empirical formula for the surge impedance of a cable, (Chapter 1).

When current chopping takes place, or under impulse conditions, the dispersion of the field in the metal no longer appears to have a noticeable effect on the propagation. This was confirmed by the frequency measurements, which showed that, beyond about 5×10^4 c/s, for all elements of the system the inductances appeared to have reached a minimum value. However, under these surge or high frequency conditions, the physical size of the network elements may have to be considered, particularly those elements in a connected system near the point of measurement. For a cable or overhead line this problem is readily solved using Bergeron's graphical method, but for the transformer and generator the actual

physics of wave propagation through the structure is not yet fully understood, and the results which have been obtained cannot be fully explained.

There has appeared a considerable need for a further theoretical investigation of the problems of wave propagation through the various elements examined. The problems are complex, and in attempting solutions the experimental evidence will be of great assistance, for it can help in leading the analysis in the right direction.

The most useful data in this connection would be impedance measurements over a frequency range of 20 c/s to about 50 Mc/s., and there appears the need for the development of an impedance bridge capable of measuring impedances varying from about 10 ohms to 10,000 ohms over a frequency range from 20 c/s to about 500 Kc/s. A 'Q' meter can be used beyond 500 Kc/s.

Considerable care has to be taken when making measurements of the system parameters with the instrument isolated from earth, because of the very large earth capacitance of the system.

PART 2

A Theoretical Investigation of the Propagation of Electromagnetic Waves through the Elements of a Power System

PART 2.

It has appeared from the work described in Part 1 that further theoretical investigation into the transient behaviour of the power system elements is necessary. The usual approach to such problems has been to develop equivalent circuits. In this, several physical assumptions are made, and the structure replaced by a network of lumped inductances, capacitances, and resistances. The merits and weaknesses of the method rest, respectively, in the simplicity of the solution and its reliability. The replacement of the complicated structure of the generator or transformer by an equivalent circuit leads to a simple explanation of the phenomena, and permits readily the consideration of the effects of variations in structure, etc.

However, it cannot be said that the physical explanations given are entirely satisfactory, and that the solutions are completely reliable. The reason is that the approximations made are of a physical nature, in that they imply certain distribution of flux, etc., and are seldom supported by any rigorous mathematical analysis.

It seemed therefore necessary to attempt some

rigorous studies of the propagation of electromagnetic waves through the system elements, and here four separate problems have been tackled. First a study is made of the propagation of waves along a cable with individual sheaths, the basis of this analysis being the general treatment of the cable problem by Schelkunoff. Then a chapter is devoted to an investigation into the factors influencing propagation through a generator, considering in detail the effects of the laminations. This is followed by two chapters on the behaviour of a transformer, the first dealing with the effect of laminated core, and the second examining the present theories of wave propagation through transformers and showing the development of a theory for a coil replaced by a sheath.

The method of tackling the problems has been to start with Maxwell's field equations, and this has meant, in each case, the consideration of geometrically simple structures representing each element. Although the results obtained, at least in the generator and transformer problems, may have no immediate value, the information that has been obtained does help to provide adequate physical explanations for most of the experimental results presented in Part 1, and may lead to the development of more comprehensive theories.

CHAPTER 6.

Wave propagation along cables with individual sheaths

6.1 Introduction

The only published work on the transient performance of this type of cable was a paper by Gosland[11]. He showed how currents flowing in the conductors induced voltages in the sheaths, and how the resulting currents flowed along the sheaths and through the bonds. In that paper the sheath circuit is considered as an inductive loop, no account being taken of its finite length.

In this chapter, there is a more rigorous study of the problem, taking into account the skin and proximity effects, and considering the distance between bonds. This analysis is based on a general treatment of the coaxial cable given in a paper by Schelkunoff[15].

6.2 Propagation Along a Coaxial Pair

The problem considered first is that of two cores surrounded by concentric cylindrical lead sheaths, Fig. 21. For the moment, the effects of bonds will not be considered.

The magnitude of a magnetic field between the sheaths due to time varying currents in the cores is affected by the sheaths. This is because electromagnetic waves, propagated outwards from the cores in a radial direction, are partially reflected at the boundaries of the sheaths and the dielectric, and attenuated in the lead. The coefficients of reflection and attenuation are functions of the frequency and the conductivity of the sheath, and so, as the frequency varies, the coupling between the fields of the two currents also varies. The coupling is a maximum at zero frequency, and decreases to zero as the frequency approaches infinity, when the fields are confined to the space between the core and the sheath as in a waveguide.

The sheaths therefore act as shields whose behaviour has been studied by Schelkunoff[15,16]. He showed that the analysis of such problems is facilitated by the use of the surface and transfer impedances. For a solid conductor the surface impedance relates the total current flowing to the electric intensity at the surface. While, for a hollow conductor, with return paths either external or internal to the conductor, or both, the surface impedances relate the electric intensity at a surface to the return current adjacent to that surface. In the

derivation of the transfer impedance, it is supposed that if the currents in the return paths are I_a inside and I_b outside the hollow conductor, then a current $-I_a$ flows along the inside surface and $-I_b$ along the outside surface. The transfer impedance then represents the interaction of these two currents. The cable system (Fig. 21) can therefore be represented by the series of transmission lines with coupling via the transfer impedance between lines 2 and 3, and lines 4 and 5 (Fig. 22). (The impedances connected across the end are the surge impedances, which have been included here merely to show the circuit more clearly.)

The electric intensities in the Z direction at the surface of the core and sheath are, according to the definitions given above

$$E_1 = Z_1 I_1$$

$$E_2 = Z_2 I_1 + Z_{23} I_2$$

$$E_3 = Z_{23} I_1 + Z_3 I_2$$

where Z_1 = surface impedance of solid core

Z_2 = surface impedance on the inside of the hollow sheath

Z_3 = surface impedance on the outside of the hollow sheath

and Z_{23} = transfer impedance between the two surfaces of the hollow conductor.

Now Maxwell's equations written in integral form for a homogeneous isotropic dielectric, are

$$\int_c E\, ds = -\frac{d}{dt}\int_s B\cdot n\, da \qquad (2)$$

and

$$\int_c H\, ds = \frac{d}{dt}\int_s D\cdot n\, da \qquad (3)$$

where $\int_c$ is a contour integral, and $\int_s$ a surface integral.

Applying equation (2) round the contour indicated by the dotted rectangle 1 in Fig. 21 gives

$$\frac{\partial V_1}{\partial z} + E_1 + E_2 = -\frac{\partial}{\partial t}\int_s B\cdot n\, da = -\frac{\partial \Phi}{\partial t} \qquad (4)$$

where V_1 is the potential between the core and the sheath, and Φ is the value of the magnetic flux passing through the rectangle. By the definition of inductance the right hand of equation (4) becomes

$$\frac{\partial \Phi}{\partial t} = j\omega L_{12} I_1 = X_1 I_1$$

so that equation (4) becomes

$$\frac{\partial V_1}{\partial z} + E_1 + E_2 = - X_1 I_1 \qquad (5)$$

Applying equation (2) round the contour 2 in Fig. 21, gives similarly

$$\frac{\partial V_2}{\partial z} - 2E_3 = X_2 I_2 \qquad (6)$$

The term $-2E_3$ results from the symmetry of the system.

Now applying the second Maxwell equation (3) round the contour 3

$$2\pi a \frac{\partial H_1}{\partial z} = \frac{\partial}{\partial t} \int_s D \cdot n \, da$$

$$\doteq - \frac{\partial q}{\partial t} = - Y_1 V_1 \qquad (7)$$

where $Y_1 = j\omega C_1$ and

C_1 = capacitance per unit length between the core and sheath.

It is shown by Stratton[45], that even for a conductor with a high resistance, one can write

$$2\pi a \, H_x = I_1$$

so that equation (7) becomes

$$\frac{\partial I_1}{\partial z} = Y_1 V_1 \tag{8}$$

Applying equation (3) round the surface of the sheath gives similarly

$$\frac{\partial I_2}{\partial z} = - Y_2 V_2 = j\omega C_2 V_2 \tag{9}$$

where C_1 = capacitance per unit length between the sheaths.

Assuming that all components vary as $\exp.-\Gamma z$ equations (5),(6),(8) and (9) become

$$\begin{aligned} -\Gamma V_1 + E_1 + E_2 &= - X_1 I_1 \\ -\Gamma V_2 - 2 E_3 &= X_2 I_2 \\ -\Gamma I_1 &= -Y_1 V_1 \\ -\Gamma I_2 &= - Y_2 V_2 \end{aligned} \tag{10}$$

Now substituting for E_1, E_2, and E_3 from equations (1) and elminating the currents I_1 and I_2 get the equations

$$V_1\left[\Gamma^2 - Y_1(Z_1 + Z_2 + X_1)\right] + V_2 Z_{23} Y_2 = 0$$

$$V_1 \cdot 2 Z_{23} Y_1 + V_2\left[\Gamma^2 - Y_2(2Z_3 + X_2)\right] = 0 \qquad (11)$$

In order that these two equations shall be consistent, the determinant of the coefficients must vanish, so that

$$\begin{vmatrix} \Gamma^2 - Y_1(Z_1 + Z_2 + X_1) & Z_{23} Y_2 \\ 2 Z_{23} Y_1 & \Gamma^2 - Y_2(2Z_3 + X_2) \end{vmatrix} = 0$$

which becomes

$$\Gamma^4 - \Gamma^2\left[Y_1(Z_1 + Z_2 + X_1) + Y_2(2Z_3 + X_2)\right] + Y_1 Y_2 (Z_1 + Z_2 + X_1)(2Z_3 + X_2) - 2 Z_{23}^2 Y_1 Y_2 = 0 \qquad (12)$$

It is obvious that, since the values of the surface impedances are themselves complicated functions, there is no simple solution to the equation (12), and therefore of the general problem. Fortunately, however, a simplifying assumption can be made. In the actual

problem the sheaths are bonded together at regular intervals. The structure is therefore of a periodic nature, and, for a rigorous determination of the surge impedance and the propagation constant, the methods outlined by Brillouin[49] would have to be used. However, if the distance between the bonds is very much smaller than the wavelength, then it may be assumed that the variation of current and voltage between the bonds is negligibly small. It follows that there can be no potential between the sheaths, i.e. $V_2 = 0$ Equation (10) can therefore be written

$$\begin{aligned} -\Gamma V_1 + E_2 + E_1 &= -X_1 I_1 \\ -2E_3 &= X_2 I_2 \\ -\Gamma I_1 &= -Y_1 V_1 \end{aligned} \qquad (13)$$

Substituting for E_1, E_2, and E_3 as before, and eliminating I_2 gives

$$\Gamma V_1 - \left[(Z_1 + Z_2 + X_1) - \frac{2Z_{23}^2}{2Z_3 + X_2}\right] I_1 = 0 \qquad (14)$$

$$Y_1 V_1 - \Gamma I_1 = 0$$

In order that these equations shall be consistent, the determinant of the coefficients must vanish

$$\begin{vmatrix} \Gamma & -\left[(Z_1+Z_2+X_1) - \dfrac{2Z_{23}^2}{2Z_3+X_2}\right] \\ Y_1 & -\Gamma \end{vmatrix} = 0$$

which leads to

$$\Gamma^2 = Y_1\left[(Z_1+Z_2+X_1) - \frac{2Z_{23}^2}{2Z_3+X_2}\right] \tag{15}$$

The phase velocity is therefore given by

$$v = R.P.\sqrt{\frac{j\omega}{Y_1\left[(Z_1+Z_2+X_1) - \dfrac{2Z_{23}^2}{2Z_3+X_2}\right]}} \tag{16}$$

and the surge impedance by

$$Z_c = \frac{2V}{I_1} = 2\frac{\Gamma}{Y_1} = 2\sqrt{\frac{1}{Y_1}\left[(Z_1+Z_2+X_1) - \frac{2Z_{23}^2}{2Z_3+X_2}\right]} \tag{17}$$

6.3 The Evaluation of the Surge Impedance and Wave Velocity

To evaluate the expressions given by equations (15),(16) and (17), it is necessary to determine the various impedances. These have already been given by Schelkunoff[16], and are

$$Z_1 = \frac{i\omega\mu_1}{2\pi a g_1} \frac{I_0(\sigma_1 a)}{I_1(\sigma_1 a)}$$

$$Z_2 = \frac{i\omega\mu_2}{2\pi b g_2} \frac{I_0(\sigma_2 b) K_1(\sigma_2 c) + K_0(\sigma_2 b) I_1(\sigma_2 c)}{I_1(\sigma_2 c) K_1(\sigma_2 b) - I_1(\sigma_2 b) K_1(\sigma_2 c)}$$

$$Z_3 = \frac{i\omega\mu_2}{2\pi c g_2} \frac{I_0(\sigma_2 c) K_1(\sigma_2 b) + K_0(\sigma_2 c) I_1(\sigma_2 b)}{I_1(\sigma_2 c) K_1(\sigma_2 b) - I_1(\sigma_2 b) K_1(\sigma_2 c)} \qquad (18)$$

$$Z_{23} = \frac{1}{2\pi g_2 a b \left[I_1(\sigma_2 c) K_1(\sigma_2 b) - I_1(\sigma_2 b) K_1(\sigma_2 c) \right]}$$

where I_0, K_0, I_1, and K_1 are the modified Bessel functions and

μ_1 = permeability of copper conductor

μ_2 = permeability of lead sheath

$\sigma_1 = \sqrt{j\omega\mu_1 g_1}$: $\sigma_2 = \sqrt{j\omega\mu_2 g_2}$

g_1 = conductivity of copper conductor

g_2 = conductivity of lead sheath

$$X_1 = j\omega \frac{\mu}{2\pi} \log_e \frac{b}{a} \qquad (19)$$

$$X_2 = j\omega \frac{\mu}{2\pi} \log_e \frac{p}{c}$$

In these expressions no account has been taken of the proximity effects. If the frequency is so high that the proximity effect has almost reached its ultimate value, the impedances Z_3 and X_2 can be written as

$$X_2 = j\omega \frac{\mu}{2\pi} \cosh^{-1}\left[\frac{p^2}{2c^2} - 1\right]$$

$$Z_3 = \frac{1}{2\pi c}\sqrt{\frac{j\omega\mu_2}{g_2}}\left[1 - 4\frac{p^2}{c^2}\right]^{-\frac{1}{2}} \qquad (20)$$

For a more accurate determination of the impedances X_2 and Z_3 the reader is referred to a paper by Mr. S.P. Mead[17].

These exact formulae are complicated functions, but approximations can be easily obtained when the arguments of the Bessel functions are either less than one or greater

approximately 10. These limits, for the cable considered here (Chapter 1), correspond to frequencies of the order of 5×10^2 and 10^5 c/s respectively.

The expressions for large arguments have already been tabulated by Schelkunoff, and curves showing these impedances as functions of the frequency are drawn in Figs. 23, 24 and 25. It is noted how the transfer impedance or coupling approaches zero as the frequency increases.

In the low frequency region the expressions may be expanded using the approximations for small arguments given by

$$
\begin{aligned}
I_0(u\sqrt{i}) &= 1 + j\frac{u^2}{4} \\
I_1(u\sqrt{i}) &= \frac{u}{2\sqrt{i}}\left(-\frac{u^2}{8} + i\right) \\
K_0(u\sqrt{i}) &= (0.1159 - \log_e u) - i\frac{\pi}{4} \\
K_1(u\sqrt{i}) &= \frac{1}{u\sqrt{i}} - \sqrt{i}\left[u/2 + u/2(0.1159 - \log_e u)\right]
\end{aligned}
\qquad (21)
$$

The impedances then become

$$Z_1 = \frac{1}{\pi a^2 g_1} + j\frac{\omega \mu_1}{8\pi} = R_c + j\omega L_c$$

$$Z_2 = \frac{1}{\pi g_2 (c^2 - b^2)} + j\omega \cdot \frac{\mu_2 b^2}{4\pi (c^2 - b^2)} \doteq R_s + \tfrac{1}{2} j\omega L_s \qquad (22)$$

$$Z_3 = \frac{1}{\pi g_2 (c^2 - b^2)} + j\omega \frac{\mu_2 c^2}{4\pi (c^2 - b^2)} \doteq R_s + \tfrac{1}{2} j\omega L_s$$

$$Z_{23} = \frac{1}{\pi g_2 (c^2 - b^2)} = R_s$$

where R_c = d.c. resistance of core

R_s = d.c. resistance of lead sheath

L_c = internal inductance of core

L_s = internal inductance of sheath

Asymptotic expressions can now be derived for the frequency tending to infinity and to zero.

(a) $f \longrightarrow \infty$. From Fig. 25 it is observed that as the frequency increases, $Z_{23} \longrightarrow 0$; and it can be shown that the impedances Z_1 and Z_2 become negligible with respect to X_1.

In this limit

$$\Gamma^2 \longrightarrow Y_1 X' \tag{23}$$

and

$$Z \longrightarrow 2\sqrt{\frac{X_1}{Y_1}} = 2\sqrt{\frac{L_1}{C_1}} \tag{24}$$

These expressions indicate that at high frequencies the waves are confined to the area between the sheath and the conductor.

(b) $f \longrightarrow 0$ From equations (15) and (22)

$$\Gamma^2 \longrightarrow Y_1\left[R_c + i\omega L_c + R_s + \tfrac{1}{2} i\omega L_s + X_1 - \frac{2R_s^2}{R_s + \frac{1}{2} i\omega L_s + i\omega L_2}\right] \tag{25}$$

Since $R_s >> i\omega(L_s + L_2)$ then equation (25) becomes

$$\Gamma^2 \longrightarrow Y_1\left[R_c + R_s + i\omega(L_c + \tfrac{1}{2}L_s + L_1) - R_s + i\omega(\tfrac{1}{2}L_s + L_2)\right] \tag{26}$$

$$= Y_1\left[R_c + i\omega(L_c + L_s + L_1 + L_2)\right]$$

and

$$Z \longrightarrow 2\sqrt{\frac{1}{Y_1}\left[R_c + i\omega L_T\right]} \tag{27}$$

where $$L_T = L_c + L_s + L_1 + L_2$$

This indicates that the sheath resistance no longer affects the result, implying that there is no current flow in the sheath. It is also noted that the inductance $2L_T$ equals the core to core inductance if the sheaths are neglected.

In the evaluation of the expressions (16) and (17) in the intermediate frequency region, two assumptions are made. It is assumed first of all that the proximity of the sheaths only affects the impedances X_2 and Z_3. This seems a reasonable assumption since it can be shown, from a numerical calculation, that at the higher frequencies, when the proximity effect becomes a maximum, the penetration of the field through the sheaths is small, and the effect of the external inductance becomes almost negligible.

Secondly, it is assumed that in the high frequency region, i.e. in this case for frequencies greater than 10^4 c/s, the impedances Z_3 and X_2 are given by their high frequency values, equations (20), while for the low frequencies these impedances are given by equations (18) and (19).

Curves showing the variation of surge impedance, wave velocity and attenuation are plotted in Figs. 26, 27

and 28. These all show how, as the frequency increases, the fields tend to be confined to the dielectric area (assumed lossless) between the cores and sheaths. The minimum and maximum values in the attenuation curve are due to a phase shift in the current density from the surface of the conductor

This analysis is dependent on the assumption that the distance between the bonds is very much smaller than the signal wavelength. Now for the cable described in Chapter 1, which has bonds at intervals of 300 yards, this is only valid below frequencies of approximately 5×10^4 c/s. However, since the bonds are connected to the outside of the sheaths, and it is already evident that beyond frequencies of 10^4 c/s there is little field penetration of the sheath, the assumption can be considered as valid over the whole frequency range.

6.4 A Three-Phase Cable with Individual Sheaths

A cross section of the cable is shown in Fig. 29. It is assumed that currents I_{1a}, I_{2a} and I_{3a} flow in conductors 1, 2 and 3 respectively, and that, as before, the sheath currents, denoted by I_{1c} and I_{1b} etc., flow along the inside and outside surfaces. The sheaths

are bonded together so that the previous assumption regarding the electric field is valid. Since the cable is considered to be symmetrical, the various surface impedances are equal, and so the electric intemsities at the conductor surfaces are given by

$$\begin{aligned} E_{1a} &= Z_a I_{1a} \\ E_{1b} &= Z_{bb} I_{1a} + Z_{bc} I_{1c} \\ E_{1c} &= Z_{bc} I_{1a} + Z_{cc} I_{1c} \end{aligned} \tag{28}$$

$$\begin{aligned} E_{2a} &= Z_a I_{2a} \\ E_{2b} &= Z_{bb} I_{2a} + Z_{bc} I_{2c} \\ E_{2c} &= Z_{bc} I_{2a} + Z_{cc} I_{2c} \end{aligned} \tag{29}$$

$$\begin{aligned} E_{3a} &= Z_a I_{3a} \\ E_{3b} &= Z_{bb} I_{3a} + Z_{bc} I_{3c} \\ E_{3c} &= Z_{bc} I_{3a} + Z_{cc} I_{3c} \end{aligned} \tag{30}$$

Applying Maxwell's equation (2), as before, to the region between core and sheath, and assuming that all

field components vary as $\exp -\Gamma z$ gives

$$
\begin{aligned}
-\Gamma V_1 + E_{1a} + E_{1b} &= -X_1 I_{1a} \\
-\Gamma V_2 + E_{2a} + E_{2b} &= -X_1 I_{2a} \\
-\Gamma V_3 + E_{3a} + E_{3b} &= -X_1 I_{3a}
\end{aligned}
\tag{31}
$$

where V_i is the potential between the core and sheath, and X_1 is the core to sheath reactance.

Now applying equation (3) to the region between the sheaths

$$
\begin{aligned}
-\Gamma V_{12} + E_{1c} - E_{2c} &= -\tfrac{1}{2} X_2 (I_{1c} - I_{2c}) \\
-\Gamma V_{23} + E_{2c} - E_{3c} &= -\tfrac{1}{2} X_2 (I_{2c} - I_{3c}) \\
-\Gamma V_{31} + E_{3c} - E_{1c} &= -\tfrac{1}{2} X_2 (I_{3c} - I_{1c})
\end{aligned}
\tag{32}
$$

where V_{ik} is the potential between sheaths i and k and X_2 is the sheath to sheath reactance.

Since the sheaths are bonded it can be assumed, as before, that V_{ik} is equal to zero; so that

$$E_{1c} - E_{2c} = -\tfrac{1}{2} X_2 (I_{1c} - I_{2c})$$

$$E_{2c} - E_{3c} = -\tfrac{1}{2} X_2 (I_{2c} - I_{3c}) \qquad (33)$$

$$E_{3c} - E_{1c} = -\tfrac{1}{2} X_2 (I_{3c} - I_{1c})$$

Applying the second Maxwell equation (3) to the region between the sheath and core gives

$$-\Gamma I_{1a} = Y_1 V_1$$

$$-\Gamma I_{2a} = Y_1 V_2 \qquad (34)$$

$$-\Gamma I_{3a} = Y_1 V_3$$

Eliminating the sheath currents and surface intensities from equations (33) and (34), get after some manipulation

$$\Gamma (V_1 - V_2) - Z_0 (I_1 - I_2) = 0$$

$$\Gamma (V_2 - V_3) - Z_0 (I_2 - I_3) = 0 \qquad (35)$$

$$\Gamma (V_3 - V_1) - Z_0 (I_3 - I_1) = 0$$

and

$$Y_1(V_1 - V_2) - \Gamma(I_1 - I_2) = 0$$

$$Y_1(V_2 - V_3) - \Gamma(I_2 - I_3) = 0 \qquad (36)$$

$$Y_1(V_3 - V_1) - \Gamma(I_3 - I_1) = 0$$

where

$$Z_o = Z_a + Z_{bb} + X_1 - \frac{2Z_{bc}^2}{2Z_{cc} + X_2} \qquad (37)$$

Eliminating the voltages and currents one gets

$$\Gamma^2 = Y_1 Z_o$$

which is the same as equation (15) when only two conductors were considered.

To determine the surge impedances for various faults, further conditions regarding the currents and voltages are necessary. These are shown in Table 1.

TABLE 1.

Fault	Boundary Conditions	Surge Impedance
Phase 1 to earth	$I_2 = I_3 = 0$	$\sqrt{\frac{Z_0}{Y_1}}$
Phase 1 to Phase 2.	$I_3 = 0$, $I_2 = -I_1$ $V_2 = -V_1$	$2\sqrt{\frac{Z_0}{Y_1}}$
Phase 1 opening to clear three-phase fault.	$V_2 = V_3$ $I_1 = -2I_2 = -2I_3$	$\frac{3}{2}\sqrt{\frac{Z_0}{Y_1}}$

6.5 Conclusions

This analysis indicates quite clearly how the lead sheaths limit the magnetic fields between the sheaths, and therefore the coupling between the core currents.

Since it has been shown that beyond frequencies of 10^4 c/s there is little penetration of the sheaths, it can be deduced that the fields of the steep fronted voltage surges and chopped current waves travel along the cable only in the region between the core and sheaths. This is in agreement with the results of the experimental work of Chapter 1.

The assumption made originally by Gosland[11] that, with bonds between the sheaths, the sheath to sheath circuit has only inductance and resistance, has been justified for the cable examined here. It appears that the validity of this assumption is dependent on the distance between the bonds, and the size and material of the sheaths.

It has appeared from the analysis that the inclusion of the proximity effect has only a slight influence on the parameters, the important factor being the transfer impedance between the two surfaces of the lead sheaths.

The analysis for the three-phase cable could be extended to include the effect of a metal pipe, but this would only influence the results at frequencies below about 500 c/s.

CHAPTER 7.

Wave propagation through generator windings

7.1 Introduction

Interest in the transient behaviour of generators has not been very great, mainly because it is perhaps the least vulnerable element of the power system, and also because of the complexity of the problem. All the analysis carried out, so far, has been made using circuit theory. Friedlander[37], for example, considers the winding as a chain of inductances and capacitances, representing the self and mutual inductances of conductors and their ground and mutual capacitances respectively (Fig. 57). He neglects the effects of overhangs and the coupling between remote parts of the winding, and so reduces the complexity of the equivalent circuit. Since this circuit has the characteristics of a low pass filter, only waves below a critical frequency can propagate along the winding, those of a higher frequency being attenuated exponentially.

Robinson[38,39], in two recent papers, includes in analyses the effects of close coupling between remote parts of the winding, and he shows that for a machine winding with two coil sides per slot, there will be two waves of

different velocities, the amplitudes of which reduce to zero at different critical frequencies.

The evaluation of the circuit constants has presented a considerable problem. As Robinson says in Reference (38), 'Although the capacitances can be obtained from more or less direct measurement the inductances must be estimated from oscillograms which will permit the determination of the critical frequency, the surge impedance and the wave velocity'; and again from Reference (39), 'The evaluation of the circuit constants can be carried out in a concentric conductor machine only if the assumptions that the mutual inductances are equal to the self inductances are valid. It is then possible to obtain expressions for the wave velocities and, hence, with a knowledge of the capacitances, to calculate the inductances'.

There does appear, therefore, to be some need for an investigation of the behaviour of these parameters, and since they are dependent on certain field distributions in the generator this implies an investigation of the fields using Maxwell's equations. The structure of a generator, however, is such that it is not possible to obtain a complete solution by these means, and so the problem has to be tackled by a process of analysis and synthesis. This means, first of all, determining the

various structural influences on the propagation, and investigating each one separately in as rigorous a way as possible. The contribution which each makes to the whole generator response can then be judged, leading either to a comprehensive theory from these results, or the determination of the equivalent system of capacitances and inductances.

In this chapter these various structural influences are listed, and two of them investigated rigorously.

7.2 The features of the propagation of waves through generator windings

The generator in its most general form consists of coils of copper wire inserted in slots of laminated iron, as shown in Fig. 30. By inspection, the structure is seen to exhibit periodicity in several forms.

(a) Since the conductors in a slot are joined to form the turns of a coil, the voltage and current of each conductor, at any cross-section of the slot, are related by some kind of periodic function of the turn length.

(b) The electromagnetic field travelling along the slot encounters the periodic nature of the lamination.

(c) The wave is alternately travelling along the slot, and along the overhangs.

(d) Different windings in the generator may be closely coupled at periodic intervals.

Wave propagation in periodic structures exhibits well-known characteristics, notably band pass effects, and the response of the winding will be the super-position of the characteristics of these periodic forms.

A factor which affects the transmission of waves at the lower frequencies is the dispersion of the field in the metal. This is due to its finite conductivity and this, together with its high permeability are the features necessary for the satisfactory operation of an electrical machine.

The rotor also affects the propagation of waves. Its influence will be dependent on the dimensions of the air gap, the slot width and depth.

Here only the effects of dispersion in the lamination, and its periodic nature, are examined. To reduce analytical labour, the simplest type of generator structure is assumed, the copper winding being replaced by an infinite plane parallel to the solid iron core representing one turn in a slot, with the laminations and the dielectric between, as shown in Fig. 31. The width of the laminations and insulation (here assumed to be

space) is exaggerated. It is assumed that a voltage source is connected between the copper plane and the iron core. This corresponds to the condition of a fault to earth or a lightning surge arriving at the generator.

7.3 The effects of dispersion in the iron

The longitudinal section of the theoretical structure, shown in Fig. 31, indicates the similarity between it and the corrugated waveguide, on which considerable work has been done (corrugated waveguides are designed to reduce the phase velocity of electromagnetic waves). In the analysis of the corrugated waveguide, the slots or stubs (not to be confused with the actual generator slot) are assumed to act as shorted sections of a smooth waveguide, and the field in them to be T.E.M. The field pattern in the guide itself, however, is more complicated, as shown in Fig. 32. This pattern can be expressed as the sum of a fundamental component corresponding to the field variation in a smooth waveguide, and a Fourier series representing the periodic field variations along the corrugated guide.

Since the lamination pitch p will be small compared with the fundamental wavelength, at frequencies even as high as 10^8 c/s, the phase shift per slot will be

an almost negligible quantity, and it can be assumed that the fields in adjacent slots have the same magnitude and phase.

Neglecting the losses in the metal and the dielectric, the field in the slot will be of the simplest type (T.E.M.) with components given by

$$E_z = B \sin ky \qquad H_z = H_y = E_x = E_y = 0$$

$$H_z = B \frac{j\omega\epsilon}{k} \cos ky$$

$$k = \frac{\omega}{c}$$

ϵ = permittivity of dielectric

Now with the metal of finite conductivity, it can be shown that the field in the slot remains approximately the same, and that the current density at the metal surface is related to the magnetic field at the boundary by the vector relationship

$$J = \bar{n} \times H \tag{3}$$

leading to, in this case

$$J_y = - H_x \tag{4}$$

It follows, therefore, that the variation of the current magnitude along the slot is given by

$$I \sim \cos ky \tag{5}$$

Since $k = \omega/c = 0.53 \times 10^{-9}$ f (for free space), with a slot depth of 0.1 m., the frequency would have to be greater than 10^8 c/s. before there would be any appreciable variation of current along the slot. With these assumptions it is therefore possible to compute the total current flowing in different sections of the guide.

The distribution of current in a plane conductor is given by the formula

$$J = A\epsilon^{p\xi} + B\epsilon^{-p\xi} \qquad (6)$$

$$\text{or } J = C \sinh p\xi + D \cosh p\xi \qquad (6a)$$

where $p^2 = -i\omega\mu\sigma$

ξ is the coordinate normal to the surface of the metal,

and $A, B, C,$ and D are constants determined from the boundary conditions.

Considering first the current flowing between points a and b in Fig. 33, and neglecting end effects, the current density is given by

$$J = A\epsilon^{py} \qquad (7)$$

B must be zero since J can have no value at $Y = -\infty$

If the current density at the surface is J' then

$$J = J' \epsilon^{\beta Y} \tag{7a}$$

and the total current flowing is given by

$$i_1 = \int_{-\infty}^{0} J' \epsilon^{\beta Y} dY = \frac{J'}{\beta} \tag{8}$$

This represents the total current flowing along the guide, and must equal the current flowing in the copper conductor in the opposite direction.

Now considering the current flowing in the lamination, since the current density at the opposite surfaces has the same value but different sign, the density at any point is given by the odd function

$$J = C \sinh \beta Z \tag{9}$$

and since J' is the density at the surface, i.e. at Z = a, then

$$J = \frac{J'}{\sinh \beta a} \cdot \sinh \beta Z \tag{9a}$$

This function is shown in Fig. 33.

For a more rigorous derivation of equation (9a) the reader is referred to Appendix 8.

From the equation (9a), the current flowing up the lamination can be found, and is given by

$$i_2 = \int_0^a \frac{J'}{\sinh \beta a} \cdot \sinh \beta z \, dz$$

$$= \frac{J'}{\beta \sinh \beta a} \cdot (\cosh \beta a - 1) \qquad (10)$$

$$= i_1 \cdot \frac{\cosh \beta a - 1}{\sinh \beta a} \qquad (10a)$$

It is therefore seen that the ratio of the current flowing up the lamination to the total current is a function of β and therefore of the frequency. Curves of this ratio have been drawn inserting typical values for the constants, and they are shown in Fig. 34. From these curves it is observed that, at high frequencies, there is little or no interaction between the fields penetrating from the two sides of the iron lamination, and all the current flows along the lamination, i.e. $i_2 = i_1$. As the frequency decreases, however, increasing interaction results in a reduction of the current i_2 until at zero frequency no current flows, $i_2 = 0$, and the field in the metal has the same value

at all points. It follows from this that at any intermediate frequency the current divides, one part travelling up and round the top of the lamination, the other part travelling across the bottom. Now since the width of the lamination is approximately ten times that of the insulating varnish, for the purposes of evaluating approximately the surge impedance, the system may be represented as that shown in Fig. 35, current i_2 flowing along the surface of the laminations, and i_3 along the solid iron core.

To evaluate the characteristic impedance, it is convenient to imagine the system as a three wire transmission line as shown in Fig. 36. It is assumed that the lines 2 and 3 are at the same potential. This assumption is justifiable, since the potential difference between the points b and c in Fig. 33 is the voltage drop due to the current flowing up the lamination, and this is small compared with the voltage between opposite sides of the guide.

Considering the three wire system, the voltage-current relationships are:-

$$e_1 = Z_{12} i_2 + Z_{13} i_3 \qquad (11)$$

$$0 = Z_{12} i_1 - Z_{23} i_3 \qquad (12)$$

$$0 = Z_{13} i_1 - Z_{23} i_2 \tag{13}$$

$$i_1 = i_2 + i_3 \tag{14}$$

where Z_{ik} represents the characteristic impedances between conductors i and k.

The equivalent characteristic impedance is given by

$$\begin{aligned} Z = e_1/i &= Z_{12} i_2/i_1 + Z_{13} i_3/i_1 \\ &= Z_{13} + i_2/i_1 (Z_{12} - Z_{13}) \end{aligned} \tag{15}$$

The ratio i_2/i_1 has already been evaluated, and so it remains to determine the characteristic impedances Z_{12} and Z_{13}.

7.4 The evaluation of the impedance Z_{12}

The impedance Z_{12} is the impedance for a current i_2 travelling along the surface of the lamination. It can therefore be determined by considering the propagation of electromagnetic waves between parallel planes of copper and of iron. This is shown in Fig. 37.

The analysis is carried out using Maxwell's equations.

Maxwell's equations are:

$$\nabla \times E + \frac{\partial B}{\partial t} = 0 \quad \text{I} \qquad \nabla \cdot B = 0 \quad \text{III}$$

$$\nabla \times H - \frac{\partial D}{\partial t} = J \quad \text{II} \qquad \nabla \cdot D = \rho \quad \text{IV} \tag{16}$$

It is assumed that the field components vary as $\exp j(hz - \omega t)$ and that they do not vary in the x direction, i.e. $\partial/\partial x = 0$

In a homogeneous conducting medium Maxwell's equations become

$$\nabla \times E + \mu \frac{\partial H}{\partial t} = 0 \qquad \mu \nabla \cdot H = 0$$

$$\nabla \times H - \sigma E = 0 \qquad \epsilon \nabla \cdot E = 0 \tag{17}$$

These can be expanded in cartesian coordinates.

$$\frac{\partial H_z}{\partial y} - jh H_y = \sigma E_x \tag{18}$$

$$jh H_x = \sigma E_y \tag{19}$$

$$-\frac{\partial H_x}{\partial y} = \sigma E_z \tag{20}$$

$$\frac{\partial E_z}{\partial y} - jh E_y = j\omega\mu H_x \tag{21}$$

$$jh E_x = j\omega\mu H_y \tag{22}$$

$$-\frac{\partial E_x}{\partial y} = j\omega\mu H_z \tag{23}$$

Combining equations (19), (20) and (21) get

$$\frac{\partial^2 E_z}{\partial y^2} = -(j\omega\mu\sigma - h^2) E_z$$

It can be shown that h^2 is very small compared with $j\omega\mu\sigma$ in the frequency range considered, and so

$$\frac{\partial^2 E_z}{\partial y^2} = -j\omega\mu\sigma E_z = p^2 E_z \qquad (24)$$

where

$$p^2 = -j\omega\mu\sigma \qquad (25)$$

The solution of this equation is

$$E_z = P\epsilon^{py} + Q\epsilon^{-py} \qquad (26)$$

Now from equations (19) and (21)

$$H_x = \frac{1}{j\omega\mu}\frac{\partial E_z}{\partial y} \qquad (27)$$

It follows, therefore, that

$$H_x = \frac{1}{j\omega\mu} p\cdot[P\epsilon^{py} - Q\epsilon^{-py}] \qquad (28)$$

It is convenient for the boundary conditions to determine the vertical impedance Z_y

$$Z_y = -\frac{E_z}{H_x} = -\frac{j\omega\mu}{p}\frac{P\epsilon^{py} + Q\epsilon^{-py}}{P\epsilon^{py} - Q\epsilon^{-py}} \qquad (29)$$

Since no field can exist in the copper at $Y = +\infty$ then in equation (29) $P = 0$ and so

$$Z_Y = \frac{j\omega\mu_c}{p_c} \tag{30}$$

Similarly in the iron the field cannot exist at $Y = -\infty$ and so

$$Z_Y = -\frac{j\omega\mu_I}{p_I} \tag{31}$$

where the subscripts c and I refer to the constants of the copper and iron respectively.

In a homogeneous dielectric medium ignoring losses Maxwell's equations are

$$\nabla \times E + \mu \frac{\partial H}{\partial t} = 0 \tag{32}$$

$$\nabla \times H - \epsilon \frac{\partial E}{\partial t} = 0 \tag{33}$$

$$\mu \nabla \cdot H = 0 \tag{34}$$

$$\epsilon \nabla \cdot E = P \tag{35}$$

Expanding these equations in cartesian coordinates get

$$\frac{\partial E_z}{\partial Y} - jhE_Y = j\omega\mu H_x \tag{39}$$

$$jhE_x = j\omega\mu H_Y \tag{37}$$

$$-\frac{\partial E_x}{\partial Y} = j\omega\mu H_z \tag{40}$$

$$\frac{\partial H_z}{\partial Y} - jhH_Y = -j\omega\epsilon E_x \tag{39}$$

$$jh\, H_x = -j\omega\epsilon\, E_y \tag{40}$$

$$-\frac{\partial H_x}{\partial y} = -j\omega\epsilon\, E_z \tag{41}$$

Equations (36), (40) and (41) yield

$$\frac{\partial^2 E_z}{\partial y^2} = -\lambda^2 E_z \tag{42}$$

where

$$\lambda^2 = k^2 - h^2 \tag{43}$$

and $$k^2 = \omega^2 \mu \epsilon \tag{44}$$

Equation (42) has a solution

$$E_z = A \sin \lambda y + B \cos \lambda y \tag{45}$$

and since

$$H_x = -\frac{j\omega\epsilon}{\lambda^2} \cdot \frac{\partial E_z}{\partial y}$$

$$H_x = \frac{j\omega\epsilon}{\lambda} \left[A \cos \lambda y - B \sin \lambda y\right] \tag{46}$$

so that

$$Z_y = -\frac{E_z}{H_x} = \frac{\lambda}{j\omega\epsilon} \frac{A \sin \lambda y + B \cos \lambda y}{A \cos \lambda y - B \sin \lambda y} \tag{47}$$

The boundary conditions are satisfied by equating the vertical impedances. ((45) page 532).

Thus at $y = 0$

$$-\frac{i\omega\mu_I}{\sqrt{-i\omega\mu_I\sigma_I}} = \frac{\lambda}{i\omega\epsilon}\cdot\frac{B}{A}$$

ie. $$B/A = \frac{\omega^2\mu_I\epsilon}{\lambda\sqrt{-i\omega\mu_I\sigma_I}} \qquad (48)$$

and at $y = a$

$$\frac{i\omega\mu_c}{\sqrt{-i\omega\mu_c\sigma_c}} = \frac{\lambda}{i\omega\epsilon}\cdot\frac{A\sin\lambda a + B\cos\lambda a}{A\cos\lambda a - B\sin\lambda a} \qquad (49)$$

which becomes

$$B/A = -\frac{\tan\lambda a + X}{1 - X\tan\lambda a} \qquad (50)$$

where

$$X = -\frac{\omega^2\mu_c}{\lambda\sqrt{-i\omega\mu_c\sigma_c}} \qquad (51)$$

Since it can be shown that λa will be very small, then $\tan\lambda a \simeq \lambda a$ and so

$$B/A = -\frac{\lambda a + X}{1 - X\lambda a} \qquad (52)$$

Combining equations (48) and (52) gives

$$\lambda^2 = -\frac{\epsilon}{\sqrt{2}a}\cdot\frac{\omega^2}{\sqrt{\omega}}\left[\sqrt{\frac{\mu_I}{\sigma_I}}+\sqrt{\frac{\mu_c}{\sigma_c}}\right]+j\left[\frac{\epsilon}{\sqrt{2}a}\cdot\frac{\omega^2}{\sqrt{\omega}}\cdot\left(\sqrt{\frac{\mu_I}{\sigma_I}}+\sqrt{\frac{\mu_c}{\sigma_c}}\right)-\omega^3\epsilon^2\sqrt{\frac{\mu_I\mu_c}{\sigma_I\sigma_c}}\right]$$

which can be written approximately, neglecting the last term

$$\lambda^2 = -k^2\,\frac{(1+j)}{\sqrt{2}a}\cdot\frac{1}{\sqrt{\omega}}\left[\sqrt{\frac{\mu_I}{\sigma_I}}+\sqrt{\frac{\mu_c}{\sigma_c}}\right] \qquad (54)$$

but $\lambda^2 = k^2 - h^2$

so that

$$h^2 = k^2(1+\Delta k^2) \qquad (55)$$

where

$$\Delta k^2 = \frac{1+j}{\sqrt{2}a}\left(\sqrt{\frac{\mu_I}{\sigma_I}}+\sqrt{\frac{\mu_c}{\sigma_c}}\right)\frac{1}{\sqrt{\omega}} \qquad (56)$$

The phase velocity is therefore

$$v = R.P.\ \frac{\omega}{h} \qquad (57)$$

$$= R.P.\ \frac{c}{(1+\Delta k^2)^{\frac{1}{2}}} \qquad (58)$$

where c is the velocity of light.

To obtain the surge impedance, relationships have to be derived for the current in the metal and the

voltage difference between the two planes. The magnetic field is given by

$$J = n \times H \tag{59}$$

Since current is flowing only in the Z direction then

$$J_z = H_x \tag{60}$$

Thus for a width S of the planes

$$I_z = S\, H_x = I \tag{61}$$

Now from equation (40)

$$E_y = \frac{k}{\omega \epsilon} H_x = \frac{k(1+\Delta k^2)^{\frac{1}{2}}}{\omega \epsilon} \times \frac{I}{S}$$

so that

$$V = \int_a^b E_y \, dy = \frac{k(1+\Delta k^2)^{\frac{1}{2}}}{\omega \epsilon} \frac{b-a}{S} I \tag{62}$$

and therefore the surge impedance

$$Z = \frac{V}{I} = \frac{k}{\omega \epsilon} \frac{b-a}{S} (1+\Delta k^2)^{\frac{1}{2}} = \sqrt{\frac{\mu}{\epsilon}} \cdot \frac{b-a}{S} (1+\Delta k^2)^{\frac{1}{2}} \tag{63}$$

7.5 Derivation of the impedance Z_{13}

The impedance Z_{13} is the characteristic impedance obtained when the current flows along the solid iron core, and not in the laminations. Under these conditions the laminations can be considered as an anisotropic homogeneous medium conducting only in the directions x and y. (Fig. 38.)

For the laminated iron Maxwell's equations can be written

$$\frac{\partial E_z}{\partial y} - jh E_y = j\omega\mu_2 H_x \tag{64}$$

$$jh E_x = j\omega\mu_2 H_y \tag{65}$$

$$-\frac{\partial E_x}{\partial y} = j\omega\mu_2 H_z \tag{66}$$

$$\frac{\partial H_z}{\partial y} - jh H_y = \sigma_2 E_x \tag{67}$$

$$jh H_x = \sigma_2 E_y \tag{68}$$

$$-\frac{\partial H_x}{\partial y} = -j\omega\epsilon_2 E_z \tag{69}$$

where ϵ_2 represents the equivalent permittivity of the metal and varnish.

These equations give

$$\frac{\partial^2 E_z}{\partial y^2} = -\lambda_2^2 E_z \tag{70}$$

where $$\lambda_2^2 = \omega^2 \mu_2 \epsilon_2 \tag{71}$$

Therefore

$$E_z = C \sin \lambda_2 y + D \cos \lambda_2 y \tag{72}$$

and $$H_x = \frac{\lambda_2}{i\omega\mu_2} (C \cos \lambda_2 y - D \sin \lambda_2 y) \tag{73}$$

It follows that

$$Z_y = -\frac{E_z}{H_x} = -i\sqrt{\frac{\mu_2}{\epsilon_2}} \frac{C \sin \lambda_2 y + D \cos \lambda_2 y}{C \cos \lambda_2 y - D \sin \lambda_2 y} \tag{74}$$

As before:

In the copper

$$Z_y = \frac{i\omega\mu_4}{\sqrt{-i\omega\sigma_4\mu_4}} \tag{30}$$

In the dielectric

$$Z_y = \frac{\lambda_3}{i\omega\epsilon_3} \frac{A \sin \lambda_3 y + B \cos \lambda_3 y}{A \cos \lambda_3 y - B \sin \lambda_3 y} \tag{47}$$

In the iron

$$Z_y = \frac{i\omega\mu_1}{\sqrt{-i\omega\sigma_1\mu_1}} \tag{31}$$

Since the boundary conditions are satisfied by equating the impedances Z_y, then at $y = 0$

$$-j\sqrt{\frac{\mu_2}{\epsilon_2}}\cdot\frac{D}{C}=-\frac{j\omega\mu_1}{\sqrt{-j\omega\sigma_1\mu_1}} \tag{75}$$

at $y=a$

$$-j\sqrt{\frac{\mu_2}{\epsilon_2}}\;\frac{C\sin\lambda_2 a+D\cos\lambda_2 a}{C\cos\lambda_2 a-D\sin\lambda_2 a}=\frac{\lambda_3}{j\omega\epsilon_3}\;\frac{A\sin\lambda_3 a+B\cos\lambda_3 a}{A\cos\lambda_3 a-B\sin\lambda_3 a} \tag{76}$$

and at $y=b$

$$\frac{\lambda_3}{j\omega\epsilon_3}\;\frac{A\sin\lambda_3 b+B\cos\lambda_3 b}{A\cos\lambda_3 b-B\sin\lambda_3 b}=\frac{j\omega\mu_4}{\sqrt{-j\omega\sigma_4\mu_4}} \tag{77}$$

It can be assumed that $\lambda_3\binom{a}{b}$ and $\lambda_2\binom{a}{b}$ are small so that $\tan\lambda\binom{a}{b}\simeq\lambda\binom{a}{b}$. Eliminating the constants A, B, C and D from equations (75), (76) and (77) gives

$$\lambda_3\Big[a^2\,\frac{\epsilon_2}{\epsilon_3}\sqrt{\frac{\omega\mu_1\epsilon_2}{-j\sigma_1\mu_2}}-j\omega^2\epsilon_2\sqrt{\frac{\mu_1\mu_4\epsilon_2}{\mu_2\sigma_1\sigma_4}}+ab\,\frac{\epsilon_2}{\epsilon_3}\sqrt{\frac{\omega\mu_1\epsilon_2}{-j\sigma_1\mu_2}}$$

$$+ab\sqrt{\frac{\omega\mu_1\epsilon_2}{-j\sigma_1\mu_2}}+ab\sqrt{\frac{\epsilon_2\mu_4\omega}{-j\sigma_4\mu_2}}+a^2b\,\omega\sqrt{\mu_2\epsilon_2}$$

$$+\frac{b}{\omega\epsilon_3}\sqrt{\frac{\epsilon_2}{\mu_2}}-\frac{a}{\omega\epsilon_3}\sqrt{\frac{\epsilon_2}{\mu_2}}\Big]$$

$$=-\sqrt{\frac{\omega\mu_1\epsilon_2}{-j\sigma_1\mu_2}}-jb\omega^2\epsilon_3\sqrt{\frac{\mu_1\mu_4\epsilon_2}{\sigma_1\sigma_4\mu_2}}+ja\omega^2\epsilon_2\sqrt{\frac{\mu_1\mu_4\epsilon_2}{\sigma_1\sigma_4\mu_2}}$$

$$+ j a \omega^2 \epsilon_3 \sqrt{\frac{\mu_1 \mu_4 \epsilon_2}{\sigma_1 \sigma_4 \mu_2}} - \omega \sqrt{\mu_2 \epsilon_2} \cdot a - a b \omega^3 \epsilon_3 \sqrt{\frac{\epsilon_2 \mu_2 \mu_4}{-j \omega \sigma_4}}$$

$$+ a^2 \omega^3 \epsilon_3 \sqrt{\frac{\epsilon_2 \mu_2 \mu_4}{-j \omega \sigma_4}} + \omega \sqrt{\frac{\epsilon_2 \mu_4}{-j \omega \sigma_4 \mu_2}} \qquad (78)$$

If typical values for the physical constants are inserted most of the terms are found to be negligible, and equation (78) reduces to

$$\lambda_3^2 = \omega^2 \cdot \frac{a}{b-a} \cdot \mu_2 \epsilon_3 \qquad (79)$$

and since $\lambda_3^2 = h^2 - k^2$ it follows that

$$h = k \left(1 + \frac{\mu_2}{\mu_3} \cdot \frac{a}{b-a}\right)^{\frac{1}{2}} \qquad (80)$$

To evaluate the surge impedance it is necessary to determine the voltage between the copper plane and the solid iron. This is made up of a voltage drop across the dielectric plus a drop across the laminated iron. The latter voltage can be neglected since the laminations conduct in that direction, and so the surge impedance can be expressed as before in equation (63) by

$$Z_c = \sqrt{\frac{\mu_3}{\epsilon_3}} \frac{b-a}{S} \left(1 + \Delta k^2\right)^{\frac{1}{2}}$$

where S is the width of the guide.

Therefore

$$Z_{13} = \sqrt{\frac{\mu_3}{\epsilon_3}} \cdot \frac{b-a}{s} \left(1 + \frac{\mu_2}{\mu_3} \frac{a}{b-a}\right)^{\frac{1}{2}} \qquad (81)$$

and the wave velocity

$$v = \frac{\omega}{h} = \frac{c}{\left(1 + \frac{\mu_2}{\mu_3} \cdot \frac{a}{b-a}\right)^{\frac{1}{2}}} \qquad (82)$$

7.6 The characteristic impedance of the corrugated structure

From equation (15) the characteristic impedance is

$$Z_c = Z_{13} + \frac{i_2}{i_3} (Z_{12} - Z_{13})$$

Setting $T = \frac{i_2}{i_3}$ and inserting the values for Z_{12} and Z_{13} gives

$$Z_c = \sqrt{\frac{\mu_3}{\epsilon_3}} \cdot \frac{b-a}{s} \left\{\left(1 + \frac{\mu_2}{\mu_3} \cdot \frac{a}{b-a}\right)^{\frac{1}{2}} (1-T) + T\right\} \qquad (83)$$

It follows, therefore, that the phase velocity is given by

$$v = \frac{c}{\left\{\left(1 + \frac{\mu_2}{\mu_3} \cdot \frac{a}{b-a}\right)^{\frac{1}{2}} (1-T) + T\right\}} \qquad (84)$$

Inserting typical values for the constants, the relationships between the phase velocity, the surge

impedance, and the frequency can be found. Figs. , 39 and 40 show these curves. It is observed how the wave velocity increases with the frequency approaching the velocity of light in the dielectric. It is also interesting to note the effect of the thickness of the laminations. As the thickness decreases, the rate of change of phase velocity and the surge impedance, from the low frequency values, is smaller.

7.7 The general features of wave propagation in periodic structures

Several papers have been written on this problem, notably by Brillouin[40], and Lines, Nichol, and Woodward[41]. Two theoretical methods of treatment are possible. The first analyses the fields in the corrugated guide using Maxwell's equations. The fields in the stubs or corrugations are matched at the common boundary with the field in the main guide. The second method gives a qualitative understanding of the problem from an equivalent circuit treatment.

So far the mathematical analysis using Maxwell's equations has not been completely examined under the conditions existing in the generator problem, but here, a short account will be given of the main features of the

results obtained from the equivalent circuit approach. This analysis is included in the paper by Lines, Nichol and Woodward.

The corrugated guide can be represented as a smooth line loaded periodically with an impedance equal to the input impedance of the stub. This is shown in Fig. 41.

If the phase change across one element of the structure is ϕ, and Θ is the phase change in the transmission line between the loading points, the frequency characteristic of the structure is given by

$$\cos\phi = \cos\Theta + j\frac{Z_1}{2Z_0}\sin\Theta \qquad (86)$$

where Z_1 is the load impedance,

and Z_2 is the characteristic impedance of the transmission line.

The input impedance of the stub is given by

$$Z_1 = jZ\tan\psi = +jZ\tan\frac{L}{d}\Theta \qquad (87)$$

where Z is the characteristic impedance of the stub.

Equation (86) becomes

$$\cos\phi = \cos\Theta - \tan\frac{L}{d}\Theta \cdot \sin\Theta \cdot \frac{Z}{2Z_0} \qquad (88)$$

Fig. 42 illustrates the general form of the

frequency characteristic. Since $\Theta = \pi$ corresponds, roughly, for the dimensions of a generator, to a frequency of 10^9 c/s. the part of the curve of interest is that part from $0 < \Theta < \pi$

$$\text{Since } \Theta = \frac{\omega d}{c} \quad \text{and} \quad \phi = \frac{\omega d}{v}$$

where c = velocity of light

and v = phase velocity,

it is possible to derive the relationship between the phase velocity and the frequency. This has been drawn in Fig. 43. It is seen that for small frequencies the phase velocity equals the velocity of light, and that it decreases as the frequency increases till at a frequency corresponding to $\Theta = \pi$ no further propagation can occur.

7.8 The combined characteristic

The effects of dispersion and periodicity have each been considered separately. The combined characteristic will be a superposition of these and the curve of phase velocity is shown in Fig. 44. This curve, of course, only indicates the relationship in a qualitative way.

7.9 Conclusions

This enquiry into the behaviour of a generator has resolved into the examination of several different problems. In this chapter, two of these problems have been examined in detail, namely the periodic nature of the lamination structure and the field dispersion at low frequencies. In the latter it has been shown, for the propagation of a signal between the core and the coil, how the currents flow in the lamination, and the effect on the wave velocity and surge impedance. The results from this analysis confirm the experimental results described in Chapter 1 which showed that the surge impedance of the winding, subject to a steep fronted surge, was approximately equal to the value calculated assuming the slot walls homogeneous and infinitely conducting. This is, in fact, the only definite result obtained so far, for there is yet no experimental verification of the effects of the periodicnature of the lamination, nor any confirmation of the effects of lamination thickness.

Once the study of the various factors influencing the propagation is complete, it may be possible either to develop an equivalent circuit for the whole winding, or a comprehensive theory by investigating the coupling of the various characteristics already obtained. This might possibly be done in the way outlined by Pierce.

CHAPTER 8.

Wave propagation along transformer coils

1. Low frequency behaviour

The next two chapters are devoted to an investigation of the propagation of electromagnetic waves along single layer transformer coils. In this chapter the effects of the core on the fields at low frequency are examined, and in the analysis, the coil is replaced by a sheath conducting in one direction. The following chapter is concerned with the high frequency behaviour, the core being replaced by a cylinder of infinite conductivity.

8.1 Examination of the present theories

Many investigators of the recovery voltage of systems have given experimental data on the frequency dependence of transformer inductance. Fig. 5 shows a typical curve. This phenomenon is known, in general, to be the result of eddy currents. Hammarlund[10] mentions in his thesis, 'Transient Recovery Voltage', that it is possible to account mathematically for the decrease of inductance with frequency, and he refers the reader to

a paper by Gosland and Dunne[12] for an attempt at an analytical approach to the problem.

Gosland and Dunne, in this paper, consider the transformer as part of a simple network, and show that the voltage transient will be of the form

$$V = A\left[L_2' - L_2''\left(1 - \epsilon^{-\alpha_2 t}\right)\cos 2\pi f_2 t\right] \qquad (1)$$

where L_2' and L_2'' refer to the leakage inductance of the transformers, L_2' varying with time, and L_2'' varying with frequency f_2, the natural frequency of the circuit. Then they show that L_2'' is made up of two components, a constant gap inductance, and a copper inductance which is a function of frequency. In this calculation the effects of eddy currents in the core are considered negligible.

Since the frequency dependence is due to eddy currents forcing the flux from the copper windings, it should follow that if a transformer has a large copper area, a large decrease of inductance would be expected. Hammarlund has carried out frequency dependence tests on many transformers and he states that 'this tendency cannot be said to exist with certainty, although the low tension transformer curves point at such conditions'.

It is accepted by the author that a reduction

of inductance due to the displacement of flux from the copper will occur as the frequency increases, but this should be completed by a relatively low frequency. The author does not accept the reason given by Gosland for the continued reduction of inductance beyond this low frequency, as due to flux passing through the coil in an axial direction. This flux would result from a phase difference between the currents in adjacent turns. For a frequency of 10^4 c/s the wavelength would be approximately 1.5×10^4 meters, so obviously the phase difference would be extremely small.

It is, in fact, difficult to estimate the validity of Gosland's analysis. This is because the physical nature of the phenomenon is not very clear. Gosland's approach to the problem is based on the established concepts of power analysis. In that respect, it is wrong because it attempts to extend these concepts, valid under certain conditions, into a region where the conditions are not clearly understood. In the author's opinion, before such assumptions are made regarding, as in the paper by Gosland, the paths of the flux and the effect of the iron, the true picture of the phenomenon must be established as rigorously as possible.

There have been two attempts at a rigorous

mathematical analysis of the problem of electromagnetic waves in transformer windings. The first, by Rudenberg[28], replaced the core and the earthed secondary by concentric isotropic surfaces, and considered the winding as an infinitely thin sheath conducting in one direction only. Since, in a transformer, the radial distance between the core and the coil is small, the curvature was neglected, reducing the complexity of the problem. The results obtained from this analysis showed that the velocity of waves remained constant for all frequencies, while the surge impedance, sensibly constant up to a fairly high frequency, reduced slowly to zero as the frequency increased. This paper, though by no means providing a complete solution to the problem, does show the possibilities of the fundamental approach using Maxwell's equation.

A later paper by Poritsky, Abetti and Jerrard[29] treated the problem from a similar approach, and the results of their analytical work show excellent agreement with measured data on a specially designed coil. This coil had two electrostatic shields inserted, one on each side of the coil. These were cut in a direction parallel to the coil axis to prevent eddy currents, and were assumed to represent the core and the secondary winding open

circuited. Unfortunately, they do not show any measured results from actual transformers to confirm these assumptions. Also they have treated the effect of a magnetic core by considering the iron of infinite permeability, and then make the rather vague statement that the effective permeability of the iron core (assumed in the work to be infinite) actually decreases with increasing frequency. A further point in their paper is the criticism of the assumption made by Rudenberg that the curvature could be neglected. They state, without any proof, that this assumption is incorrect. Apparently it has been based on the comparison of the relationships of the phase velocity and surge impedance. In their work they find that the phase velocity decreases as the frequency decreases, while Rudenberg finds that the velocity is constant. If they believe that the curvature produces this result they are quite wrong, because it can be shown that for an ideal case the phase velocity increases as the frequency approaches zero.

8.2 Statement of the Problem

The cross section of a typical single phase transformer is shown in Fig. 45. Since the effect of the frequency on the penetration of the field into the

copper is known in general, it will be assumed in the analysis that the winding is of infinite conductivity. Also, since here it is the effect of the laminated core which is being investigated, it is sufficient to consider the problem of a coil of infinite conductivity surrounding a laminated iron core, as shown in Fig. 46.

In the analysis the winding will be considered of infinite length. This permits a better insight into the problem, since the natural modes of propagation and the wave impedances are obtained in the easiest way.

The problem is therefore like that of a coaxial line with, of course, different boundary conditions at $r = a$ and $r = b$, Fig. 46. At $r = b$, the coil surface will be considered as a sheath conducting in one direction only, Fig. 47. This representation has been used in the reactance calculations of coils, and also in the mathematical investigation of electromagnetic wave propagation along a helix. In the latter case, it has been shown that the results obtained using the sheath model compare favourably with those obtained from the more accurate representation of the coil by a tape.

The boundary presented by the iron core is a much more difficult one to consider, and it may be helpful, at this stage, to examine the behaviour of a laminated

core in a magnetic field. Considering, at first, a stack of laminations between two parallel current sheets, Fig. 48. (The space between the laminations has been exaggerated). The time varying currents flowing in the sheets will produce a magnetic field H , which may be considered as constant at all points in the dielectric since the dimensions will be very small compared to the free space wavelength. This magnetic field, H , induces an eddy current flowing round the lamination cross section, the magnitude of which, is dependent on the penetration of the field into the metal, and therefore the frequency. The ratio of the current, which can flow at a particular frequency, to the maximum current, has previously been derived (neglecting end effects) and is given by

$$i/i_T = \frac{\cosh pa - 1}{\sinh pa} \qquad (2)$$

where i_T is the maximum current

$p = \sqrt{j\omega\mu\sigma}$ and ω = angular frequency

μ = permeability of the iron

σ = conductivity of the iron

$2a$ = thickness of lamination

Graphs of this ratio for various values of 'a' are shown in Figs. 49, 50. It is seen that the current flow is

zero at zero frequency and increases to a maximum at infinite frequency. This current flows round each lamination cross section and since the thickness of the insulation between laminations is less than 10% of the metal thickness, then as far as the fields outside the core are concerned, it may be considered as a surface current. This surface current is zero at zero frequency, and reaches a maximum value at infinite frequency. At zero frequency, therefore, the core may be considered as a homogeneous anisotropic medium; in other words, a core made up of infinitely thin laminations; while at a high frequency the core behaves like homogeneous isotropic material.

8.3 Core as an anisotropic homogeneous medium

Now considering the actual problem at low frequencies with the assumption that the core is a homogeneous anisotropic medium, it can be seen from Fig. 46, that the physical structure is going to cause considerable analytical difficulties. The geometry of the boundaries immediately suggests the use of cylindrical coordinates, while, on the other hand, the core is anisotropic in the directions x and y. Therefore, it is necessary at this stage to alter the physical set-up to permit a solution.

Since the main feature of these laminations is the prevention of current flow in the θ direction, considering the core non-conducting in the θ direction instead of the X direction will not alter this condition, Fig. 46. This situation fits the coordinate system.

The Maxwell field equations are:-

$$\nabla \times E + \frac{\partial B}{\partial t} = 0$$
$$\nabla \times H - \frac{\partial D}{\partial t} = J \qquad (3)$$

These can be expanded using cylindrical coordinates

$$\frac{1}{r}\frac{\partial E_z}{\partial \theta} - \frac{\partial E_\theta}{\partial z} = -\frac{\partial B_r}{\partial t}$$
$$\frac{\partial E_r}{\partial z} - \frac{\partial E_z}{\partial r} = -\frac{\partial B_\theta}{\partial t}$$
$$\frac{1}{r}\frac{\partial}{\partial r}(rE_\theta) - \frac{1}{r}\frac{\partial E_r}{\partial \theta} = -\frac{\partial B_z}{\partial t}$$
$$\frac{1}{r}\frac{\partial H_z}{\partial \theta} - \frac{\partial H_\theta}{\partial z} = i_r + \frac{\partial D_r}{\partial t} \qquad (4)$$
$$\frac{\partial H_r}{\partial z} - \frac{\partial H_z}{\partial r} = i_\theta + \frac{\partial D_\theta}{\partial t}$$
$$\frac{1}{r}\frac{\partial}{\partial r}(rH_\theta) - \frac{1}{r}\frac{\partial H_r}{\partial \theta} = i_z + \frac{\partial D_z}{\partial t}$$

It will be assumed in the following analysis that all field components vary as $\exp j(-hz + \omega t)$ and

that the field variation in the θ direction is zero i.e. $\partial/\partial\theta = 0$. With this last assumption the field equations (4) break up into two independent subsets.

For a homogeneous isotropic dielectric this yields

$$E_r = \frac{ik_z}{\lambda_z^2} \cdot \frac{\partial E_z}{\partial r}$$

$$H_\theta = \frac{i\omega\epsilon_z}{\lambda_z^2} \cdot \frac{\partial E_z}{\partial r} \qquad (5a)$$

$$\frac{1}{r}\frac{\partial}{\partial r}(rH_\theta) = i\omega\epsilon_z E_z$$

and

$$H_r = \frac{ik_z}{\lambda_z^2} \cdot \frac{\partial H_z}{\partial r}$$

$$E_\theta = -\frac{i\omega\mu_z}{\lambda_z^2} \cdot \frac{\partial H_z}{\partial r} \qquad (5b)$$

$$\frac{1}{r}\frac{\partial}{\partial r}(rE_\theta) = -i\omega\mu_z H_z$$

The first set gives the components of the circular magnetic field (or T.M. Mode) associated with currents travelling in the Z direction. The second set (5b) describes the circular electric field (or T.E. Mode) associated with eddy currents flowing round the conductor. In this case, because of the boundary conditions at the coil surface, both sets must necessarily be present.

Eliminating H_θ from the last equation in set (5a) gives

$$\frac{1}{r}\frac{\partial}{\partial r}\left(r\frac{\partial E_z}{\partial r}\right) = \lambda_z^2 E_z \tag{6}$$

or

$$\frac{\partial^2 E_z}{\partial r^2} + \frac{1}{r}\frac{\partial E_z}{\partial r} - \lambda_z^2 E_z = 0 \tag{7}$$

This is Bessel's equation with a solution

$$E_z = A I_o(\lambda_z r) + B K_o(\lambda_z r) \tag{8}$$

where $I_o(\lambda_z r)$ and $K_o(\lambda_z r)$ are the modified Bessel functions.

Since, in a typical power transformer, the ratio of the space between the coil and core, to the diameter, will be small, then for this space equation (6) can be written approximately

$$\frac{\partial^2 E_z}{\partial r^2} - \lambda_z^2 E_z = 0 \tag{9}$$

which has a solution

$$E_z = A\epsilon^{\lambda_z r} + B\epsilon^{-\lambda_z r} \tag{10}$$

This approximate form of equation (8) will be used in the following analysis.

The other components of the T.M. mode are

obtained from equation (5c) and are:

$$E_r = \frac{ih_z}{\lambda_z}\left[A\epsilon^{\lambda_z r} - B\epsilon^{-\lambda_z r}\right] \tag{11}$$

and

$$H_\theta = \frac{i\omega\epsilon_z}{\lambda_z}\left[A\epsilon^{\lambda_z r} - B\epsilon^{-\lambda_z r}\right] \tag{12}$$

The components of the T.E. mode are obtained in the same manner and are:

$$H_z = C\epsilon^{\lambda_z r} + D\epsilon^{-\lambda_z r} \tag{13}$$

$$H_r = \frac{ih_z}{\lambda_z}\left[C\epsilon^{\lambda_z r} - D\epsilon^{-\lambda_z r}\right] \tag{14}$$

$$E_\theta = -\frac{i\omega\mu_z}{\lambda_z}\left[C\epsilon^{\lambda_z r} - D\epsilon^{-\lambda_z r}\right] \tag{15}$$

In a similar way it is possible to write the field equations for the anisotropic core, describing the medium in terms of the various components of the permeability, permittivity and conductivity. Introducing these into equations (4) gives:-

$$\begin{aligned} ih\,E_\theta &= -i\omega\mu_r H_r \\ -ih\,E_r - \frac{\partial E_z}{\partial r} &= -i\omega\mu_\theta H_\theta \\ \frac{1}{r}\frac{\partial}{\partial r}(r E_\theta) &= -i\omega\mu_z H_z \end{aligned} \tag{16}$$

$$
\begin{aligned}
ih H_\theta &= (\sigma_r + i\omega\epsilon_r) E_r \\
-ih H_r - \frac{\partial H_z}{\partial r} &= (\sigma_\theta + i\omega\epsilon_\theta) E_\theta \\
\frac{1}{r}\frac{\partial}{\partial r}(r H_\theta) &= (\sigma_z + i\omega\epsilon_z) E_z
\end{aligned}
\tag{16}
$$

These yield for E_z the equation

$$
\frac{1}{r}\frac{\partial}{\partial r}\left(r\frac{\partial E_z}{\partial r}\right) = \frac{\sigma_z}{\sigma_r}(i\omega\mu_\theta\sigma_r + h^2) E_z \tag{17}
$$

Now, in thise case, $\sigma_z = \sigma_r$, and putting

$$
\rho^2 = i\omega\mu_\theta\sigma_r + h^2 \cong i\omega\mu_\theta\sigma_r \tag{18}
$$

equation (17) has a solution

$$
E_z = C_1 I_o(\rho r) + H K_o(\rho r) \tag{19}
$$

Since the field must be finite at $r=0$ then the second function cannot exist, so that

$$
E_z = C_1 I_o(\rho r) \tag{19a}
$$

The other components of the T.M. mode are

$$
E_r = \frac{ih}{\rho} C_1 I_1(\rho r) \quad : \quad H_\theta = \frac{\sigma_r}{\rho} C_1 I_1(\rho r) \tag{20}
$$

In a similar way, the components of the T.E. mode can be obtained

$$
\begin{aligned}
H_z &= F I_o(\xi r) \quad : \quad H_r = \frac{ih}{\xi} F I_1(\xi r) \\
E_\theta &= -\frac{i\omega\mu_r}{\xi} F I_1(\xi r)
\end{aligned}
\tag{21}
$$

where

$$\xi^2 = h^2 - \omega^2 \mu_r \epsilon_\theta \tag{22}$$

For the insertion of the boundary conditions at the core surface it is sufficient to equate the radial impedances of each mode separately. These impedances are defined as

$$Z_r^{TE} = \frac{E_\theta}{H_z} \quad ; \quad Z_r^{TM} = -\frac{E_z}{H_\theta} \tag{23}$$

Therefore, in the dielectric medium 2, these are

$$Z_{r_2}^{TE} = -\frac{i\omega\mu_2}{\lambda_2} \frac{C\epsilon^{\lambda_2 r} - D\epsilon^{-\lambda_2 r}}{C\epsilon^{\lambda_2 r} + D\epsilon^{-\lambda_2 r}} \tag{24}$$

and

$$Z_{r_2}^{TM} = -\frac{\lambda_2}{i\omega\epsilon_2} \frac{A\epsilon^{\lambda_2 r} + B\epsilon^{-\lambda_2 r}}{A\epsilon^{\lambda_2 r} - B\epsilon^{-\lambda_2 r}} \tag{25}$$

In the core

$$Z_{r_1}^{TM} = -\frac{\rho}{\sigma_r} \frac{I_0(\rho r)}{I_1(\rho r)} \tag{26}$$

$$Z_{r_1}^{TE} = -\frac{i\omega\mu_r}{\xi} \frac{I_1(\xi r)}{I_0(\xi r)} \tag{27}$$

Writing

$$Z^{TM} = \frac{\lambda_2}{i\omega\epsilon_2} \tag{28}$$

and

$$Z^{TE} = \frac{i\omega\mu_2}{\lambda_2} \tag{29}$$

then from equations (24), (25) (27)

$$D = M \cdot C \, \epsilon^{2\lambda_2 a} \tag{30}$$

and $$B = -P A \cdot \epsilon^{2\lambda_2 a} \tag{31}$$

where

$$M = \frac{Z^{TE} - Z_{r_1}^{TE}}{Z^{TE} + Z_{r_1}^{TE}} \tag{32}$$

and

$$P = \frac{Z^{TM} - Z_{r_1}^{TM}}{Z^{TM} + Z_{r_1}^{TM}} \tag{33}$$

Since it is assumed the sheath is of infinite conductivity in the direction given by the angle ψ, Fig. 47, and that the current flows only in that direction then

$$E_z \sin\psi + E_\theta \cos\phi = 0 \tag{34}$$

and
$$H_z \sin\psi + H_\theta \cos\psi = 0 \tag{35}$$

where ψ is the angle of the helix. Substituting for the field components gives

$$\frac{E_z}{E_\theta} = -\cot\psi = \frac{\lambda_2}{i\omega\mu_2} \frac{A\epsilon^{\lambda_2 b} + B\epsilon^{-\lambda_2 b}}{C\epsilon^{\lambda_2 b} - D\epsilon^{-\lambda_2 b}} \tag{36}$$

and

$$\frac{H_z}{H_\theta} = -\cot\psi = \frac{\lambda_2}{j\omega\epsilon_2}\,\frac{C\epsilon^{\lambda_2 b} + D\epsilon^{-\lambda_2 b}}{A\epsilon^{\lambda_2 b} - B\epsilon^{-\lambda_2 b}} \qquad (37)$$

Eliminating $A, B, C,$ and D from the equations (30), (31), (36) and (37) gives:

$$\left(\frac{\cot\psi\, k}{\lambda_2}\right)^2 = \frac{\epsilon^{\lambda_2 b} + M\epsilon^{2\lambda_2 a}\epsilon^{-\lambda_2 b}}{\epsilon^{\lambda_2 b} - M\epsilon^{2\lambda_2 a}\epsilon^{-\lambda_2 b}} \cdot \frac{\epsilon^{\lambda_2 b} - P\epsilon^{2\lambda_2 a}\epsilon^{-\lambda_2 b}}{\epsilon^{\lambda_2 b} + P\epsilon^{2\lambda_2 a}\epsilon^{-\lambda_2 b}} \qquad (38)$$

Writing $b-a = d$ this becomes

$$\left(\frac{\cot\psi\, k}{\lambda_2}\right)^2 = \frac{\epsilon^{\lambda_2 d} + M\epsilon^{-\lambda_2 d}}{\epsilon^{\lambda_2 d} - M\epsilon^{-\lambda_2 d}}\,\frac{\epsilon^{\lambda_2 d} - P\epsilon^{-\lambda_2 d}}{\epsilon^{\lambda_2 d} + P\epsilon^{-\lambda_2 d}} \qquad (39)$$

If the values for M and P are inserted, equation (39) can be written:

$$\cot^2\psi = -Z^{TM}\cdot\frac{Z^{TM}\sinh\lambda_2 d + Z_{r_1}^{TM}\cosh\lambda_2 d}{Z^{TM}\cosh\lambda_2 d + Z_{r_1}^{TM}\sinh\lambda_2 d}$$

$$\times\frac{1}{Z^{TE}}\,\frac{Z^{TE}\cosh\lambda_2 d + Z_{r_1}^{TE}\sinh\lambda_2 d}{Z^{TE}\sinh\lambda_2 d + Z_{r_1}^{TE}\cosh\lambda_2 d} \qquad (39a)$$

$$= -\frac{Z_{in}^{TM}}{Z_{in}^{TE}}$$

The terms Z_{in}^{TM} and Z_{in}^{TE} correspond to the input impedance of, in this case, a radial transmission line, when the radial impedances at the core surface act as load impedances.

Inserting typical values for the conductivity and permeability of the iron and dielectric in equations (26) and (28), it can be shown that

$$Z_{r_1}^{TM} \ll Z^{TM}$$

Equation (39a) can therefore be written

$$\left(\frac{\cot\psi\, k}{\lambda_2}\right)^2 = \tanh \lambda_2 d \cdot \frac{\cosh \lambda_2 d + \frac{\mu_r}{\mu_2}\frac{I_1(\xi a)}{I_0(\xi a)} \sinh \lambda_2 d}{\sinh \lambda_2 d + \frac{\mu_r}{\mu_2}\frac{I_1(\xi a)}{I_0(\xi a)} \cosh \lambda_2 d} \qquad (40)$$

When the arguments of the Bessel and hyperbolic functions are large, then

$$\frac{I_1(\xi a)}{I_0(\xi a)} \longrightarrow 1 \quad , \quad \cosh \lambda_2 d \simeq \sinh \lambda_2 d$$

and equation (40) becomes

$$\left(\frac{\cot\psi\, k}{h}\right)^2 = 1 \qquad (41)$$

When the arguments are small

$$\frac{I_1(\xi a)}{I_0(\xi a)} \simeq \frac{1}{2}\xi a \simeq \frac{1}{2} h a$$

$$\sinh \lambda d \simeq hd$$

$$\cosh \lambda d \simeq 1$$

and equation (40) becomes

$$\left(\frac{\cot \psi\, k}{h}\right)^2 = hd \cdot \frac{1 + \frac{\mu_r}{\mu_2} \frac{1}{2} a d h^2}{d + \frac{\mu_r}{\mu_2} \cdot \frac{1}{2} a} \qquad (42)$$

Fig. 51 shows the form of the complete relationship between h and k, and Fig. 52 the form of the relative phase velocity $v/c = \frac{h}{k}$. The effect of varying d, the distance between the coil and core, is also shown.

8.4 Core with laminations of finite thickness

Considering now the core made up of laminations of finite thickness, the surface it presents is periodic, being alternatively iron and insulation. Since the length of one period is very much smaller than the wavelength the core can still be considered as a homogeneous medium. The effect of the lamination thickness will be implicit in the relationship for the radial impedance of the core.

The behaviour of a stack of laminations in a magnetic field has already been examined. It was shown how eddy currents were produced in these laminations, and that, as far as the magnetic field in the dielectric was concerned, these currents could be assumed to flow along

the surface. The same phenomenon occurs in the core of a transformer. These surface currents circulating around the core produce a magnetic field in the core opposing that due to the current in the coil.

The magnitude of this magnetic field is obtained from the relationship

$$H = n \times J$$

and equation (2), and is

$$\frac{H_z}{H_{z_T}} = \frac{\cosh pa - 1}{\sinh pa} \qquad (43)$$

To include the effect of this varying magnetic field in a relationship for the radial impedance of the core, it is helpful to consider the analogy of this problem with the transmission line. In this case, the field component H_z corresponds to the current, E_Θ to the voltage, Z^{TE} to the characteristic impedance of the line, Z_c, and $Z_{r_1}^{TE}$ to the load impedance, Z_L. It is required to find, in this analogy, the load impedance when the load current is known as a fraction of the load current with the end short circuited.

From transmission line theory, the current at the load end

$$I_r = \frac{V_s}{Z_c \sinh \gamma \ell + Z_L \cosh \gamma \ell}$$

where ℓ is the line length,

γ is the propagation constant,

and V_s is sending end voltage.

So that,

$$Z_L = \frac{1}{\cosh \gamma \ell} \left[V_s / I_R - Z_c \sinh \gamma \ell \right]$$

Now when $Z_L = 0$

$$I_R = \frac{V_s}{Z_o \sinh \gamma \ell} = I_{RT}$$

so that $V_s = I_{RT} Z_o \sinh \gamma \ell$

and therefore

$$Z_r = Z_c \tanh \gamma \ell \left[\frac{I_{RT}}{I_R} - 1 \right] \qquad (44)$$

The corresponding relationship for the radial impedance of the core is

$$Z_{r_2}^{TE} = Z^{TE} \tanh \lambda_2 d \left[\frac{H_{ZT}}{H_Z} - 1 \right]$$
$$= Z^{TE} \tanh \lambda_2 d \left[\frac{1}{T} - 1 \right] \qquad (45)$$

where

$$T = \frac{H_Z}{H_{ZT}}$$

So far, no account has been taken of the original impedance, $Z_{r_1}^{TE}$, presented by the core when it was assumed that no circulating current could flow.

These impedances, $Z_{r_1}^{TE}$ and $Z_{r_2}^{TE}$ may be considered as acting in parallel, so that the total impedance presented by the core surface will be

$$Z_r^{TE} = \frac{Z_{r_1}^{TE} \times Z_{r_2}^{TE}}{Z_{r_1}^{TE} + Z_{r_2}^{TE}} \qquad (46)$$

Substituting equations (27) - (29), (45) and (46) in equation (39a), gives after some rearrangement

$$\left(\frac{\cot\psi\, k}{\lambda_2}\right)^2 = \frac{\mu_0 \frac{I_1(\xi a)}{I_0(\xi a)} \left[T + (1-T)\tanh^2\lambda d\right] + \tanh\lambda d \cdot (1-T)}{\mu_0 \frac{I_1(\xi a)}{I_0(\xi a)} + \tanh\lambda d \cdot (1-T)} \qquad (47)$$

This equation cannot be solved rigorously for k, but it is possible to obtain approximate solutions valid for the dimensions of the average power transformer. From Fig. 49, it is seen that beyond about 10^6 c/s $T \sim 1$ so that equation (47) becomes

$$\left(\frac{\cot\psi\, k}{\lambda_2}\right)^2 = 1 \qquad (48)$$

which is the same as equation (41) and reduces to the result

$$v_r = v/c = \tan\psi$$

the result found by Rudenberg.

Below frequencies of about 10^6 c/s the arguments

of the Bessel and hyperbolic functions are small, and equation (47) reduces to the quadratic in h^2

$$h^4\left[\mu_0 \tfrac{1}{2} a d(1-T)\right] + h^2\left[d(1-T) + \mu \tfrac{1}{2} a T\right] - \cot^2\psi\, k^2\left[d(1-T) + \mu \tfrac{1}{2} a\right] = 0 \qquad (49)$$

This equation is of the form

$$a x^2 + b x + c = 0 \qquad (50)$$

and normally the solution is taken as

$$x = -\frac{b}{2a} \pm \frac{1}{2a}\sqrt{b^2 - 4ac} \qquad (51)$$

However, since as ω tends to infinity $(1-T)$ tends to zero, the coefficient of the term x^2 is approaching zero, the above solution is not valid. Dividing equation (50) by C, instead of by a, and completing the square, the following solution is obtained which is valid for a tending to zero.

$$x = \frac{-2c}{b \pm \sqrt{b^2 - 4ac}} \qquad (52)$$

The solution of equation (49) is therefore given by

$$h^2 = \frac{2\cot^2\psi\, k^2\left[d(1-T) + \mu \tfrac{1}{2} a\right]}{\left[d(1-T) + \mu \tfrac{1}{2} a T\right] \pm \sqrt{\left[d(1-T) + \mu \tfrac{1}{2} a\right]^2 + 4\cot^2\psi\, k^2\left[d(1-T) + \mu_r \tfrac{1}{2} a\right]\left[\mu \tfrac{1}{2} a d(1-T)\right]}}$$

It can be shown that the second term under the square root is negligibly small so that

$$h^2 = \infty \quad , \quad \frac{\cot^2\psi\, k^2 \left[d(1-T) + \mu \tfrac{1}{2} a\right]}{d(1-T) + \mu \tfrac{1}{2} a T}$$

The first solution is trivial so that

$$h = \pm \cot\psi\, k \cdot \sqrt{\frac{d(1-T) + \mu \tfrac{1}{2} a}{d(1-T) + \mu \tfrac{1}{2} a T}} \qquad (53)$$

Since for a transformer $d \ll \mu a$ equation (53) becomes

$$h = \pm \cot\psi\, k \sqrt{\frac{1}{\frac{2d}{\mu a} + T}} \qquad (54)$$

It follows, therefore, that the relative phase velocity

$$v_r = \text{R. P. } \tan\psi \sqrt{\frac{2d}{\mu a} + T} \qquad (55)$$

To evaluate the surge impedance it is necessary to find the expressions for the voltage and current in the windings. The line integral of the electric field between the coil and the core gives the voltage V at the point considered.

Thus

$$V = \int_a^b E_r \, dr \tag{67}$$

$$= \frac{ik}{\lambda_2} A \int_a^b \left[\epsilon^{\lambda_2 r} + \epsilon^{2\lambda_2 a} \epsilon^{-\lambda_2 a} \right] dr$$

using equations (11) and 31)

$$\text{so} \quad V = \frac{ik}{\lambda_2^2} A \cdot \epsilon^{\lambda_2 a} \cdot 2 \cdot \sinh \lambda_2 d \tag{68}$$

From the boundary condition

$$H = n \times J$$

where J is a surface current, the component of the current flowing in the x direction

$$J_x = H_z \tag{69}$$

J_x is related to the actual current I flowing in the turns by

$$J_x = J \cos\psi = n I \cos\psi \tag{70}$$

where n is the number of turns per unit length of the coil.

So at $r = b$

$$I = \frac{H_z}{n\cos\psi} = \frac{1}{n\cos\psi} C\left[\epsilon^{\lambda_2 b} + M\epsilon^{2\lambda_2 a}\epsilon^{-\lambda_2 b}\right] \quad (71)$$

using equations (30) and (13)

Therefore the surge impedance is given by

$$Z_c = \frac{V}{I} = n\cos\psi \; \frac{ih}{\lambda_2^2} \cdot \frac{2\sinh\lambda_2 d}{\epsilon^{\lambda_2 d} + M\epsilon^{-\lambda_2 d}} \cdot \frac{A}{C} \quad (72)$$

To obtain the ratio A/C is necessary to use equation (36), substituting the values for B and D given by equations (30) and (31), and putting $P = 1$; so

$$\frac{A}{C} = -\frac{i\omega\mu_2\cot\psi}{\lambda_2} \cdot \frac{\epsilon^{\lambda_2 d} - M\epsilon^{-\lambda_2 d}}{\epsilon^{\lambda_2 d} - \epsilon^{-\lambda_2 d}}$$

Therefore

$$Z_c = -n\cos\psi \cdot \frac{ih}{\lambda_2^3} \cdot i\omega\mu_2\cot\psi \cdot \frac{\epsilon^{\lambda_2 d} - M\epsilon^{-\lambda_2 d}}{\epsilon^{\lambda_2 d} + M\epsilon^{-\lambda_2 d}} \quad (73)$$

which, on substitution for M and h from equations (32) and (53), becomes

$$Z_c = n\frac{h}{\lambda_2^3}\omega\mu_2\cot\psi \tanh\lambda d \cdot \frac{\mu\frac{I_1(\xi a)}{I_0(\xi a)} + \tanh\lambda_2 d\,(1-T)}{\mu\frac{I_1(\xi_1 a)}{I_0(\xi_1 a)} \cdot T + \tanh\lambda_1 d\,(1-T)}$$

(74)

For high frequencies when $T \rightarrow 1$

$$Z_c \rightarrow n\sqrt{\frac{\mu_2}{\epsilon_2}} \cdot \frac{\tanh \lambda_2 d}{\lambda_2} \qquad (75)$$

corresponding to equation (38) in Rudenberg's paper.

For frequencies below about 10^6 c/s, and making the same approximations as before

$$Z_c = n\sqrt{\frac{\mu_2}{\epsilon_2}} \cdot d \cdot \sqrt{\frac{d(1-T) + \mu \cdot \frac{1}{2}a}{d(1-T) + \mu \frac{1}{2} a T}}$$

$$\simeq n.d.\sqrt{\frac{\mu_2}{\epsilon_2}} \cdot \frac{1}{\sqrt{T + \frac{2d}{\mu a}}} \qquad (76)$$

It is useful to derive rigorous expressions for the self inductance ℓ and capacitance C of the coil. The wave velocity and surge impedance may be defined as

$$v = \frac{1}{\sqrt{\ell c}} \quad , \quad Z = \sqrt{\frac{\ell}{c}}$$

and so

$$\ell = \frac{Z}{v} \quad , \quad c = \frac{1}{Z v}$$

In the frequency range $0 < f < 10^6$ c/s

$$\ell = R.P. \frac{\mu_2 n d}{\tan \psi \left[T + \frac{2d}{\mu a}\right]} \qquad (77)$$

$$C = \frac{\epsilon_2}{n d \tan \psi}. \qquad (78)$$

Figure 53 shows the variation of phase velocity with the frequency. This is due to the dispersion of the field in the metal, an effect which decreases as the frequency increases, till at frequencies beyond 10^6 c/s, in this case, the field is confined to the dielectric, and the waves travel along the wires with the velocity of light. The velocity at zero frequency is given from equation (55) by $v_r = \tan\psi\sqrt{\frac{2d\mu_2}{\mu_r a}}$, and this for a transformer core is of the order of $2.5 \times 10^{-3} \times \tan\psi$.

In Fig. 54 the variation of attenuation with frequency is shown. It is seen that, for each lamination considered, the attenuation reaches a maximum at a particular frequency. This is due to the change of phase of the current density at different distances, in the lamination, from the surface.

Figs. 55 and 56 show the change of surge impedance and inductance. The effects of dispersion are again clearly shown.

8.5 Conclusions

This analysis does indicate how the laminations affect the current flow in the core of a transformer, and how this influences the zero sequence inductance. Currents in a homogeneous isotropic metal core would tend

to flow round the core in the same helical direction as in the coil (different sign, of course). With a laminated core, however, the magnitude of the component of that current in the θ direction, Fig. 46, is determined by the lamination thickness, conductivity, and permeability, no current being able to flow at zero frequency, and the maximum current at infinite frequency. This varying constraint on the angular core current, and its field, produces the variation of inductance shown in Fig. 56.

It will be necessary to obtain experimental confirmation of the results obtained, e.g. the effect of lamination thickness, and justification for the alteration of the theoretical core made to facilitate the analysis.

It does appear that for frequencies beyond about 10^4 c/s the laminated core can be considered as a homogeneous isotropic metal, so that in the examination of the high frequency behaviour of the transformer, the core may be considered as a homogeneous medium of infinite conductivity.

A determination of the effect of the laminated core on the positive sequence inductance will be of great value. This could be found rigorously from the analysis derived here by considering a finite coil with a source

connected between the two ends. An approximate solution might be found by stating from the start that since no current I_z can flow in the core, there can be no component H_θ at the core surface.

Further theoretical work could also be carried out to include the effects of coils of finite thickness and conductivity and the metal tanks.

CHAPTER 9.

Wave propagation along transformer coils

2. High frequency behaviour

9.1 Introduction

The first transformers put into commission were designed according to the requirements of power operation. However, faults in the windings produced by surges forced an investigation of the transient behaviour of windings, and, as a result, the design requirements for such operation have become an important consideration.

The understanding of this phenomenon, described in terms of the circuit parameters, is generally considered to be almost complete (e.g. the capacitive initial distribution for a winding subject to a rectangular wave is accepted as correct). The author will attempt to show that the basis of the assumptions made is not very sound, and that a reinvestigation of the whole phenomenon would be valuable.

The problem is then tackled in three different ways, first using the circuit equations and making no assumptions regarding the limitations of the coupling,

and then using integral equations to include the effects of retardation. Although both of these analyses are incomplete, it is found that they contain an arbitrary factor which can only be resolved by a consideration of the source. For this purpose, the problem is then tackled using Maxwell's field equations, considering the winding as a sheath conducting in only one direction and the core as an infinitely conducting cylinder. Although the work on this last section is not complete, the general result obtained indicates the presence of a fast wave, which may account for the well-known instantaneous voltage distribution along coils.

9.2 Development and discussion of the present theories of wave propagation

In the original attempts to visualise and determine the transient phenomena in transformers, the winding was considered as differing little from a smooth transmission line with self-inductance and capacitance. This conception of a winding did not explain why surges caused the breakdown of windings within the first few turns, and so about 1914 various theoretical investigations were carried out and several papers published in Germany and America. The theories propounded then have formed

the basis of all further work on this problem. As Weed[18] said in his paper in 1915:

"These questions have been the subject of special investigations, with the result that a new epoch in transformer design has been initiated based on a better knowledge of the physics involved."

In this original work, the transformer was considered as a network of lumped inductances and capacitances, Fig. 57, and Wagner[19] was the first to show that the response of the network to a steep fronted surge could be divided into three periods:

(a) an initial period when the voltage distribution would be determined by the capacitive network,
(b) a transient period, and
(c) a final period when the voltage would be determined by the inductance distribution.

The transient period is the transition from the initial to the final, and takes the form of damped oscillations. These can be expressed by a Fourier series, thus giving the solution the name 'Standing Wave Theory'. It has been developed by Bewley[20] and Makin[21], using the Duhamel integral, to find the response to different types of wave, and by many other investigators to tackle more complicated windings.

A later theory developed by Rudenberg[22], called the 'Travelling Wave Theory', considers first of all, an infinite winding with an equivalent circuit as Fig. 57. The voltage and current distribution is obtained from the solution of two partial differential equations, and is in the form of travelling waves for frequencies below, and an exponential distribution for frequencies above, a critical frequency. The response of a finite winding is obtained by considering the reflections from the termination as in transmission line theory.

A comparison of the two theories will be given later. For the moment, it will be interesting to consider briefly the development of the theories and the difficulties which appeared.

The original theories published in 1914 were not supported by any detailed experimental evidence, for it was not until the 1920's that cathode ray tube techniques were developed. These investigations merely sought to explain why a transformer winding should tend to break down within the first few turns, and on that basis, the theories produced were quite adequate.

With the development of the cathode ray oscillograph, investigators were induced to attempt more comprehensive analyses, and it was natural that these should

develop from the original work. However, they soon found difficulty in interpreting the various parameters of the circuit in terms of the actual structure and, as a result, various slightly divergent theories have been produced. (For an account of these different theories the reader is referred to a paper by Pirenne[23] who examines the approximations involved in each, and shows how they are all derived from a single comprehensive theory.)

The first assumption that is made and accepted by all investigators is that the voltage distribution at high frequencies is determined by a capacitive circuit. The evidence for such a conclusion is not direct, for there is no published account of any high frequency measurement of transformer impedance. It has been deduced from the oscillographic evidence of an instantaneous distribution of voltage along a winding, subject to steep fronted surge. Now it is possible to explain this distribution as the result of a fast attenuated wave, and this would be a physically possible solution. Of course, it can be argued that the instantaneous distribution produced by the capacitive circuit is merely an approximation of the fast wave, but before such a representation can be accepted implicitly, it is necessary to have more knowledge of the limits in which it is valid.

Another difficulty is in the meaning of the inductance of the coil. This is due to the fact that the inductance value is, in one sense, dependent on a knowledge of the current distribution along the winding. Since this presupposes, at least, a knowledge of the form of the solution, the difficulties are obvious.

In the same connection, the assumptions regarding the paths of the transient flux are numerous. For example, Fruhauf[24] and Pirenne[23] think that the core flux common to all turns, is important; Blume, Boyajian[25], and Bewley[20], consider the transverse flux between elements of the winding to be of primary importance; while Rudenberg[22] emphasizes the axial flux.

The extent of the coupling between turns or coils is another aspect of the same problem about which there appears to have been no rigorous investigation. In all the theories developed so far, the capacitance network is made up of capacitances between turns or coils and earth, and between adjacent turns or coils. The coupling between a turn and turns beyond the adjacent, is neglected. On the other hand, the equivalent inductance is not represented simply as an interturn inductance, but is given usually as some function of the total leakage inductance of the winding, and includes the effects of

inductive coupling between one turn and all other turns. To limit the capacitive coupling to adjacent turns, but to consider inductive coupling between many turns, is a considerable assumption to make without adequate proof. The basis of this is probably the conception of the core as a medium of infinite permeability.

The fundamentals of the two theories, 'The Standing Wave Theory' and 'The Travelling Wave Theory', have already been described breifly. In a recent book, 'Transformer Engineering', Blume and Boyajian criticised severely the 'Travelling Wave Theory' of Rudenberg, on the basis that "experiment does not exhibit a rectangular wave front progressively advancing along the winding turns". This is a strange statement for, in fact, there has been considerable evidence obtained for nearly rectangular wavefronts, e.g. Makin's thesis[21]. This view of the problem is probably based on their conception of the whole transformer winding as a connection of lumped capacitances and inductances. It forgets the physical nature of wave propagation and the structure of a coil which, in fact, lends itself to a travelling wave approach. The two theories are actually equivalent from a mathematical point of view, for the standing wave solution is a particular solution of the more general travelling

wave solution, taking in account some further boundary condition, in this case, the impedance at the end of the winding. The reason for the divergence of the theories is partly due to the simplification and approximations that are made. The standing wave solution, although in its original form, not as rigorous in its derivation, does lend itself to a more reliable approximate solution. This is because approximations are made by considering only a finite number of terms of an infinite series. In other words, the approximation is an arithmetical or mathematical one, whose reliability is accurately known. On the other hand, in the travelling wave solution some physical condition may be assumed such as, that the coil length does not affect the initial distribution of voltage. This is not an assumption which can be relied upon since the conditions may vary from coil to coil, and over the frequency range. For a rigorous approach of this problem, the reader is referred to Makin's thesis.

In Makin's thesis there is also some criticism of Rudenberg's work. First he criticises him for neglecting the effect of the core on the lower frequencies, 'an inadmissible approximation'. In the thesis Makin considers that for frequencies less than 5 Kc/s the core produces a linear distribution of voltage. He does not

indicate how this frequency is decided, and it appears that in his calculations of the voltage response of the coil to surges, this effect has been neglected. Then he writes that Rudenberg 'mixes the standing wave and travelling wave solutions because the standing wave method only accepts very definite frequencies, whereas the travelling wave method accepts all frequencies'. No matter what type of solution is used, the transformer must accept and react to all frequency components of a wave.

Another of Makin's criticisms shows the confusion which can exist when an equivalent circuit approach is used. Makin is suggesting that the travelling wave solution may be valid but points out that, from a physical point of view, a wave travelling along the winding should have a finite velocity. Rudenberg showed that when a rectangular wave was applied to a coil, there was an instantaneous distribution of voltage along it. According to Makin this violates the physical condition mentioned above, but, of course, the use of an equivalent circuit of lumped elements representing, for example, the coupling between turns implies that the time for a signal to travel from one turn to the other though the capacitance, is negligible. A lumped circuit representation will only be valid if that condition is fulfilled.

9.3 Wave propagation along a coil using Kirchoff's equations

At first the general problem of a coil of n turns with interaction between all turns, will be considered. It is assumed that both the core and the coil are of infinite conductivity.

If one considers the voltages and currents on the conductors at points cut by a line parallel to the coil axis, Fig. 58, then the similarity between this problem and that of a multiconductor line over an earth plane is obvious. One can therefore write down the voltage current relationships of all conductors

$$-\frac{\partial}{\partial x}(e) = [L]\frac{\partial}{\partial t}(i) \qquad (1)$$

$$-\frac{\partial}{\partial x}(i) = [C]\frac{\partial}{\partial t}(e) \qquad (2)$$

where (e) and (i) are column matrices for the voltages and currents on all the conductors, and where $[L]$ and $[C]$ are square symmetrical matrices of rank n of the inductance and capacitance coefficients respectively. Now the inductance and capacitance matrices are related to Maxwell's coefficients by the equations

$$[L] = \frac{1}{U_c^2}[P] \qquad (3)$$

$$\text{and} \qquad [C] = [\not{p}]^{-1} \tag{4}$$

where U_c is the velocity of light in the dielectric. Substituting for $[L]$ and $[C]$ in equations (1) and (2), and eliminating the column matrix (i) gives

$$\frac{\partial^2}{\partial x^2}(e) = \frac{1}{U_c^2}[u]\,\frac{\partial^2}{\partial t^2}(e) \tag{5}$$

where $[u]$ is the unit matrix.

If the voltages vary as $\epsilon^{i\omega t}$ then the solution of equation (5) can be written

$$(e) = \left[A\,\epsilon^{i\frac{\omega}{U_c}x} + B\,\epsilon^{-i\frac{\omega}{U_c}x}\right]\epsilon^{i\omega t} \tag{6}$$

This solution indicates that the voltage wave travels along the wires with the velocity of light, and also that this velocity is independent of any condition imposed upon the values of the voltages on adjacent conductors.

In the above relationships there has been no indication of the periodic nature of the structure. This is shown best if the coil is split along the line parallel to the axis, and the core considered as a plane. Since the electromagnetic state must be the same at both edges of the coil, the representation may be repeated in both

directions. In this way the entire η, ξ plane in Fig. 59 is covered with a lattice of spaced conductors. It has already been shown that waves in the direction x along the conductors travel with the velocity of light, so that the wavelength of a sinusoidal signal in that direction must always be related to the frequency by the equation $\lambda = {}^{v_c}/_{f}$ However, because of the periodic nature of the structure there is some ambiguity concerning the wavelength in the direction η, and hence the velocity of propagation along the coil.

The physical meaning of the ambiguity in the wave length may be seen from Fig. 60. The crosses give the voltage at points on the conductors, say along the line $\xi = 0$. Through these positions, three possible sine waves have been drawn, and all three waves give equally good descriptions of the wave motion, as far as the voltages at these points are concerned. The solid line gives the fundamental and represents a wave travelling in the direction η with a phase velocity equal to $c \tan \varphi$, where c is the velocity of light in the x direction, and φ is the angle of the coil, Fig. 59. It has, therefore, a wave number given by

$$h_0 = \frac{\omega}{c \tan \varphi} \qquad (7)$$

The dashed curve, on the other hand, corresponds to a wave number of $h_0 + \frac{2\pi}{d}$ and the dotted curve to $h_0 - \frac{2\pi}{d}$ where d is the circumference of the coil. It is obvious that the solid and dashed curves must propagate in the same direction, while the dotted curve propagates in the opposite direction. There is, in fact, no restriction to the possible number of sine waves which can pass through these points and, in general, the wave number for propagation in the η direction is

$$h_m = h_0 + \frac{2m\pi}{d} \qquad (8)$$

A plot of h_m against frequency given by $h_0 = \frac{\omega}{c \tan\psi}$ for different values of m is shown in Fig. 61. It is noticed how for any value of m the phase velocity k/h can change from $-\infty$ to $+\infty$ while the group velocity, given by the slope of the lines remains either $\pm \omega/c \tan\psi$

The solution for the voltage distribution in the η direction will therefore be of the form

$$e(\eta) = \sum_{m=-\infty}^{+\infty} \left[A(m) \epsilon^{-ih_0\eta} + B(m) \epsilon^{+ih_0\eta} \right] \epsilon^{i\left(\frac{2m\pi}{d}\eta + \omega t\right)}$$

so that for a complete solution it will be necessary to take into account the source and the type of signal it generates.

9.4 Wave propagation along coils using the complete circuit equations

So far, no account has been taken of the finite velocity of wave propagation between turns. It has been implicit in the conception of inductive and capacitive coupling that these retardation effects are negligible. An attempt was made to find a solution to the problem taking this into account; but it has not been possible. It is interesting, however, to consider the method used and the difficulties involved, for it enables the definition of the various regions in which the retardation and coupling are negligible.

The method employed was that developed by Fowler[27] to solve the problem of propagation along helical coils. When conductors in a medium occupy only a small proportion of the total volume it is permissible to replace the system of conductors by phantom currents flowing in the dielectric. Then for the space occupied by the conductors Fowler showed that the potentials and currents must satisfy the equations

$$\frac{\partial}{\partial x}\phi(x) = -\frac{1}{\sigma_c}\frac{\partial}{\partial t} i(x,t) - \frac{\mu}{4\pi}\int_S \frac{1}{r}\frac{\partial}{\partial t} i\left(x+s, t-\frac{r}{c}\right) ds$$

$$\frac{\partial}{\partial t}\phi(x,t) = -\frac{1}{4\pi\epsilon}\int_s \frac{1}{r}\frac{\partial}{\partial x} i\left(x+s, t-\frac{r}{c}\right) ds \qquad (10)$$

where ϕ = scalar potential

i = current

σ_c = conductivity of conductor.

and x, s, and r are as shown in Fig. 62. Equations (10) constitute what Fowler has called the complete circuit equations. The similarity to the transmission line equations is evident.

The main snag in the application of these equations to an ideal transformer coil is the presence of the core. (Fowler in his paper examines the natural modes of single and double helical structures). It might be imagined that a coil with a core could be treated as the double helical structure, Fig. 63, considering the inside helix as the image of the coil. However, this is not so because the core shields one side of the coil from the other. In an open structure, a current at a point 'a', Fig. 64, influences the voltage at b as a result of a wave travelling along the straight line ab.

If, however, it is possible to consider the coil flattened out as in Fig. 59, then the interaction with the images does not violate the effect of the screening. The

winding will therefore be considered as an infinite series of parallel conductors. Applying equation (10) to give the potential and current along the n^{th} conductor (considering a coil of infinite turns), and neglecting losses

$$\frac{\partial \phi_n}{\partial x} = -\frac{\mu}{4\pi}\sum_{p=-\infty}^{\infty}\int_{-\delta}^{\delta}\frac{1}{r_{n,n+p}}\cdot\frac{\partial}{\partial t}\left[i_{n+p}\right]^{*}ds$$

$$-\frac{\mu}{4\pi}\sum_{p=-\infty}^{+\infty}\int_{-\delta}^{\delta}\frac{1}{r_{n,n+p'}}\cdot\frac{\partial}{\partial t}\left[i_{n+p'}\right]^{*}ds.$$

$$\frac{\partial \phi_n}{\partial t} = -\frac{1}{4\pi\epsilon}\sum_{p=-\infty}^{\infty}\int_{-\delta}^{\delta}\frac{1}{r_{n,n+p}}\cdot\frac{\partial}{\partial x}\left[i_{n+p}\right]^{*}ds \qquad (11)$$

$$-\frac{1}{4\pi\epsilon}\sum_{p=-\infty}^{+\infty}\int_{-\delta}^{\delta}\frac{1}{r_{n,n+p'}}\cdot\frac{\partial}{\partial x}\left[i_{n+p'}\right]^{*}ds$$

where p refers to the number of conductors from the n^{th}, and p' the number of image conductors from the n^{th}. The range of integration is determined by the relative diameter of the core and coil. Since the interaction can only take place along straight lines, the limit will be when this line becomes a tangent to the core, Fig. 64.

Since the conductor $n+p'$ is the image of conductor $n+p$ then

$$i_{n+p} = -\, i_{n+p'}$$

Assuming that the solution is of the form

$$\begin{aligned} \phi &= \Phi \exp. -j(hx - \omega t) \\ i &= I \exp. -j(hx - \omega t) \end{aligned} \tag{12}$$

equation (11) becomes

$$h\,\Phi_n = \frac{\mu\omega}{4\pi} I_n \sum_{p=-\infty}^{\infty} \epsilon^{ihpd} \int_{-\delta}^{\delta} \left[\frac{\epsilon^{-ikr_{n,n+p}}}{r_{n,n+p}} - \frac{\epsilon^{-ikr_{n,n+p'}}}{r_{n,n+p'}} \right] \epsilon^{ihx}\, ds \tag{13}$$

$$\omega\,\Phi_n = \frac{h}{4\pi\epsilon} I_n \sum_{p=-\infty}^{\infty} \epsilon^{ihpd} \int_{-\delta}^{\delta} \left[\frac{\epsilon^{-ikr_{n,n+p}}}{r_{n,n+p}} - \frac{\epsilon^{-ikr_{n,n+p'}}}{r_{n,n+p'}} \right] \epsilon^{ihx}\, ds$$

Since $r_{n,n+p} = r_{n,n-p}$

and $r_{n,n+p'} = r_{n,n-p'}$

equations (13) can be written

$$h\underline{\Phi}_n = \frac{\mu\omega}{4\pi} I_n \left\{ \int_{-\delta}^{\delta} \left[\frac{\epsilon^{-ikr_{n,n}}}{r_{n,n}} - \frac{\epsilon^{-ikr_{n,n'}}}{r_{n,n'}} \right] \epsilon^{ihx} ds \right.$$

$$\left. + 2 \sum_{1}^{\infty} \cosh pd \int_{-\delta}^{+\delta} \left[\frac{\epsilon^{-ikr_{n,n+p}}}{r_{n,n+p}} - \frac{\epsilon^{-ikr_{n,n+p'}}}{r_{n,n+p'}} \right] \epsilon^{ihx} ds \right\}$$

$$\omega\underline{\Phi}_n = \frac{h}{4\pi\epsilon} \underline{I}_n \left\{ \int_{-\delta}^{\delta} \left[\frac{\epsilon^{-ikr_{n,n}}}{r_{n,n}} - \frac{\epsilon^{-ikr_{n,n'}}}{r_{n,n'}} \right] \epsilon^{ihx} ds \right. \qquad (14)$$

$$\left. + 2 \sum_{1}^{\infty} \cosh pd \int_{-\delta}^{\delta} \left[\frac{\epsilon^{-ikr_{n,n+p}}}{r_{n,n+p}} - \frac{\epsilon^{-ikr_{n,n+p'}}}{r_{n,n+p'}} \right] \epsilon^{ihx} ds \right\}$$

Eliminating $\underline{\Phi}_n$ and $\underline{I}_n$ from equation (14) get as before from equation (6).

$$h = \pm \omega \sqrt{\epsilon\mu}$$

showing again that waves of all frequencies travel along the wires with the velocity of light.

Now, since

$$r_{n,n+p} = \sqrt{(p+q)^2 + a^2} \qquad (15)$$

and $r_{n,n+p'} = \sqrt{(p+q)^2 + a^2 + (2\ell)^2}$

where q = distance between turns

a = radius of conductor

ℓ = distance between coil and core

as in Fig. 65, then as p increases $r_{n,n+p}'$ tends to $r_{n,n+p}$.

It is therefore possible to estimate the rate of convergence of the sum in equations (14), and, for an approximate solution of the equations, to select the terms which contribute most to the sum. This means that a zone in which coupling is important can be defined.

It is also possible to define a region in which the retardation effects are negligible. The argument of the exponential functions in equations (14) is

$$k r_{n,n+p} = \frac{\omega}{c} r_{n,n+p} \qquad (16)$$

When this is very small, i.e. for small ω and r, the exponential function approaches unity. This has been defined by King as the near zone, and within it the parameters of inductance and capacitance can be used. The reader is referred to King's book, page 402, for further information on these frequency and distance limits.

No general solution has been found for these equations. Its form, however, would be similar to that obtained in section 9.3, with the arbitrariness due to the

periodicity still present. Also there would be, as before, considerable difficulty when considering a coil with a finite number of turns due to the end effects. This particular problem has been tackled, in general, for a periodic structure by Brillouin[49]

9.5 Sheath model of coil

Both analyses have shown that to obtain a complete solution, the type and position of the source has to be considered. In the case of a transformer this implies a knowledge of how the connection to the coil is made. Two different connections which might produce different results are shown in Fig. 66.

There are two methods of attacking this problem. The first would use an approach similar to that described in section 9.4. The methods are those developed for the study of aerials and other high frequency networks.[50,51]

The other method, which is the one used here, is to find a solution of Maxwell's differential equation satisfying the boundary conditions. Rudenberg[28] and Poritsky, Abetti and Jerrard[29] have already considered the problem in this way. They have, however, both neglected the periodic nature of the coil and the effect of a source. In both cases the coil was considered as a homogeneous

sheath conducting in one direction only. This, of course, is a considerable simplification of the problem, since the interturnspacing is neglected and any possible flow of current across a turn prevented. These factors, as will be shown, do not appear to be vitally important to the phenomena; the coupling and retardation effects between different sections of the winding remain, being implicit in the solution of Maxwell's differential equations.

A considerable amount of work has been carried out recently on the problem of the propagation of electromagnetic waves along a helix, in connection with the development of the travelling wave tube. The original analyses were formulated using the sheath model mentioned above, first neglecting the periodicity of the structure, , and then later including it. Various other attempts at a more accurate analysis were published about 1950. Sollfrey[31], for example, introduced a set of helical coordinates to make the inclusion of a finite wire diameter possible. However, the wave equation in helical coordinates cannot be solved using a separation of variables technique, and so only an approximate result could be found for the fundamental mode. Fowler's analysis has already been mentioned in section 9.4. He developed expressions for what he called partial inductances and capacitances,

but he did not tackle the problem of a source.

In a thesis, Sensiper[32] introduced the tape helix, Fig. 67. This is developed from the sheath model by considering the tape current as an infinite sum of sheath currents of varying amplitude, as in a Fourier series. To obtain a complete solution the current distribution across the tape has to be assumed, and Sensiper has considered two cases

(a) when the tape width is large compared with the interturn spacing,

(b) when the tape is narrow compared with the interturn spacing.

In case (a) current flow across the tape was permitted. Sensiper showed that results from both did not differ greatly, and also that they compared favourably with the results obtained from the sheath model. It appears, therefore, that the use of a sheath model is fairly justifiable.

Sensiper appears to be the only investigator who has, so far, considered the presence of a source. The results from the source-free case are, of course, very valuable, yielding the natural modes of propagation, and giving a good idea of the behaviour of the structure.

However, as has been shown, it is important in the transformer problem to consider the source and the types of modes it can generate. In Sensiper's thesis it is mainly the simple helix which is considered and the source is placed in a gap in the infinite coil. The source, in this case, will be connected between the coil and the core.

In previous analyses[28,29], the coil has been considered as an infinitely thin sheath between the core and the casing. For the purposes here, all the relevant information can be obtained with an infinitely conducting coil and core, by assuming that the coil extends to infinity in the radial direction, Fig. 46. The extension of the sheath in the radial direction is not important, so long as it is stated that all the current returns by the core and not partly, or wholly, by any external conductor.

To simplify the analysis slightly, by replacing Bessel functions by circular and hyperbolic functions, the coil will be split along a line parallel to its axis, and flattened out on the x, z plane, Fig. 68. The electromagnetic fields will now be periodic in the direction x. This simplification was first used by Rudenberg[28], and it seems fairly justifiable at this stage.

Because of the infinite conductivity of the core and coil the problem is therefore to find a solution of

the wave equation in the dielectric, satisfying certain boundary conditions. The wave equation in cartesian coordinates is

$$\frac{\partial^2\phi}{\partial x^2} + \frac{\partial^2\phi}{\partial y^2} + \frac{\partial^2\phi}{\partial z^2} - \mu\epsilon \frac{\partial^2\phi}{\partial t^2} = 0 \qquad (17)$$

where μ and ϵ are the permeability and permittivity of the dielectric respectively, and ϕ is any field component.

It will now be assumed that all the field components vary as

$$\exp.-j(hz + \alpha x - \omega t) \qquad (18)$$

where $\alpha = \frac{n\pi}{d}$, n varying from $-\infty$ to $+\infty$

and d = circumference of coil.

Equation (18) becomes

$$\frac{d^2\phi}{dy^2} - p^2\phi = 0 \qquad (19)$$

where

$$p^2 = h^2 + \alpha^2 - k^2 \qquad (20)$$

and has a solution

$$\phi = A\epsilon^{+py} + B\epsilon^{-py} \qquad (21)$$

Since four of the six field components can be written in terms of the other two, and since ϕ may represent any one of these components, then

$$E_z = A\epsilon^{py} + B\epsilon^{-py} \qquad (22)$$

$$H_z = C\epsilon^{\beta y} + D\epsilon^{-\beta y} \tag{23}$$

and the other components can be evaluated from the equations

$$\begin{aligned}
E_x &= -\frac{1}{\Gamma^2}\left(j\omega\mu\frac{\partial H_z}{\partial y} + jh\frac{\partial E_z}{\partial x}\right) \\
H_x &= \frac{1}{\Gamma^2}\left(j\omega\epsilon\frac{\partial E_z}{\partial y} - jh\frac{\partial H_z}{\partial y}\right) \\
E_y &= \frac{1}{\Gamma^2}\left(j\omega\mu\frac{\partial H_z}{\partial x} - jh\frac{\partial E_z}{\partial y}\right) \\
H_y &= -\frac{1}{\Gamma^2}\left(j\omega\epsilon\frac{\partial E_z}{\partial x} - jh\frac{\partial H_z}{\partial y}\right)
\end{aligned} \tag{24}$$

where

$$\Gamma^2 = h^2 - k^2 \tag{25}$$

From equations (22), (23) and (24)

$$E_x = \frac{1}{\Gamma^2}\left[(\alpha hA - j\omega\mu\beta C)\epsilon^{\beta y} + (\alpha hB + j\omega\mu\beta D)\epsilon^{-\beta y}\right] \tag{26}$$

$$H_x = \frac{1}{\Gamma^2}\left[(j\omega\epsilon\beta A + \alpha hC)\epsilon^{\beta y} - (j\omega\epsilon\beta B - \alpha hD)\epsilon^{-\beta y}\right] \tag{27}$$

$$E_y = \frac{1}{\Gamma^2}\left[(\omega\mu\alpha C - jh\beta A)\epsilon^{\beta y} + (\omega\mu\alpha D + jh\beta B)\epsilon^{-\beta y}\right] \tag{28}$$

The constants A, B, C and D will be determined from the boundary conditions. These are

(i) at $y = 0$, $E_x = E_z = 0$

(ii) at $y = a$, since it is assumed that the conductivity of the sheath in the direction given by the angle ψ, Fig. 68, is infinite, and that no current can flow across the conductors, then the electric and magnetic fields in direction given by ψ are zero, i.e.

$$E_x \cos\psi + E_z \sin\psi = 0$$
$$H_x \cos\psi + H_z \sin\psi = 0 \qquad (30)$$

Condition (i) serves to eliminate the constants B and D so that

$$E_z = A \sinh \beta y$$
$$H_z = C \cosh \beta y$$
$$E_x = \frac{1}{\Gamma^2}(\alpha h A - j\omega\mu\beta C) \sinh \beta y \qquad (31)$$
$$H_x = \frac{1}{\Gamma^2}(j\omega\epsilon\beta A + \alpha h C) \cosh \beta y$$
$$E_y = -\frac{1}{\Gamma^2}(\omega\mu\alpha C + jh\beta A) \cosh \beta y$$

A factor 2 has been neglected.

Inserting equations (31) in (30) get for condition (ii)

$$\frac{1}{\Pi^2}(\alpha h A - i\omega\mu p C)\,\mathrm{Sinh}\,pa\,\cos\psi + A\,\mathrm{Sinh}\,pa\,\sin\psi = 0$$

$$\frac{1}{\Pi^2}(i\omega\epsilon p A + \alpha h C)\,\mathrm{Cosh}\,pa\,\cos\psi + C\,\mathrm{Cosh}\,pa\,\sin\psi = 0 \qquad (32)$$

Therefore, from (32), provided $\Pi^2 \neq 0$ it follows that

$$\begin{aligned} &(1)\quad [\alpha h + \tan\psi\,(h^2 - k^2)]^2 = k^2 p^2 \\ &(2)\quad \mathrm{Sinh}\,pa = 0 \qquad (33) \\ &(3)\quad \mathrm{Cosh}\,pa = 0. \end{aligned}$$

These three conditions determine the natural modes of the helix, and each will be examined in turn.

(1) <u>The natural helical modes</u>

Condition (i) gives, what may be called, the natural helix modes. The equation has three solutions

$$\begin{aligned} &(a)\quad h = k \\ &(b)\quad h = \frac{1}{\sin\psi}(\alpha\cos\psi + k) = h_1 \qquad (34) \\ &(c)\quad h = \frac{1}{\sin\psi}(\alpha\cos\psi - k) = h_2 \end{aligned}$$

The first solution may be regarded as trivial since to obtain equations (33) it was assumed that $\Gamma^2 \neq 0$ i.e. $h \neq k$ from equation (25). This spurious root results from the order of analysis, by beginning with the wave equation and then deriving the field components.

The modes (b) and (c) are similar to those obtained earlier in section 9.3 and 9.4 for propagation along wires. Inserting (b) and (c) in equations (32) gives for

$$\begin{aligned} h_1 \qquad & C_1 = + j\sqrt{\frac{\epsilon}{\mu}}\, A_1 \\ h_2 \qquad & C_2 = - j\sqrt{\frac{\epsilon}{\mu}}\, A_2 \end{aligned} \tag{35}$$

The general solution for these modes is obtained by substituting for C in equation (31) and taking the sum of all the α components, thus

$$E_z = \sum_{\alpha=-\infty}^{\infty} (A_1 \sinh p_1 y\, \epsilon^{-jh_1 z} + A_2 \sinh p_2 y\, \epsilon^{-jh_2 z}) \exp -j(\alpha x - \omega t)$$

$$H_z = \sqrt{\frac{\epsilon}{\mu}} \sum_{-\infty}^{\infty} (A_1 \cosh p_1 y\, \epsilon^{-jh_1 z} - A_2 \cosh p_2 y\, \epsilon^{-jh_2 z}) \exp -j(\alpha x - \omega t)$$

$$H_x = \sqrt{\frac{\epsilon}{\mu}} \sum_{-\infty}^{\infty} \left(-A_1 \cosh p_1 y\, \epsilon^{-ih_1 z} + A_2 \cosh p_2 y\, \epsilon^{-ih_2 z}\right) \exp.-j(\alpha x - \omega t)$$

$$E_y = \sum_{-\infty}^{\infty} \left(A_1 \cosh p_1 y\, \epsilon^{-ih_1 z} + A_2 \cosh p_2 y\, \epsilon^{-ih_2 z}\right) \exp.-j(\alpha x - \omega t)$$

where $p_1 = (h_1^2 + \alpha^2 - k^2)^{\frac{1}{2}}$

and $p_2 = (h_2^2 + \alpha^2 - k^2)^{\frac{1}{2}}$ (37)

Before the complete solution for these modes can be found, two further boundary conditions are necessary. It will be convenient first, however, to derive expressions for the voltage between the core and the sheath, and for the current in the sheath.

The line integral of the electric field between the coil and the core gives the voltage V at the point considered, thus

$$V = \int_0^a E_y \, dy.$$

$$= \sum_{-\infty}^{\infty} \left(A_1 \frac{\sinh p_1 a}{p_1} \epsilon^{-ih_1 z} + A_2 \frac{\sinh p_2 a}{p_2} \epsilon^{-ih_2 z}\right) \exp-j(\alpha x - \omega t)$$

(38)

The current in the sheath I is related to the magnetic field at the surface by the vector relationship

$$H = n \times J$$

where J is the current density

Therefore $$H_z = J_x = I \cos\psi$$

$$= \sqrt{\frac{\epsilon}{\mu}} \sum_{-\infty}^{\infty} \left(-A_1 \cosh p_1 a \epsilon^{-ih_1 z} + A_2 \cosh p_2 a \epsilon^{-ih_2 z}\right) \exp -j(\alpha x - \omega t) \tag{39}$$

Comparing these equations with the ordinary transmission line equations, the main difficulty is that, in this case, the A_1 and A_2 terms can represent waves travelling in both directions, and under certain conditions, in the same direction. It is therefore not possible to separate, in the general case, positively travelling waves from negatively travelling waves.

Suppose now that at $Z = 0$ the voltage and current are known, supplied from some external source which produces no disturbance. They can be represented by the Fourier series

$$V_0(x,0) = \sum_{-\infty}^{\infty} V_0(\alpha,0) \exp -j(\alpha x - \omega t)$$

$$I_0(x,0) = \sum_{-\infty}^{\infty} I_0(\alpha,0) \exp -j(\alpha x - \omega t) \tag{40}$$

These two conditions serve to eliminate the constants A_1 and A_2. Equations (38) and (39) become after some rearrangement, considering a particular solution

$$V(\alpha,z) = \frac{1}{D\cos\psi}\left\{\left[V_0(\alpha,0)\cosh p_2 a + I_0(\alpha,0)\sqrt{\frac{\mu}{\epsilon}}\,\frac{\sinh p_2 a}{p_2}\right]\times\right.$$
$$\times\frac{\sinh p_1 a}{p_1}\cdot\epsilon^{-ih_1 z} + \left[V_0(\alpha,0)\cosh p_1 a + I_0(\alpha,0)\sqrt{\frac{\mu}{\epsilon}}\,\frac{\sinh p_1 a}{p_1}\right]\times$$
$$\left.\times\frac{\sinh p_2 a}{p_2}\cdot\epsilon^{-ih_2 z}\right\} \qquad (41)$$

$$I(\alpha,z) = \sqrt{\frac{\epsilon}{\mu}}\cdot\frac{1}{D\cos\psi}\left\{-\left[V_0(\alpha,0)\cosh p_2 a - I_0(\alpha,0)\sqrt{\frac{\mu}{\epsilon}}\,\frac{\sinh p_2 a}{p_2}\right]\times\right.$$
$$\frac{\sinh p_1 a}{p_1}\epsilon^{-ih_1 z} + \left[V_0(\alpha,0)\cosh p_1 a + I_0(\alpha,0)\,\frac{\sinh p_1 a}{p_1}\right]\times$$
$$\left.\frac{\sinh p_2 a}{p_2}\cdot\epsilon^{-ih_2 z}\right\} \qquad (42)$$

where

$$D = \frac{\sinh p_2 a}{p_2}\cdot\cosh p_1 a + \frac{\sinh p_1 a}{p_1}\cosh p_2 a \qquad (43)$$

For the complete solution, it is now necessary to state the voltage or current at some other point along the coil. Two cases will be examined.

(a) Semi-infinite coil

It is not possible, as in the ordinary transmission line theory, to separate the two boundary conditions by considering the wave travelling outwards. This is because of the ambiguity of wave direction. The method employed is to connect an impedance Z_L at a distance ℓ along the coil, and then examine the input impedance as ℓ tends to infinity.

This input impedance is found to be

$$Z_{in} = \frac{V_0(\alpha,0)}{I_0(\alpha,0)}$$

$$= \frac{Z_L \cdot \frac{\sinh p_2 a}{p_2} \cdot \cosh p_1 a + Z_L \frac{\sinh p_1 a}{p_1} \cosh p_2 a \; \epsilon^{-2ih_0\ell}}{Z_L \sqrt{\frac{\epsilon}{\mu}} \cosh p_2 a \cdot \cosh p_1 a \,(1 - \epsilon^{-2ih_0\ell}) - \cosh p_2 a \frac{\sinh p_1 a}{p_1} - \sqrt{\frac{\mu}{\epsilon}} \frac{\sinh p_1 a \sinh p_2 a}{p_1 p_2}(1-\epsilon^{-2ih_0\ell})} \qquad (44)$$

$$- \cosh p_1 a \frac{\sinh p_2 a}{p_2} \epsilon^{-2ih_0\ell}$$

It is noticed that the term $\epsilon^{-i\alpha\ell}$ has cancelled.

So far, no account has been taken of the losses, which in an actual coil must be present. Their effect is to make the value of h_0 complex instead of real, and so it follows that if ℓ tends to infinity the exponential term in equation (44) would tend to zero. With these conditions equation (44) now becomes for $+ve\ \omega$

$$Z_{in} = \frac{V_0}{I_0} = \sqrt{\frac{\mu}{\epsilon}}\ \frac{\tanh h_2 a}{h_2} \qquad (45)$$

and for $-ve\ \omega$

$$Z_{in} = \sqrt{\frac{\mu}{\epsilon}}\ \frac{\tanh h_1 a}{h_1}$$

For $\alpha = 0$ these equations reduce to

$$Z_{in} = \sqrt{\frac{\mu}{\epsilon}}\ \frac{\tanh h_0 a}{h_0}$$

which corresponds to the equation Rudenberg[28] derived. Graphs showing the variation of impedances with frequency and α are drawn in Fig. 69.

Substituting for I_0 from equation (45) in (41) get for $+ve\ \omega$

$$V(\alpha, z) = V_0(\alpha, 0)\ \epsilon^{-i h_2 z} \qquad (46)$$

and for $-ve\ \omega$

$$V(\alpha, z) = V_0(\alpha, 0)\ \epsilon^{-i h_1 z}$$

so that the complete solution for the natural helix modes on a semi-infinite coil is

$$V(x,z,\omega) = \sum_{\alpha=-\infty}^{\infty} V(\alpha,0,\omega)\exp -j(hz+\alpha x-\omega t) \quad (47)$$

If the problem is to find the response of the coil to a surge $V(x,0,t)$ then using the Fourier integral to represent the surge

$$V(\alpha,0,\omega) = \frac{1}{4\pi d}\int_{-d}^{d} \epsilon^{i\alpha x}\,dx \int_{-\infty}^{\infty} V(x,0,t)\,\epsilon^{-j\omega t}\,dt \quad (48)$$

the voltage along the coil is

$$V(x,z,t) = \sum_{\alpha=-\infty}^{\infty} \int_{-\infty}^{\infty} V(\alpha,0,\omega)\,\epsilon^{-j(hz+\alpha x-\omega t)}\,d\omega. \quad (49)$$

Since the voltage distribution for $+ve\ z$ is given by a wave travelling in a positive direction, and

$$h = \frac{1}{\sin\psi}(\alpha\cos\psi \pm k)$$

it follows that

for $+ve\ \omega$ $\quad h > 0$ $\qquad$ and so $\frac{k}{\sin\psi} > -\alpha\cot\psi$

and for $-ve\ \omega$ $\quad h < 0$ $\qquad$ and so $\frac{k}{\sin\psi} > +\alpha\cot\psi$

for all values of α.

This means that on an $h\alpha$ plane there must be

forbidden regions, corresponding roughly to the pass and attenuation bands of a filter. These are shown in Fig. 70. Since the general solution contains positive and negative values of α, if the mode of propagation is such that one of the α values lies within a forbidden region, then the distribution in the x direction is determined by a travelling wave: if both values lie outside, then the distribution is a standing wave.

For waves travelling in a positive direction equation (49) is written

$$V(x,z,t) = \sum_{\alpha=-\infty}^{0} \left\{ \int_{-\infty}^{0} V(\alpha,0,\omega)\, \epsilon^{-j(h_z z-\omega t)}\, d\omega + \int_{|\alpha\cos\psi|}^{\infty} V(\alpha,0,\omega)\, \epsilon^{-j(h_z z-\omega t)}\, d\omega \right\} \epsilon^{-j\alpha y} + \sum_{\alpha=0}^{\infty} \left\{ \int_{-\infty}^{-|\alpha\cos\psi|} V(\alpha,0,\omega)\, \epsilon^{-j(h_z z-\omega t)}\, d\omega + \int_{0}^{\infty} V(\alpha,0,\omega)\, \epsilon^{-j(h_z z-\omega t)}\, d\omega \right\} \epsilon^{-j\alpha x} \qquad (50)$$

The function $V(\alpha,0,\omega)$ may be written as $V(\alpha,0) \cdot V(\omega)$ Now since any distribution of voltage at $z=0$, as for example in Fig. 71, will be given by an even function

of x , then it follows that

$$V(\alpha,0) = V(-\alpha,0)$$

Further, since for the application of a unit function at $Z=0$, $V(\omega) = \frac{1}{j\omega}$ then one can write

$$V(-\alpha,0,-\omega) = -V(\alpha,0,\omega) \qquad (51)$$

Equation (50) can therefore be written

$$V(x,z,t) = \sum_{0}^{\infty}\Bigg\{-\int_{0}^{\infty} V(\alpha,0,\omega)\,\epsilon^{j(h_2 z-\omega t)}\,\epsilon^{j\alpha x}\,d\omega + \int_{0}^{\infty} V(\alpha,0,\omega)\,\epsilon^{-j(h_2 z-\omega t)}\,\epsilon^{-j\alpha x}\,d\omega - \int_{-\infty}^{-\alpha\cos\gamma} V(\alpha,0,\omega)\,\epsilon^{+j(h_2 z-\omega t)}\,\epsilon^{j\alpha x}\,d\omega + \int_{-\infty}^{-\alpha\cos\gamma} V(\alpha,0,\omega)\,\epsilon^{-j(h_2 z-\omega t)}\,\epsilon^{-j\alpha x}\,d\omega\Bigg\}$$

$$= -2\sum_{0}^{\infty} V(\alpha,0)\Bigg\{\int_{0}^{\infty}\frac{1}{\omega}\sin(h_2 z+\alpha x-\omega t)\,d\omega + \int_{-\infty}^{-\alpha\cos\gamma}\frac{1}{\omega}\sin(h_2 z+\alpha x-\omega t)\,d\omega\Bigg\} \qquad (52)$$

If ξ is the coordinate along the coil then from Fig. 68

$$Z = \xi\sin\gamma \quad ; \quad x = \xi\cos\gamma. \qquad (53)$$

and so from equation (34) the argument of the sine function

$$h_2 z + \alpha x - \omega t = k\xi - \omega t = \omega\left(\frac{\xi}{c} - t\right) \qquad (54)$$

Therefore equation (52) can be written

$$V(x,z,t) = -2\sum_{0}^{\infty} V(\alpha,0)\left\{\int_{0}^{\infty} \frac{\sin\omega\left(\frac{\xi}{c}-t\right)}{\omega}\cdot d\omega + \int_{-\infty}^{-\alpha\cos\psi} \frac{\sin\omega\left(\frac{\xi}{c}-t\right)}{\omega}\cdot d\omega\right\}$$

$$= -2\sum_{0}^{\infty} V(\alpha,0)\left\{2\int_{0}^{\infty} \frac{\sin\omega\left(\frac{\xi}{c}-t\right)}{\omega}\cdot d\omega - \int_{0}^{\alpha\cos\psi} \frac{\sin\omega\left(\frac{\xi}{c}-t\right)}{\omega}\cdot d\omega\right\} \qquad (55)$$

From this equation it follows that the voltage distribution along the winding, due to a step function applied at $z = 0$, is the difference of two waves, a step function travelling along the wire with the velocity of light, and a wave represented by the finite sine integral also travelling along the wire with the velocity of light. For each α component of the applied voltage function this has a cut off frequency given by

$$f_c = \alpha\cos\psi = \frac{n\pi}{d}\cos\psi$$

Propagation along the coil axis will therefore

be of waves travelling with velocities $c \tan \psi$ and because of the period nature of the coil, each α component of the applied wave will be modulated at a frequency α .

An important conclusion from this analysis is that the distribution of voltage along the coil, for waves travelling in the helix modes, is independent of the position of the core.

(b) Finite coil short circuited at the end

It is assumed, in this case, that at $z = \ell$ the voltage is zero for all x .

The input impedance given by equation (44) becomes with $Z_L = 0$

$$Z_{in} = \frac{V_0}{I_0}$$

$$= \frac{\sqrt{\frac{\mu}{\epsilon}} \frac{\sinh h_2 a}{h_2} \cdot \frac{\sinh h_1 a}{h_1} \left(1 - \epsilon^{-2j h_0 \ell}\right)}{\cosh h_2 a \cdot \frac{\sinh h_1 a}{h_1} + \cosh h_1 a \frac{\sinh h_2 a}{h_2} \cdot \epsilon^{-2j h_0 \ell}} \qquad (56)$$

Substituting for I_0 in equation (41) get after some manipulation

$$V(x, z, \omega) = \left(\cosh_0 z - \cot h_0 \ell \sin h_0 z\right) +$$

$$+2\sum_{1}^{\infty} V_0(\alpha,0,\omega)\left\{\frac{\frac{\tanh h_1 a}{h_1}}{\frac{\tanh h_1 a}{h_1}+\frac{\tanh h_2 a}{h_2}}\left(\cosh h_1 z-\cosh h_2 \ell\cdot\frac{\sinh h_0 z}{\sinh h_0 \ell}\right)\right.$$

$$\left.+\frac{\frac{\tanh h_2 a}{h_2}}{\frac{\tanh h_1 a}{h_1}+\frac{\tanh h_2 a}{h_2}}\left(\cosh h_2 z-\cosh h_1 \ell\cdot\frac{\sinh h_0 z}{\sinh h_0 \ell}\right)\right\}\cos\alpha x \qquad (57)$$

The response to a surge can be found using equations (48) and (49). In this case, there will be no restriction on wave direction.

The simplification of equation (57) has not been accomplished, but some general conclusions can be derived. First of all, it is seen that the voltage distribution is dependent on the function $V_0(\alpha)$; in other words, on the method of application of the surge to the coil. It appears also that the distribution is dependent on the distance between the coil and core. This result differs from that obtained for the infinite coil, and so it would follow that one cannot use the results of an infinite winding to determine the voltage distributions along a finite winding. The results of the infinite winding would, of course, hold for a surge until the reflected wave returns from a termination.

The waveguide modes (2) and (3).

The other modes still to be considered are given by the equations (33)

(2) $\sinh pa = 0$

(3) $\cosh pa = 0$

(2.) From equations (33) it follows that

$$p = i\frac{m\pi}{a} = iq \tag{58}$$

where m is any integer between $-\infty$ and ∞

Therefore from equation (20)

$$h^2 = k^2 - \left(\frac{n\pi}{d}\right)^2 - \left(\frac{m\pi}{a}\right)^2 = h_3^2 \tag{59}$$

This equation indicates the similarity between this mode and the usual waveguide modes. It follows from equation (59) that there can be no propagation until

$$k^2 > \left(\frac{n\pi}{d}\right)^2 + \left(\frac{m\pi}{a}\right)^2 \tag{60}$$

Below this critical frequency h is imaginary, and the wave is attenuated.

The field components are found by substituting for p in equation (32) and finding C in terms of A

i.e. $$C = \frac{\omega\epsilon q \cos\psi}{\alpha h_3 \cos\psi + \sin\psi\, \Gamma_3^2} \cdot A \tag{51}$$

where $$\Gamma_3^2 = h_3^2 - k^2$$

So that from equations (31)

$$E_y = \frac{\alpha \cos\psi + h_3 \sin\psi}{\alpha h \cos\psi + \sin\psi\, \Gamma_3^2} \cdot q A \cos qy \,. \qquad (61)$$

and

$$H_z = \frac{\omega \epsilon \cos\psi}{\alpha h \cos\psi + \sin\psi\, \Gamma_3^2} \cdot q A \cos qy \qquad (62)$$

(31) Similarly from equations (33) it follows that

$$p = i\frac{s\pi}{2a} = ir \qquad (63)$$

where s is any integer except zero between $-\infty$ and $+\infty$

Therefore, from equation (20)

$$h^2 = k^2 - \left(\frac{h\pi}{d}\right)^2 - \left(\frac{s\pi}{2a}\right)^2 = h_4^2 \qquad (64)$$

The relationship between C and A is now

$$C = -\frac{\alpha h_4 \cos\psi + \Gamma_4^2 \sin\psi}{\omega \mu r \cos\psi} \cdot A \qquad (65)$$

and so from equations (31)

$$E_y = \frac{1}{\Gamma^2}(\alpha \tan\psi - h_4) A \cos ry \qquad (66)$$

and

$$H_z = -\frac{\alpha h_4 \cos\psi + \Gamma_4^2 \sin\psi}{\omega \mu \cos\psi} \cdot A \cos ry \qquad (67)$$

where

$$\Gamma_4^2 = h_4^2 - k^2 \,.$$

9.7. General Solution

The most general solution must contain all possible modes; thus

$$E_y = \sum_{\alpha=-\infty}^{\infty} \Bigg\{ \left(A_1 \cosh p_1 y \cdot \epsilon^{-ih_1 z} + A_2 \cosh p_2 y \, \epsilon^{-ih_2 z} \right)$$

$$+ \sum_{q=-\infty}^{\infty} \frac{\alpha \cos\psi + h_3}{\alpha h_3 \cos\psi + \sin\psi \, \Gamma_3^2} \cdot A_3 q \cos qy \, \epsilon^{-ih_3 z}$$

$$+ \sum_{r=-\infty}^{\infty} \frac{1}{r} (\alpha \tan\psi - h_4) A_4 \cos ry \, \epsilon^{-ih_4 z} \Bigg\} \exp -j(\alpha x - \omega t) \qquad (68)$$

Similar expressions can be derived for the other components.

To enable the evaluation of the constants $A_1 \ldots A_4$ four boundary conditions are required. It would therefore be necessary to state the actual field distribution at the boundary instead of, as in section 9.3, the voltage and current.

It is seen from equation (68) that three different types of wave may propagate along the coil. There are the natural helix modes which, for the infinite line, travel along the conductors with the velocity of light. Then there are the two wave guide modes, which may propagate along the axis with phase velocities greater than that of light, or which may be attenuated.

The possibility of these modes being present is dependent entirely on the type and position of the source. In a waveguide, for example, the source is so arranged that only one particular type of mode is generated, while, in the transformer, there is no attempt made to generate any particular type of mode.

This particular problem has not been thoroughly examined yet, but some points of interest will be given. Assuming that the source is connected between the core and the coil, then it should follow that the total axial current flowing in the coil should equal the axial current in the core. This means that the integral of the magnetic field H_x round the core surface will equal the integral of the same field round the coil surface. It therefore follows from equation (31) for H_x that propagation cannot exist solely in the natural helix mode, since the field

components of that mode vary hyperbolically in the y direction. At low frequencies, this variation will be very small (for $\alpha=0$ $\beta \simeq \frac{k}{c \sin\psi}$) and propagation will be largely in these natural modes, but as the frequency increases, to satisfy the field requirements, the other modes will become important.

This would appear to give a satisfactory explanation of the distribution of voltage along a coil subject to a steep fronted surge. The high frequency components present in the surge travel along the coil as fast attenuated waves while the low frequency components travel in the natural modes along the coil conductors.

Another important case might be when the connection to the core is made at some point along the winding. This means that no current can flow in the core at the point $z=0$, and so $H_z = H_x = 0$ at that point. Again, the presence of the waveguide modes is necessary to fulfil the above requirement.

Conclusions

1. The Kirchhoff equations do not provide a complete solution to the problem unless certain unjustifiable assumptions are made regarding the nature of the coupling. The arbitrary nature of the solution and that obtained using the complete circuit equations can only be resolved by consideration of the source, and for this purpose, the replacement of the coil by a sheath seems justifiable.

2. There are three types of modes which can exist in a helical structure

(a) Natural helix modes. These result from the periodic nature of the coil and are independent of the position of the core. They correspond to the TEM modes in ordinary waveguide theory, but they differ in that there is a field variation between the coil and core.

(b) The two waveguide modes. These correspond to the ordinary TE and TM waveguide modes. In this case, however, the principal mode becomes the natural helix mode.

3. It appears important, to control the way in which the signal is applied to the coil, i.e. the factors $V_0(\alpha)$ and $I_0(\alpha)$., since it affects the voltage distribution.

4. It would appear that in a helical structure, with the source connected as in a transformer, all modes must

be present to satisfy the requirements at the boundaries. Further, that the waveguide modes, which apparently become important at high frequencies, produce voltage distributions which might explain the attenuated instantaneous distribution often recorded.

5. It will, of course, be necessary to examine this theoretical problem in greater detail. At the same time, experimental data on ideal coils would be very useful, considering the effect of the source, of frequency and the load, on the voltage distributions.

GENERAL CONCLUSIONS TO PART II

The problems tackled in Part II of this thesis have shown the value of a fundamental approach using Maxwell's equations.

The selection of particular problems under ideal conditions, although not immediately of any practical value, does lead to a better understanding of the nature of wave propagation in the particular element.

In these problems, in which physical assumptions are often made to facilitate the analysis, it is necessary to obtain experimental evidence.

The cable problem may be said to be completely understood although the investigation of the proximity effect was not rigorous.

It has appeared from the analysis of the transformer, that the sheath model preserves all the important features of the single layer coil, and since this problem can be tackled rigorously from a mathematical point of view, the detailed results which may be obtained will be of great value.

To provide a comprehensive solution to the

generator problem from a rigorous analysis using Maxwell's equations, will be a difficult task and perhaps the only practical method of solution will be to use the circuit equations, as in the work of Robinson. The analysis given here should then help in the evaluation of the circuit constants.

The extension of Bergeron's graphical method to the solution of the problems of wave propagation in waveguides, and perhaps even the sheath model of the transformer, seems possible.

APPENDIX 1

Recovery Voltage Inductor (R.V.I.)[54]

The R.V.I. has proved a very useful instrument in the study of switching transients. The method is to record, on an oscilloscope, the voltage response to a periodic current surge, since this voltage, according to Thevenin's theorem, will correspond to the recovery voltage. The time base of the oscilloscope is synchronised with the current surges so that a standing pattern is obtained.

This particular R.V.I.[54] is a modification and development of the instrument proposed by S.Y. King[55], the triode valve of the new injection circuit, Fig. 72, replacing a diode. The triode acts as a switch, so that half sine waves of current are injected into the system under test at a rate of 50 per second. Further, with the application of a negative pulse to the grid of the triode, the current wave can be chopped at any point, and so current chopping conditions can be studied. The maximum current this instrument can inject has a peak value of 0.055 amps.

When recording transients of recovery voltage on

the cable transformer system described in Chapter 3, the oscillations were not completely damped out by the time the next half sine wave was injected, and the resultant voltage transient was difficult to analyse Fig. 7a. To overcome this difficulty, the duration of the negative chop applied to grid of the triode was extended so that every alternate half sine wave was blocked, and the transient at the beginning of the half sine wave could be examined, Fig. 7b.

APPENDIX 2

Recurrent Surge Oscillograph[54]

This particular R.S.O. can generate impulse waves and short duration pulses with a repetition rate of 50 per second. The cathode ray tube being triggered at the same rate, these surges, or the response of any network to them, are displayed as standing waves. The basic impulse generator circuit is shown in Fig. 73. The capacitor C_1 is first charged with the thyration non-conducting (in this case, a hydrogen thyration), and then discharged through it when a positive pulse is applied to its grid. The voltage between the terminals A and B is then given approximately by the difference of two exponential curves, and its shape can be altered by varying the values of R_1, R_2, C_1 and C_2. The wave can be chopped to represent the chopping of a lightning surge.

APPENDIX 3

Bergeron's graphical solution of wave problems

1. Bergeron's graphical method[43] for the solution of the wave equation under transient conditions has been found of considerable value in the analysis of the response of distributed networks to surges. In this appendix a short account will be given of the method, its applications and possible development. This will be followed by a short description of each surge diagram presented in this thesis.

Along a transmission line it can be shown that the voltage and current are given respectively by the sum and difference of two waves

$$e = F(x + Vt) + G(x - Vt) \qquad (1)$$

$$i = \frac{1}{Z}\left[F(x + Vt) - G(x - Vt)\right] \qquad (2)$$

where F and G are waves travelling in the opposite direction with the velocity V. Adding and then subtracting these equations gives

$$e - Zi = 2F(x + Vt) \tag{3}$$

$$e + Zi = 2G(x - Vt) \tag{4}$$

so that at all points and times given by $x + Vt = 0$

$$e - Zi = \text{constant} \tag{5}$$

and at all points and times given by $x - Vt = 0$

$$e + Zi = \text{constant} \tag{6}$$

The following interpretation may be given. If an imaginary observer, who can measure the instantaneous voltage and current on the line, moves in a positive direction with velocity V, then equation (5) is always satisfied, and similarly, equation (6) is satisfied for an observer moving in a negative direction. Therefore, on a voltage and current graph the point corresponding to a forward moving observer is to be found on the straight line $e + Zi = C$ while that for a negatively moving observer will be found on the line $e - Zi = C$. These lines are called surge lines and are completely determined if the values of voltage and current, at the points from which the observers depart, are known. A simple example will show how this may be applied.

The problem is to determine the transient

condition on a line terminated by a non-linear resistance, and fed by a constant voltage supply, Fig.74 . On a voltage-current graph the boundary conditions at the ends A and F, Fig. 74, are, respectively, a line representing the constant voltage source, and the resistance characteristic. It is assumed that the switch is closed at time zero, that the propagation time along the cable is unity, and that x increases positively from A to F.

At time -1 an observer is assumed to leave the end A and travel towards F, reaching F just as the switch is closed. On the voltage-current graph this is represented by a line of slope $-Z$ passing through the point $(-1\ 4)$ and crossing the resistance curve at the point OF, which gives the voltage and current at F immediately the switch is closed. The wave is reflected and travels back to A. This is represented by a line with slope $+Z$ passing through the point OF. Continuing this construction results in the surge diagram from which the voltage-time graph of the voltage across the resistance may be drawn.

The response of lumped capacitance or inductance is found approximately by changing the differential equations, involved in their voltage current relationships,

to difference equations. They can then be treated as distributed lines, the capacitance as an open circuited line, the inductance as a short circuited line. A certain suitable propagation time τ is chosen and the surge impedance for the inductance is given by $Z = \frac{L}{\tau}$ and for the capacitance $Z = \frac{\tau}{C}$

Losses in a line may be accounted for by the inclusion of lumped resistances or, more simply, assuming the line distortionless, by a method suggested by Satche and Grosse[44]. They have also shown how the method may be used to investigate the dynamic behaviour of an arc, and how to take account of the mutual inductance of a three phase line.

2. The extension of the method to the solution of the general wave equation for the electromagnetic field.

It is suggested that the method just described could be extended to solve graphically the problem of surges in waveguides.

Maxwell's equations for a homogeneous isotropic lossless dielectric are

$$\nabla \times E + \mu \frac{\partial H}{\partial t} = 0 \qquad (7)$$

$$\nabla \times H - \epsilon \frac{\partial E}{\partial t} = 0 \qquad (8)$$

It can be shown that the rectangular components of the electric and magnetic fields satisfy the wave equation

$$\nabla^2 \phi - \frac{1}{c^2} \frac{\partial^2 \phi}{\partial t^2} = 0 \qquad (9)$$

where $C = \frac{1}{\sqrt{\mu \epsilon}}$ = velocity of wave propagation in the dielectric.

The solution of the wave equation may be written in the form

$$\phi = F(r+ct) + G(r-ct) \qquad (10)$$

where $r = \sqrt{x^2+y^2+z^2}$

Hence

$$E = F(r+ct) + G(r-ct) \qquad (11)$$

and from equation (8)

$$\nabla \times H = \frac{1}{Z_0}\left[F(r+ct) - G(r-ct)\right] \qquad (12)$$

where $Z_0 = \sqrt{\frac{\mu}{\epsilon}}$

Adding and subtracting the equations (11) and (12) gives

$$E + Z_0 \cdot \nabla \times H = F(r+ct) \qquad (13)$$

$$E - Z_0 \nabla \times H = G(r-ct). \qquad (14)$$

These equations correspond to equations (3) and (4), and so it should be possible to plot surge dia grams of E and H the field vectors .

3. Short descriptions of the Surge Diagrams.

Fig. 81 shows the response to a half sine current wave of the cable with a three phase short at the remote end, and with a capacitance at the near end. In the surge diagram the losses have been neglected. The boundary conditions are as follows:-

At the end A the current is the known sinusoidal input.

At the end B there is a short and so the voltage there is always zero.

Since no electron current can flow through the capacitance its boundary must lie on the voltage axis.

Unit time is chosen as the propagation time of the cable, and the propagation time of the capacitance is taken as 1/10 of this. The voltage time graph shows the voltage at A determined from the surge diagram, the measured transient, and the transient which was derived for the line with no capacitance. In this case, the propagation value used was derived from the frequency of the measured transient and is greater than the actual value.

The surge diagram in Fig. 82 shows the response of the same cable capacitance network to a chopped half

sine wave. The boundary conditions at B and C are the same as in Fig. 81. In this case the losses of the line are included, the decrement factor used being determined from the decrement of the measured transients. The voltage-time curve shows the voltage at A found from the surge diagram, the measured transient, and also that derived for the line without the capacitance.

The value of this graphical method is illustrated in the derivation of this initial capacitance value. By a graphical process of trial and error, the value was readily found which produced a curve almost coinciding with the measured transient.

Fig. 83 shows the recovery voltage at the circuit breaker when the current has been chopped. In this case the boundary conditions are as follows:

At A the current is a chopped half sine wave.

At D and E the voltage is zero.

The propagation times of the cable AB and BC differed slightly. To draw a surge diagram with these values would be very involved, and so the value of T_{BC} was made equal to T_{AB} and an adjustment made to the surge impedance Z_{BC}.

An alteration of the propagation time, since

$T = \sqrt{LC}$, means an alteration in the values of L, or C, or both. Since the capacitance of the cable is the important parameter it is kept constant, and L altered to a new value given by

$$L_1 = \frac{T_1^2}{C} = \frac{T_1^2}{T_2^2} \cdot L$$

where L_1 is the new value of the inductance and T_1 the new time. This alteration of inductance produces an alteration of the surge impedance, and the new value is

$$Z_1 = \sqrt{\left(\frac{T_1}{T}\right)^2 \cdot \frac{L}{C}} = \frac{T_1}{T} \cdot Z$$

The voltage-time curve shows the voltage derived from the surge diagram, that derived neglecting the losses, and the measured voltage.

Fig. 84 shows the response of the generator winding, considered as a distributed line, to an impulse. The boundary conditions are:

At A the voltage is the impulse voltage shown in the voltage-time diagram.

At B the current is zero since the end is open circuited.

The voltage-time graph shows the voltage at the open circuited end of the line.

APPENDIX 4

The extension of Gosland's analysis[11]

The evaluation of the cable surge impedance according to the method outlined by Gosland[11] is a tedious process. The impedance derived here is a closed expression from which the variation can be derived directly.

Considering the case of two single phase cables, as shown in Fig. 21, it is assumed that the bonds are close enough to be able to assume that there is no electric field between the sheaths. (In the diagram the distance between the sheaths has been exaggerated).

Gosland showed that a current i flowing in the core induces an electromotive force in the sheath circuit such that

$$M \frac{di}{dt} = L_s \frac{di_s}{dt} + 2 R_s i_s \qquad (1)$$

where i = current in core

i_s = current in sheaths

M = mutual inductance between core and sheath circuits

L_s = inductance of sheath to sheath circuit

and R_s = resistance of each sheath

Now, considering the application of a ramp function

$$i = At \tag{2}$$

equation (1) becomes

$$L_s \frac{di_s}{dt} + 2R_s i_s = MA$$

which has a solution

$$i_s = \frac{MA}{2R_s}\left(1 - \epsilon^{-\frac{2R_s}{L_s}t}\right) \tag{3}$$

Now, since the sheaths are concentric with the cores

$$M = L_s \tag{4}$$

The voltage at the input to the cores is given by

$$e(t) = L_c \frac{di}{dt} + 2R_c i - M \frac{di_s}{dt} \tag{5}$$

where L_c = inductance of core to core circuit

R_c = resistance of each core

This equation becomes for $i = At$

$$e(t) = L_c A + 2R_c At - M \cdot \frac{MA}{L_s} \epsilon^{-\frac{2R_c}{L_s}t}$$

so that the inductive impedance is given by

$$x(t) = \frac{e(t)}{i(t)} = \frac{L_c}{t} + 2R_c - \frac{L_s}{t} \cdot \epsilon^{-\frac{2R_c}{L_s}t} \tag{6}$$

So far, no account has been taken of the cable capacitance. The equivalent circuit of the cable may be

represented as an inductance and capacitance in parallel. Assuming that a linear current $i = Bt$ flows through the capacitance then since $\int i.dt = vc$

$$\frac{1}{2} Bt^2 + K = vc \tag{7}$$

If it is assumed that there is no initial change, i.e. $K=0$, then the admittance

$$Y(t) = \frac{i(t)}{v(t)} = \frac{2c}{t} \tag{8}$$

Hence, the surge impedance is given by

$$Z_c = \sqrt{\frac{z_c}{Y}} = \sqrt{\left\{ \frac{L_c}{2c} + \frac{Rc}{C} t - \frac{L_s}{2c} \epsilon^{-\frac{2R_s}{L_s} t} \right\}} \tag{9}$$

APPENDIX 5

The inclusion of the instrument terminal capacitances in the determination of transformer self capacitance

When measurements with the R.V.I. and bridge circuits are made on apparatus which has a large capacitance to earth it may be necessary to include the instrument terminal capacitances. In the case considered here, measurements were made to determine the transformer self capacitance for the first phase to clear a three phase unearthed fault. The instrument is therefore connected between the points a and b, Fig. 75.

The instrument output has a certain capacitance to earth which can be represented by the mesh circuit shown in Fig. 76. With the additional capacitance C_1 connected across the terminals, as described in Ch. 2 the equivalent circuit of the transformer and instrument can be taken as that shown in Fig. 77 where C_o is the self capacitance per phase and L the inductance per phase of the transformer coil. Since the transient voltage was of essentially a single frequency, it is therefore permissible to replace C_b and C_c by

$$C_c' = \frac{1}{2}(C_b + C_c)$$

$$C_b' = \frac{1}{2} C_c' = \frac{1}{4}(C_b + C_c)$$

so that the circuit of Fig.77i reduces to the simple circuit Fig.77ii where

$$C' = \frac{2}{3}(C_0 + C_b') + C_a + C_1$$

By measuring the parameters C_a, C_b and C_c for the R.V.I. and Signal Generator, it is possible then to determine the transformer self capacitance.

APPENDIX 6

The surge impedances for different fault conditions on a double circuit line with earth wire protection

In this analysis, based on the analysis in Surge Phenomena[33], p.178, it is assumed that the conductivity of the conductors and earth is infinite.

Let 1^1, 2^1, ... 8^1 be to the images of the lines 1, 2, ... 8, lines 7 and 8 being the earth wires. The voltages and conductors of all conductors must satisfy the matrix equation

$$(e) = [Z] (i) \qquad (1)$$

where (e) and (i) are column matrices of the voltages and currents at any section of the line, and $[Z]$ is a symmetrical square matrix of rank 8, of the self and mutual surge impedances with

$$Z_{rr'} = 60 \log \frac{r-r'}{a}$$

$$Z_{rs} = 60 \log \left(\frac{r-r'}{r-s}\right) \qquad (2)$$

where $r - r^1$ is the distance between the conductor r and its image r^1, and $r - s^1$ the distance between conductor r

and the image of conductor s.

Since conductors 7 and 8 are earthed at every tower, it can be assumed that e_7 and e_8 are zero at all points along the line.

(a) Earth fault on conductor 1.

For an earth fault on conductor 1, one can write

$$i_2 = i_3 = i_4 = i_5 = i_6 = 0$$

so that from the matrix equation (1)

$$\begin{aligned} e_1 &= Z_1 i_1 - Z_{17} i_7 - Z_{18} i_8 \\ 0 &= Z_{17} i_1 - Z_{77} i_7 - Z_{78} i_8 \\ 0 &= Z_{18} i_1 - Z_{78} i_7 - Z_{78} i_8 \end{aligned} \qquad (3)$$

The surge impedance is given by $Z = e_1/i_1$ so that from (3)

$$Z = Z_{11} - \frac{(Z_{71})^2 Z_{88} + (Z_{81})^2 Z_{77} - 2 Z_{71} Z_{81} Z_{87}}{Z_{77} Z_{88} - (Z_{87})^2} \qquad (4)$$

For a single earth wire, say 7, this becomes

$$Z_1 = Z_{11} - \frac{Z_{17}^2}{Z_{77}} \qquad (5)$$

(b) Phase 1 opening a phase to phase earth fault on conductors 1 and 2.

In this case $i_3 = i_4 = i_5 = i_6 = 0$,

and so

$$Z = e_1/i_1 = Z_{11} - Z_{21}\, i_2/i_1 - Z_{71}\, \frac{i_7}{i_1} - Z_{81}\, \frac{i_8}{i_1} \qquad (6)$$

where the three current ratios can be found from a solution of the equations

$$\begin{aligned} Z_{22}\, \frac{i_2}{i_1} + Z_{27}\, \frac{i_7}{i_1} + Z_{28}\, \frac{i_8}{i_1} &= Z_{21} \\ Z_{72}\, \frac{i_2}{i_1} + Z_{77}\, \frac{i_7}{i_1} + Z_{78}\, \frac{i_8}{i_1} &= Z_{71} \\ Z_{82}\, \frac{i_2}{i_1} + Z_{78}\, \frac{i_7}{i_1} + Z_{88}\, \frac{i_8}{i_1} &= Z_{81} \end{aligned} \qquad (7)$$

(c) Phase 1 clearing a three phase to earth fault

The conditions are $i_4 = i_5 = i_6 = 0$ and so

$$Z_1 = \frac{e_1}{i_1} = Z_{11} - Z_{21}\, \frac{i_2}{i_1} - Z_{31}\, \frac{i_3}{i_1} - Z_{71}\, \frac{i_7}{i_1} - Z_{81}\, \frac{i_8}{i_1} \qquad (8)$$

where the current ratios are found from

$$\begin{aligned} Z_{22}\, \frac{i_2}{i_1} + Z_{23}\, \frac{i_3}{i_1} + Z_{27}\, \frac{i_7}{i_1} + Z_{28}\, \frac{i_8}{i_1} &= Z_{21} \\ Z_{32}\, \frac{i_2}{i_1} + Z_{33}\, \frac{i_3}{i_1} + Z_{37}\, \frac{i_7}{i_1} + Z_{38}\, \frac{i_8}{i_1} &= Z_{31} \end{aligned}$$

$$Z_{72}\frac{i_2}{i_1} + Z_{73}\frac{i_3}{i_1} + Z_{77}\frac{i_7}{i_1} + Z_{78}\frac{i_8}{i_1} = Z_{71}$$

$$Z_{82}\frac{i_2}{i_1} + Z_{83}\frac{i_3}{i_1} + Z_{87}\frac{i_7}{i_1} + Z_{88}\frac{i_8}{i_1} = Z_{81}$$

APPENDIX 7

The evaluation of the input impedance of the generator from measurements using a 'Q' meter

The basic circuit of the meter is shown in Fig. 78. If a voltage e is injected at the resonant frequency into the series circuit, the voltage V developed across the circuit will be approximately,

$$V = \frac{e\,\omega L}{R_L + R_c}$$

The magnification factor of the complete circuit is the ratio of the developed voltage V to the injected e.m.f. e, that is

$$Q = V/e$$

$$= \frac{1}{\frac{R_L}{\omega L} + \frac{R_c}{\omega L}} = \frac{1}{\frac{1}{Q_L} + \frac{1}{Q_c}}$$

i.e.

$$\frac{1}{Q} = \frac{1}{Q_L} + \frac{1}{Q_c}$$

The circuit used in the measurement of the input impedance of the generator is that shown in Fig. 79. The first measurement was made with the points a.b. short circuited. C^1 was adjusted until the point of resonance

was reached. Since the losses in C^1 and C are small, then

$$Q_1 \simeq Q_L$$

Now with the generator connected, and C^1 adjusted to a new resonance point the value of Q is given by

$$\frac{1}{Q_2} = \frac{1}{Q_L} + \frac{1}{Q_c} = \frac{1}{Q_1} + \frac{1}{Q_c}$$

$$\text{i.e.} \quad Q_c = \frac{Q_1 Q_2}{Q_1 - Q_2} \tag{1}$$

Q_c is also defined as

$$Q_c = \frac{\text{series resistance of arm db}}{\text{series resistance of arm db}}$$

$$= \frac{X_{db}}{R_{db}} \tag{2}$$

Now, it can be shown that, if the generator is represented as a resistance R and capacitance C in series

$$R_{db} = \frac{R/\omega C_2'^2}{R^2 + 1/\omega K_2^2} \simeq R\left(\frac{K_2}{C_2'}\right)^2 \tag{3}$$

$$X_{db} = \frac{K_2}{\omega C_2 K_1} \tag{4}$$

where

$$K_1 = \frac{CC_0}{C_0 + C} \quad , \quad K_2 = \frac{C \cdot C_0 C_2'}{CC_0 + C_0 C_2' + C_2' C}$$

Substituting (1), (3) and (4) in (2) get

$$R = \frac{C_2'(Q_1 - Q_2)}{\omega K_1 K_2 Q_1 Q_2} \tag{5}$$

$$C = \frac{C_0(C_0 + C_1' - C_2')}{C_2' - C_1'} \qquad (6)$$

If the input impedance of the generator winding is inductive then $C_1^1 > C_2^1$, and at resonance $C_1^1 = C_2^1$.

APPENDIX 8

The current distribution in a generator lamination

The ideal generator structure shown in Fig. 28 is assumed. It has already been shown in Chapter 7 that for the frequency range considered, there is a negligible variation of current density round the surface of the lamination slot, and that between the points a and b, Fig. 28, the current density varies from the surface as $\epsilon^{-\beta y}$ where $\beta = \sqrt{j\omega\mu\sigma}$. These conditions will be assumed in the following analysis.

The problem is, therefore, to find the current distribution within the metal slab, Fig.33, subject to the conditions described above. In Fig. 80 the lamination has been redrawn and different coordinates used. The joint between the lamination and the core is assumed to be perfect, and the core is considered as extending to infinity.

It is assumed that the current variation in the Z direction is zero so that the current distribution is found from a solution of the equation

$$\frac{\partial^2\phi}{\partial x^2} + \frac{\partial^2\phi}{\partial y^2} = -j\omega\mu\sigma\phi \qquad (1)$$

where μ = permeability of the metal

σ = conductivity of metal

and ϕ represents any of the rectangular components of the current density.

The solution must satisfy the following boundary conditions

$$0 < x < b \quad \begin{cases} y = a & i_y = 0 \;,\; i_x = +J \\ y = -a & i_y = 0 \;,\; i_x = -J \end{cases} \qquad (2)$$

$$b < x < \infty \quad \begin{cases} y = a & i_y = f(x) = J\epsilon^{-p(x-b)} \;,\; i_x = 0 \\ y = -a & i_y = f(x) \;,\; i_x = 0 \end{cases} \qquad (3)$$

Considering the component i_x, it is obvious from the boundary conditions that it is an odd function of y, and so it is therefore only necessary to consider the section $0 < y < a$ knowing that at $y = 0$, $i_x = 0$. Since the values of the function i_x are known at $y = 0, a$ and $x = 0, \infty$ the differential equation (1) can be solved by applying a finite Fourier sine transform in the y direction, and a Fourier sine transform in the x direction.

i.e. $$\Phi(h,k) = \int_0^a \int_0^\infty \phi(x,y) \sin \frac{n\pi}{a} y \sinh x \, . \, dy \, . \, dx \qquad (4)$$

and by the Fourier inversion theorem

$$\phi(x,y) = \sum_{1}^{\infty} \int_{0}^{\infty} \Phi(n,h) \sin \frac{n\pi}{a} y \sinh x \, dx \qquad (5)$$

The terms

$$\int_0^a \int_0^\infty \frac{\partial^2 \phi}{\partial x^2} \sin \frac{n\pi}{a} y \sinh x \, dy.dx. = h \underset{x=0}{G(n)} - h^2 \Phi(n,h) \qquad (6)$$

and

$$\int_0^a \int_0^\infty \frac{\partial^2 \phi}{\partial y^2} \sin \frac{n\pi}{a} y \sinh x. \, dy.dx$$

$$= \frac{n\pi}{a} \left\{ \underset{y=0}{F(h)} - \cos n\pi \underset{y=a}{F(h)} \right\} - \left(\frac{n\pi}{a}\right)^2 \Phi(n,h) \qquad (7)$$

In this case

$$\underset{x=0}{G(n)} = 0 \quad \text{since} \quad i_x = 0 \quad \text{at } x = 0$$

$$\underset{y=0}{F(h)} = 0 \quad \text{since} \quad i_x = 0 \quad \text{at } y = 0$$

$$\underset{y=a}{F(h)} = \int_0^\infty F(x) \sinh x \, dx$$

and

$$F(x) = J \quad - \quad 0 < x < b$$

$$0 \qquad b < x < \infty$$

So that $\underset{Y=a}{F(h)} = \frac{J}{h}(1-\cosh b)$

Multiplying equation (1) by $\sin\frac{n\pi}{a}y \sin hx$ and integrating therefore gives

$$-h^2\bar{\Phi} - \left(\frac{n\pi}{a}\right)^2\bar{\Phi} - \frac{n\pi}{a}\cos n\pi\frac{J}{h}(1-\cosh b) - p^2\bar{\Phi} = 0$$

i.e.

$$\bar{\Phi}(n,h) = -\frac{n\pi}{a}J\cos n\pi\,\frac{1-\cosh b}{h\left(h^2+\left(\frac{n\pi}{a}\right)^2+p^2\right)} \qquad (8)$$

Expanding the R.H.S. and setting $\xi^2 = \left(\frac{n\pi}{a}\right)^2 + p^2$

$$\bar{\Phi}(n,h) = \frac{n\pi}{a}\frac{J\cos n\pi}{\xi^2}\left\{\frac{\cosh b}{h} - \frac{1}{h} - \frac{h\cosh b}{h^2+\xi^2} + \frac{h}{h^2+\xi^2}\right\} \qquad (8a)$$

Using the inversion theorem, equation (5)

$$\phi(x,y) = \frac{2}{\pi}\sum_1^{\infty}{}'\left\{\frac{n\pi}{a}\frac{J\cos n\pi}{\xi^2}\sin\frac{n\pi}{a}y \times \right.$$

$$\left. \times \int_0^{\infty}\left[\frac{\cosh b}{h} - \frac{1}{h} - \frac{h\cosh b}{h^2+\xi^2} + \frac{h}{h^2+\xi^2}\right]\sin hx\,dx\right\} \qquad (9)$$

These sine integrals are tabulated in a book by Bateman[52] and are :

$f(h)$	$f(x)$	
$\frac{\cosh b}{h}$	0	$0 < x < b$
		$b < x < \infty$
$\frac{1}{h}$	$\pi/2$	
$\frac{h \cosh b}{h^2 + \xi^2}$	$-\frac{1}{2}\pi \epsilon^{-\xi b} \sinh \xi x$	$0 < x < b$
	$+\frac{1}{2}\pi \epsilon^{-\xi x} \sinh \xi b$	$b < x < b$
$\frac{h}{h^2 + \xi^2}$	$\frac{1}{2}\pi \epsilon^{-\xi x}$	

So therefore, in the region $0 < x < b$

$$\Phi(x,y) = \sum_{1}^{\infty} \frac{n\pi}{a} \frac{J \cosh n\pi}{\xi^2} \left(-1 + \epsilon^{-\xi b} \sinh \xi x - \epsilon^{-\xi x}\right) \sin \frac{n\pi}{a} y \quad (10$$

Now $\xi^2 = \left(\frac{n\pi}{a}\right)^2 + j\omega\mu\sigma$

Taking $\mu = 300 \times \mu_0 = 12\pi \times 10^{-5}$

$\sigma = 10^7$ U/m

$a = 2.54 \times 10^{-4}$ $m.$

then $\xi = \left(n.\, 2.54 \times 10^8 + j\omega \times 376 \times 10^4\right)^{\frac{1}{2}}$

It follows, therefore, that in equation (10), unless for $x \to 0$ and $x \to \infty$ the expression

$$\left(-1 + \epsilon^{-\xi b} \sinh \xi x - \epsilon^{-\xi x}\right) \longrightarrow -1$$

and so, in the region $0<x<b$, except very near the limits $x=0, b$, equation (10) can be written

$$\phi(x,y) = -\sum_{1}^{\infty} \frac{n\pi}{a} \frac{J\cos n\pi}{\xi^2} \cdot \sin \frac{n\pi}{a} y \qquad (11)$$

If one writes

$$I_1 = \int_0^a \sinh \beta y \sin \frac{n\pi}{a} y \cdot dy \;, \quad I_2 = \int_0^a \cosh \beta y \cos \frac{n\pi}{a} y \cdot dy \qquad (12)$$

then integrating by parts

$$I_1 = -\frac{a}{n\pi} \sinh \beta d \cos n\pi + \frac{a\beta}{n\pi} I_2$$

and $$I_2 = -\frac{a\beta}{n\pi} I_1$$

Eliminating I_2 from these two equations gives

$$I_1 = -\frac{\frac{n\pi}{a} \cdot \sinh \beta a \cdot \cos n\pi}{\left(\frac{n\pi}{a}\right)^2 + \beta^2}$$

$$= -\frac{n\pi}{a} \cdot \cos n\pi \; \frac{\sinh \beta a}{\xi^2} \qquad (13)$$

Making use of the Fourier sine inversion theorem, one may write this result in the form

$$\sinh \beta y = \sum_{1}^{\infty} I_1 \sin \frac{n\pi}{a} y$$

so that

$$\frac{\sinh \beta y}{\sinh \beta a} = -\sum_{1}^{\infty} \frac{n\pi}{a} \cos n\pi \frac{1}{\xi^2} \sin \frac{n\pi}{a} y \qquad (14)$$

So, therefore, equation (11) becomes

$$\phi(x,y) = \frac{J \sinh py}{\sinh pa} \qquad (15)$$

which is the result obtained previously.

This confirms that the current divides, and that the disturbance caused by the change in current direction only appears at the end of the lamination and close to the joint between it and the core. For a complete solution it would be necessary to determine the component i_y.

BIBLIOGRAPHY

RECOVERY VOLTAGE

1. HILLIARD, J.D. — disc., Tr. A.I.E.E., 46 (1927), p.312.

2. SLEPIAN, J. — 'Extinction of an A.C. Arc'. A.I.E.E., 47 (1928), 4, p.1398.

3. PARK, R.H., and SKEATS, W.F. — 'Circuit Breaker Recovery Voltage, Magnitudes, and Rates of Rise'. Tr. A.I.E.E., 50 (1931), p.238.

4. KOPLEOWITSCH, J. and BROWN, J.K. — 'Influence of Wave Form of the Recovery Voltage on Performance of Circuit Breaker'. Electrician, 108 (1932), p.93.

5. BOEHNE, E.W. — 'The Determination of Circuit Recovery Rates'. A.I.E.E., 54 (1935) p.530.

6. CASSIE, A.M. — 'Some Aspects of the Problem of the Calculation of Transients of Restriking Voltages'. World Power, 24 (1935), 139, p.13.

7. EVANS and WITZKE. — 'Practical Calculation of Electrical Transients on Power Systems'. Electrical Engineering, 57, 1943, p.690.

8. EVANS and MONTEITH. — 'System Recovery Voltage Determination of Analytical and A.C. Calculating Board Methods'. Electrical Engineering, 56 (1937), p.695.

9. MORTLOCK, J.R. — 'The Evaluation of Restriking Voltages'. J.I.E.E., 92, 2, (1945), p.562.

10. HAMMARLUND, P. 'Transient Recovery Voltage'. Aeta Polytechnica, Elect. Eng. Series Vol. 1.

11. GOSLAND, L. 'Measurement and Calculation of Restriking Voltage Transients at a Sub-station Fed by Single Core Cables.' J.I.E.E., 1939, p.269.

12. GOSLAND, L. and DUNNE, W.F.M. 'Calculation and Experiment on Transformer Reactance in Relation to Transients of Restriking Voltage.' J.I.E.E., 87, 1940, p.163.

13. VOSPER, J.S. 'Restriking Voltage Characteristics: Self Capacitances of H.V. Transformers, Reactors and Busbars.' E.R.A. Technical Report G/T272, 1953.

CABLE

14. GOSLAND, L. and WHITNEY. 'Circuit-breaker Location at a Major Sub-station on a Large 33 kV. Power Distribution System.' Beama Journal, 1937, Vol. 41, p.117.

15. SCHELKUNOFF, S.A. 'Electromagnetic Theory of Coaxial Transmission Lines and Cylindrical Shields.' Bell System Technical Journal, Oct. 1934, 13, 4, p.532.

16. SCHELKUNOFF, S.A. and ODARENKO, T.M. 'Cross Talk between Coaxial Transmission Lines.' ibid, 16, 2, 1937, 144.

17. MEAD, S.P. 'Wave Propagation over Parallel Tubular Conductors: the Alternating Current Resistance.' Bell Sys. Tech. Jour. p.327, April, 1925.

TRANSFORMERS AND COILS

18. WEED, J.M. 'Abnormal Voltages in Transformers'. Tr. A.I.E.E., 34, 1915.

19. WAGNER, K.N. 'Progress of Waves in Windings.' Elek. u. Masch. Feb. 1915.

20. BEWLEY. 'Travelling Waves on Transmission Systems.' J. Wiley, 1951.

21. MAKIN. 'Surges in Transformer Windings.' Ph.D. Thesis, London 1953.

22. RUDENBERG, R. 'Performance of Travelling Waves in Coils and Windings.' Tr. A.I.E.E., 59, 1940, p.1031.

23. PIRENNE, J. 'Theorie Generale des Phenomenes Oscillatoires dans les Enroulements des Transformateur.' Revue Generale de l'Electricite, 47, 1940, 19.

24. FRUHAUF, G. 'Phenomenes Transitoires dans les Enroulements de Transformateurs Abordes par des Ondes Mobiles.' Comptes Rendus du Congres International d'Electricite, 5, 939, (1932).

25. BLUME, S.F. and BOYAJIAN, A. 'Abnormal Voltages Within Transformers.' Tr. A.I.E.E., 38, 1919.

26. BLUME, BOYAJIAN, CAMILLI, LENNOX, MINNECI and MONTSINGER. 'Transformer Engineering', Wiley, 1951.

27. FOWLER, V. 'Analysis of Helical Transmission Lines by Means of the Complete Circuit Equations.' Tr. I.R.E.

28. RUDENBERG, R. 'Electromagnetic Waves in Transformer Coils Treated by Maxwell's Equations.' Jour. Appl. Phys. 12, 1941, p.219.

29. PORITSKY, H., ABETTI, P.A. and JERRARD, R.P. 'Field Theory of Wave Propagation along Coils.' Tr.A.I.E.E. 72. III. 1953.p930.

30. PIERCE, J.R. and TIEN. 'Coupling of Modes in Helices.' Proc. I.R.E., 42, p.1386, 1954.

31. SOLLFREY, W. 'Wave Propagation on Helical Wires.' Jour. Appl. Phys., 22, 7, 1951.

32. SENSIPER, S. 'Electromagnetic Wave Propagation on Helical Conductors.' Tech. Report No. 194, Research Laboratory of Electronics, Massachusetts Institute of Technology, May 1951.

33. SURGE PHENOMENA. E.R.A., Reference S/T35, 1941.

OVERHEAD LINE

34. CARSON, J.R. A.I.E.E., 38, p.345, 1919.

35. PELISSIER, R. 'La Propagation des Ondes Transitoires et Periodiques le Long des Ligues Electriques.' Revue Generale de l'Electricite, T.59, 9, p.379, 1950.

36. FALLOU, M.J. 'Propagation des Courants de Haute Frequence Polyphases le Long des Ligues Aerienals de Transport D'Energie. Affectees de Courts Circuits on Defauts d'Isolement.' Bull. Soc. Franc. Elect. 5, 2, 1952, p.787.

GENERATOR

37. FRIEDLANDER, E. 'Travelling Waves in High Voltage Alternator Windings.' J.I.E.E., 1942, 89, Pt. II, p.492.

38. ROBINSON, B.C. 'The Propagation of Surge Voltages Through High Speed Turbo-Alternators with Single-Conductor Windings.' J.I.E.E., 1953, 100, Pt. II, p.453.

39. ROBINSON, B.C. 'The Propagation of Surge Voltages Through Turbo-Alternators with Concentric-Conductor-Type Windings.' Proc. I.E.E., 103, A, Aug. 1956, p.355.

40. BRILLOUIN, L. 'Wave Guides for Slow Waves.' Jour. Appl. Phys. 19, 1948, p.1023.

41. LINES, A.W., NICOLL, G.R. and WOODWARD, A.M. 'Some Properties of Waveguides with Periodic Structures.' Proc. I.E.E., 97, III, 1950, p.263.

42. PIERCE, J.R. 'Coupling of Modes of Propagation.' Jour. Appl. Phys. 25, 1954, p.179.

BERGERON'S GRAPHICAL METHOD

43. BERGERON, L. 'Du Coup de Belier en Hydraulique au Coup de Foudre en Electricite.' Dunod, 1950.

44. SATCHE, P. and GROSSE, V. 'The Calculation of Recovery Voltages and Internal Voltage Surges by Means of Bergeron's Method.' C.I.G.R.E., 1950, Report No. 128.

45. STRATTON. 'Electromagnetic Theory.' McGraw-Hill, 1941.

46. RAMO, S. and WHINNERY, J.R. 'Fields and Waves in Modern Radio.' J. Wiley, 1953.

47. BEWLEY. 'Travelling Waves in Transmission Systems.' J. Wiley, 1951.

48. KING. 'Electromagnetic Engineering.' Vol. 1, Fundamentals. McGraw-Hill, 1945.

49. BRILLOUIN. 'Wave Propagation in Periodic Structures.' McGraw-Hill, 1946.

50. PIDDUCK, F.B. 'Currents in Aerials and High Frequency Networks.' Oxford, 1946.

51. WATSON, W.H. 'Wave Guide Transmission and Antennae Systems.' Oxford, 1947.

52. BATEMAN. 'Tables of Integral Transforms.' McGraw-Hill, 1954.

53. SNEDDON, I.N. 'Fourier Transforms.' McGraw-Hill, 1951.

R.S.O. AND R.V.1.

54. FINES, R.R. 'Recurrent Surge Investigations.' Thesis for Ph.D. Glasgow 1954.

55. KING, S.Y. 'Determination of Restriking Transients on Power Networks by a Half-Wave Injection Method.' J.I.E.E., II, 96, 1949.

ACKNOWLEDGEMENTS

The author wishes to express his gratitude to the Belmos Co., Ltd., Bellshill, for the provision of a generous scholarship during the three years of research. He wishes to thank the South of Scotland Electricity Board, and the Belmos Co., Ltd. for permission to make measurements on the power system components. Thanks are also due to Professor F.M. Bruce, Department of Electrical Engineering, Royal College of Science and Technology, for his guidance, valuable criticism, and encouragement of the work, to Mr. B. Noble of the Mathematics Department of the same college for his criticism of the theoretical analysis, and to members of the Department of Electrical Engineering for their very kind assistance.

TRANSIENT PERFORMANCE OF POWER SYSTEMS

PART 3

DIAGRAMS, OSCILLOGRAMS AND GRAPHS

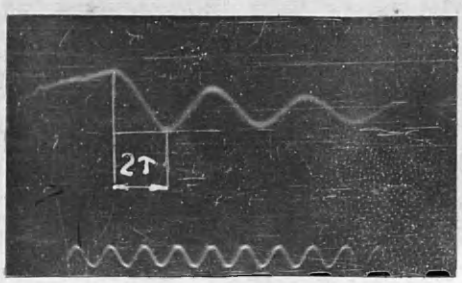

(a)

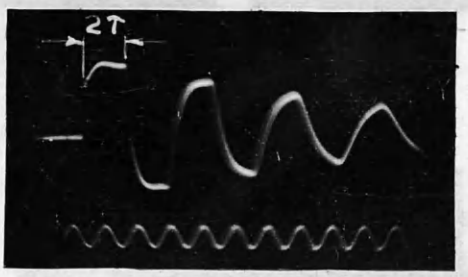

(b)

Fig. 1. Transient voltage response of cable to half sine current wave

(a) with no chop

(b) with chop.

τ = propagation time of cable

Calibration oscillation - 25 Kc/s.

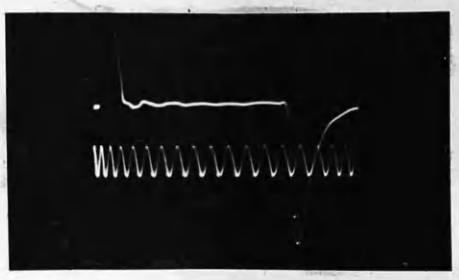

$R_L = 0$

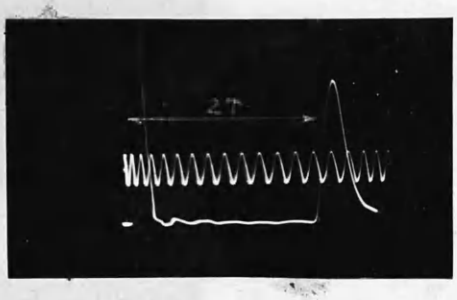

$R_L = \infty$

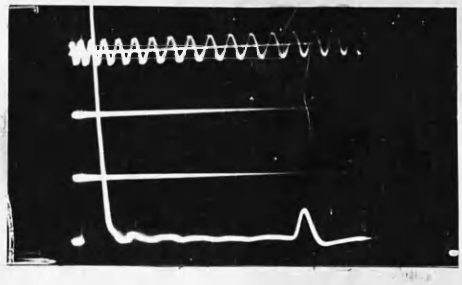

$R_L = 55$

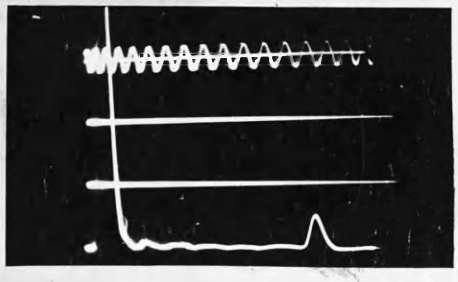

$R_L = 65$

$R_L = 60$

Fig. 2. Measurement of surge impedance of cable using R.S.O.

R_L is the variable resistance at remote end of cable.

τ is the propagation time.

The calibrating frequency is 250 Kc/s.

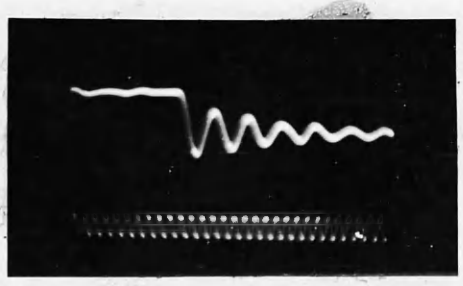

(a)

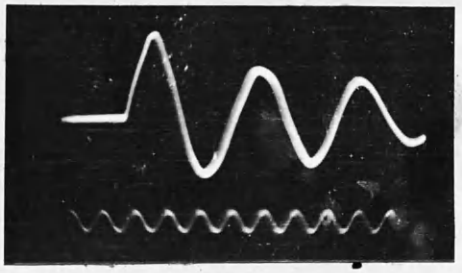

(b)

Fig. 3. Transient voltage response of transformer to half sine current wave

(a) with no chop

(b) with chop.

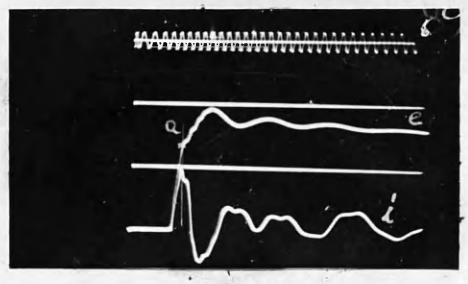

Fig. 4. Transient current response i of transformer to voltage impulse e. Surge impedance calculated at point a.

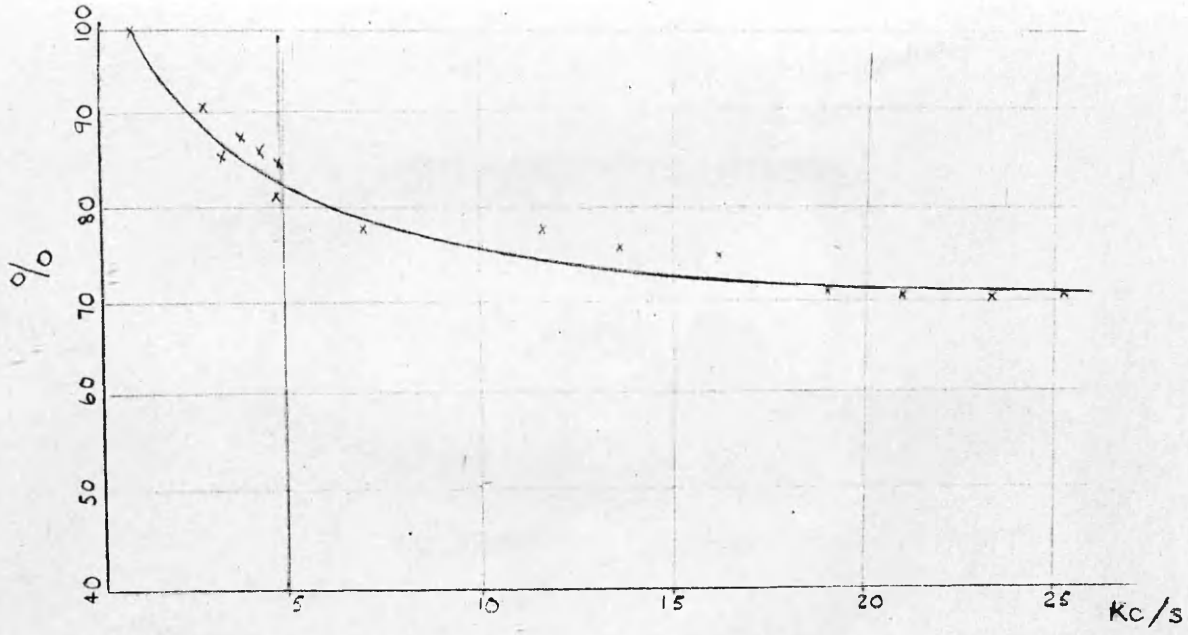

Fig. 5. Frequency dependence of transformer inductance % of the inductance at 1000c/s.

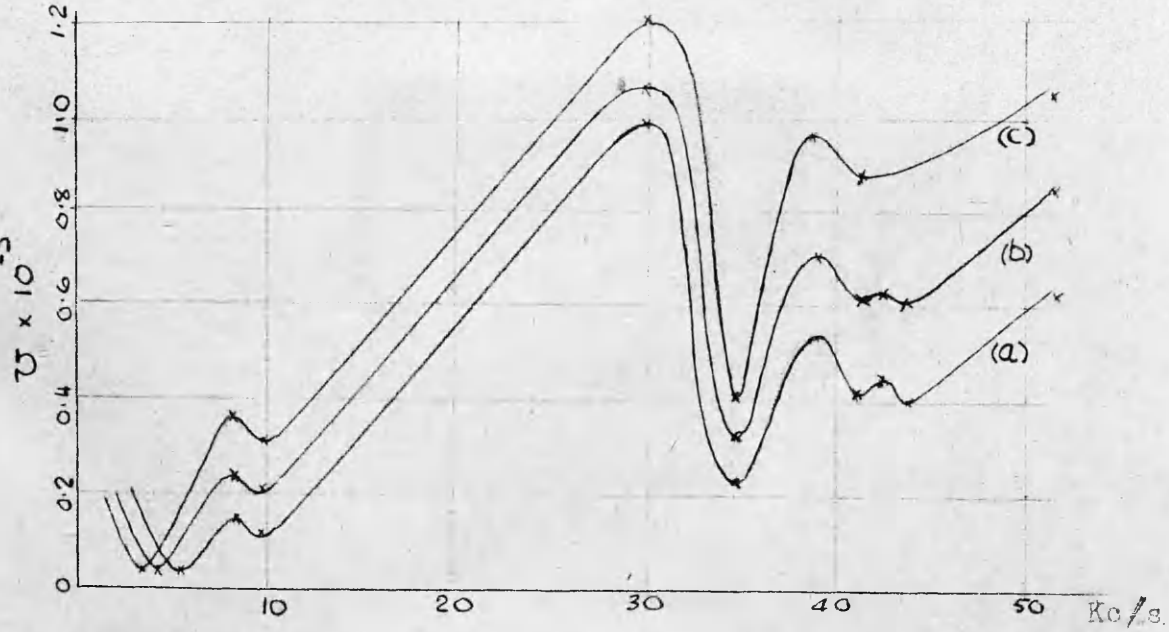

Fig. 6. Admittance of transformer with extra capacitance C connected across the terminals.

(a) $C^1 = 0$, (b) $C^1 = 0.00169\mu F$. (c) $C^1 = 0.00448\mu F$

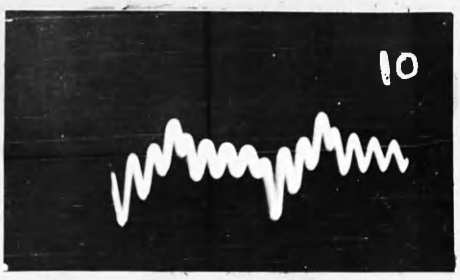

(a)

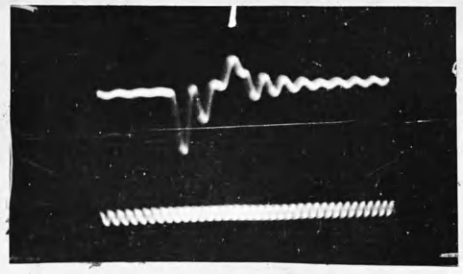

(b)

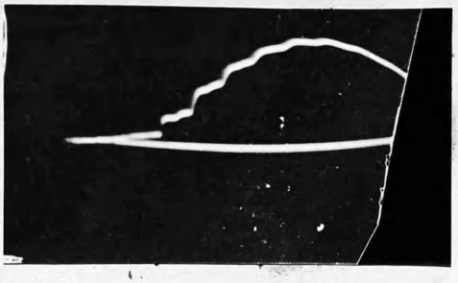

(c)

Fig. 7. Transient voltage response of system 3 to half sine wave with

(a) Current waves injected at rate of 50/sec. with no chop.

(b) Current waves injected at rate of 25/sec. with no chop.

(c) Current chopped (faster time-base).

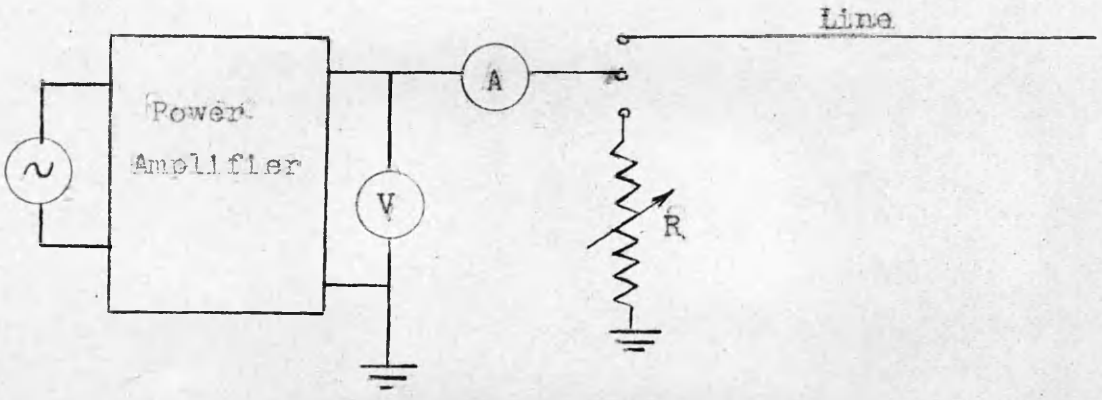

Fig. 8. Circuit (a) for measurement of line impedance.

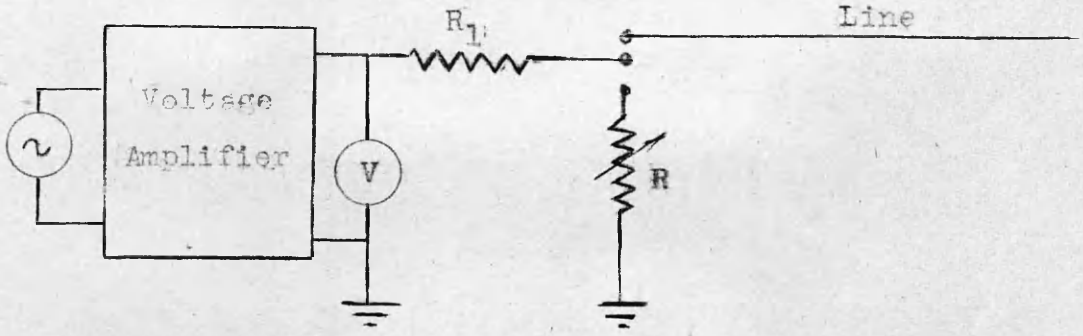

Fig. 9. Circuit (b) for the measurement of line impedance.

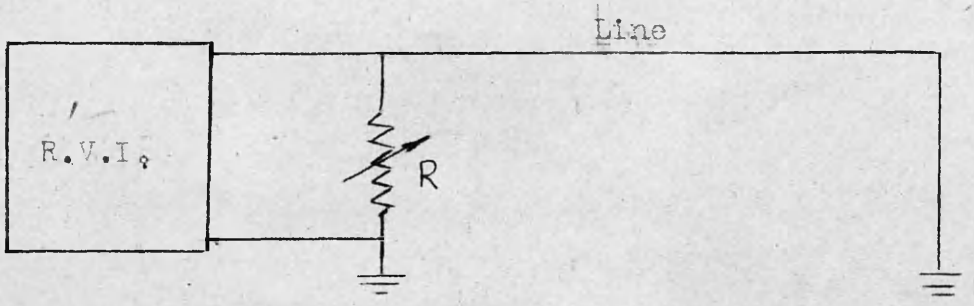

Fig. 10. Circuit (d) for the measurement of line impedance.

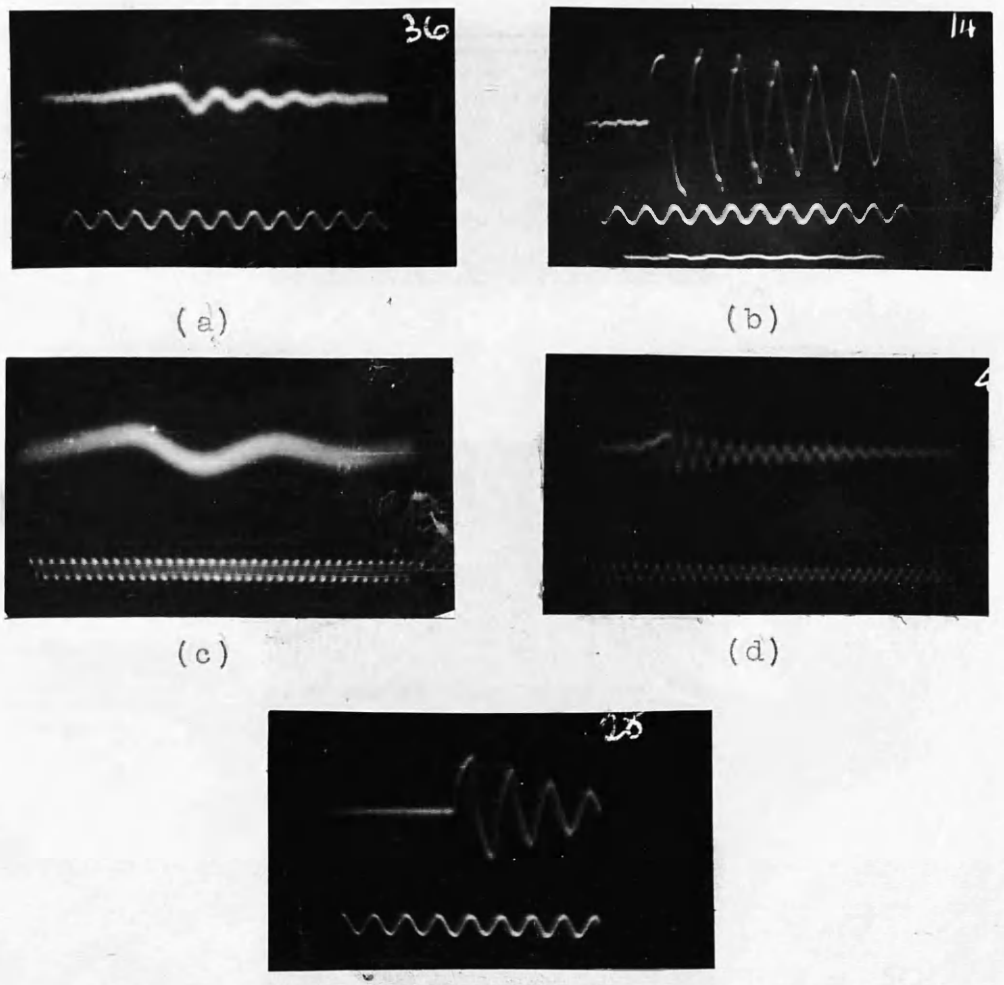

Fig. 11. Transient voltage response of overhead line to half sine current wave.

(a) Unearthed fault with no chop.
(b) Unearthed fault with chop.
(c) Earthed fault with no chop.
(d) Earthed fault with no chop and capacitance 400 μμF. connected.
(e) Earthed fault with chop.

(1) R = 800
(2) 700
(3) 600
(4) 500
(5) 400

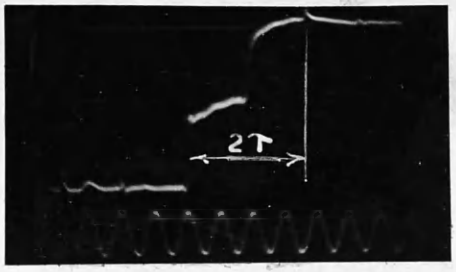

R = 540

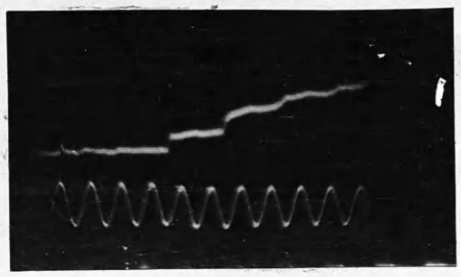

R = 50

Fig. 12. Measurement of surge impedance and propagation time of the overhead line using R.V.I. R is the variable resistance connected across the line.

τ is the propagation time of the line.

The calibrating frequency is 25 Kc/s.

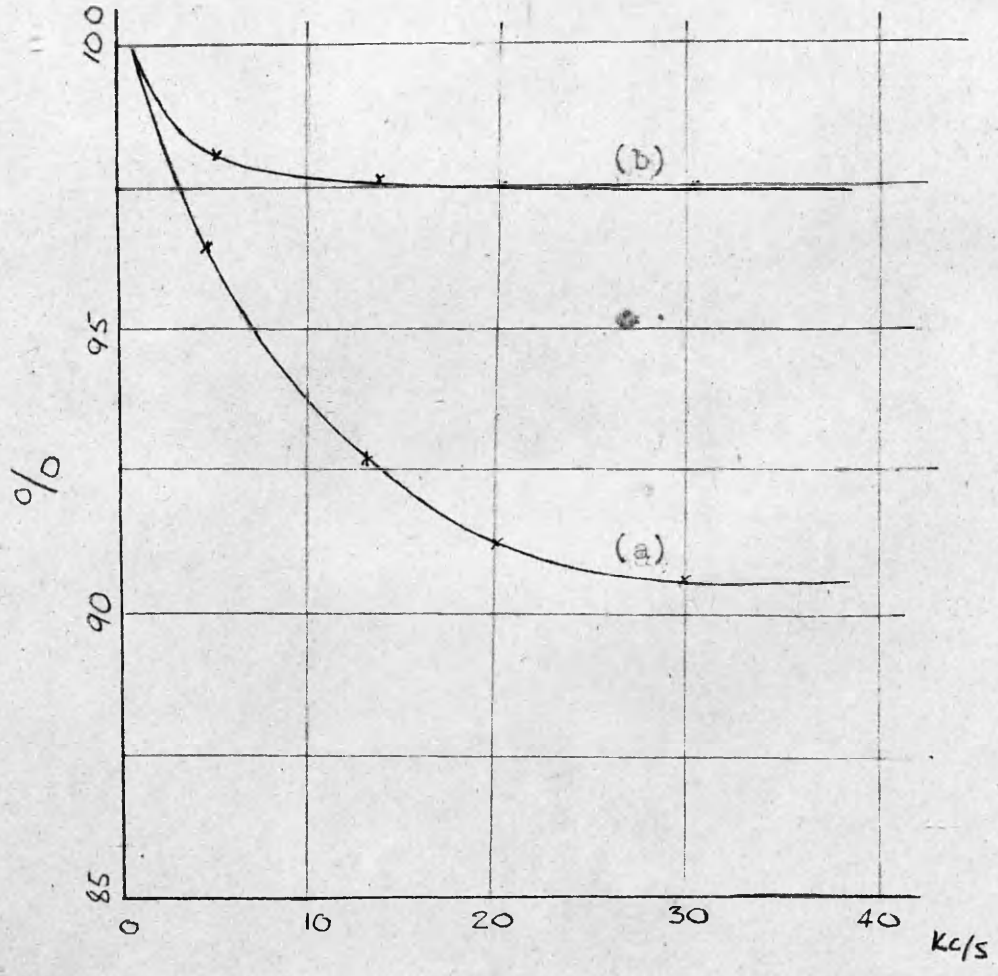

Fig. 13. Variation of line surge impedance with frequency.

% of impedance at 1000c/s.

(a) Earth return.

(b) Wire return.

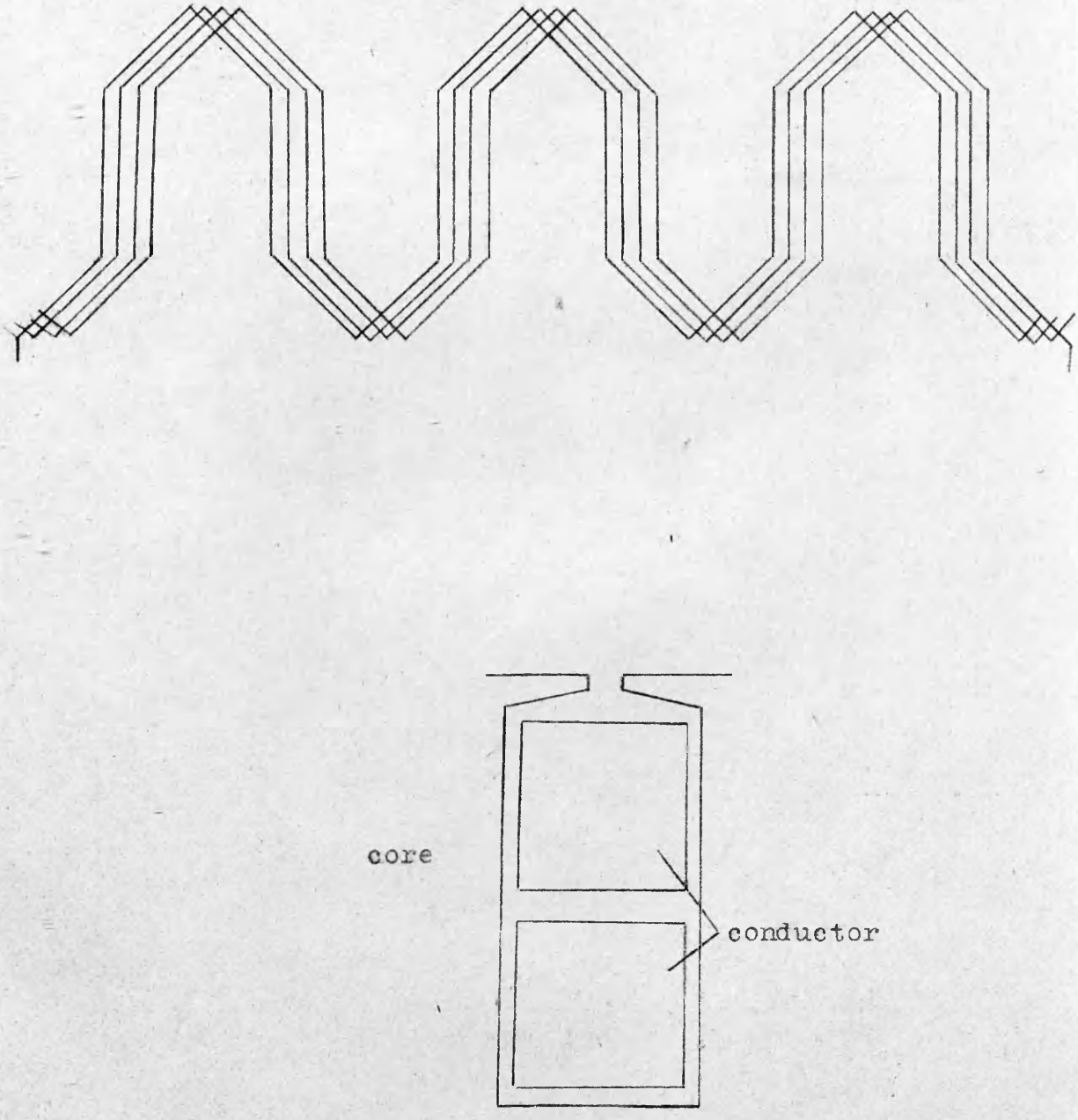

Fig.14. Generator winding (one phase shown), and slot.

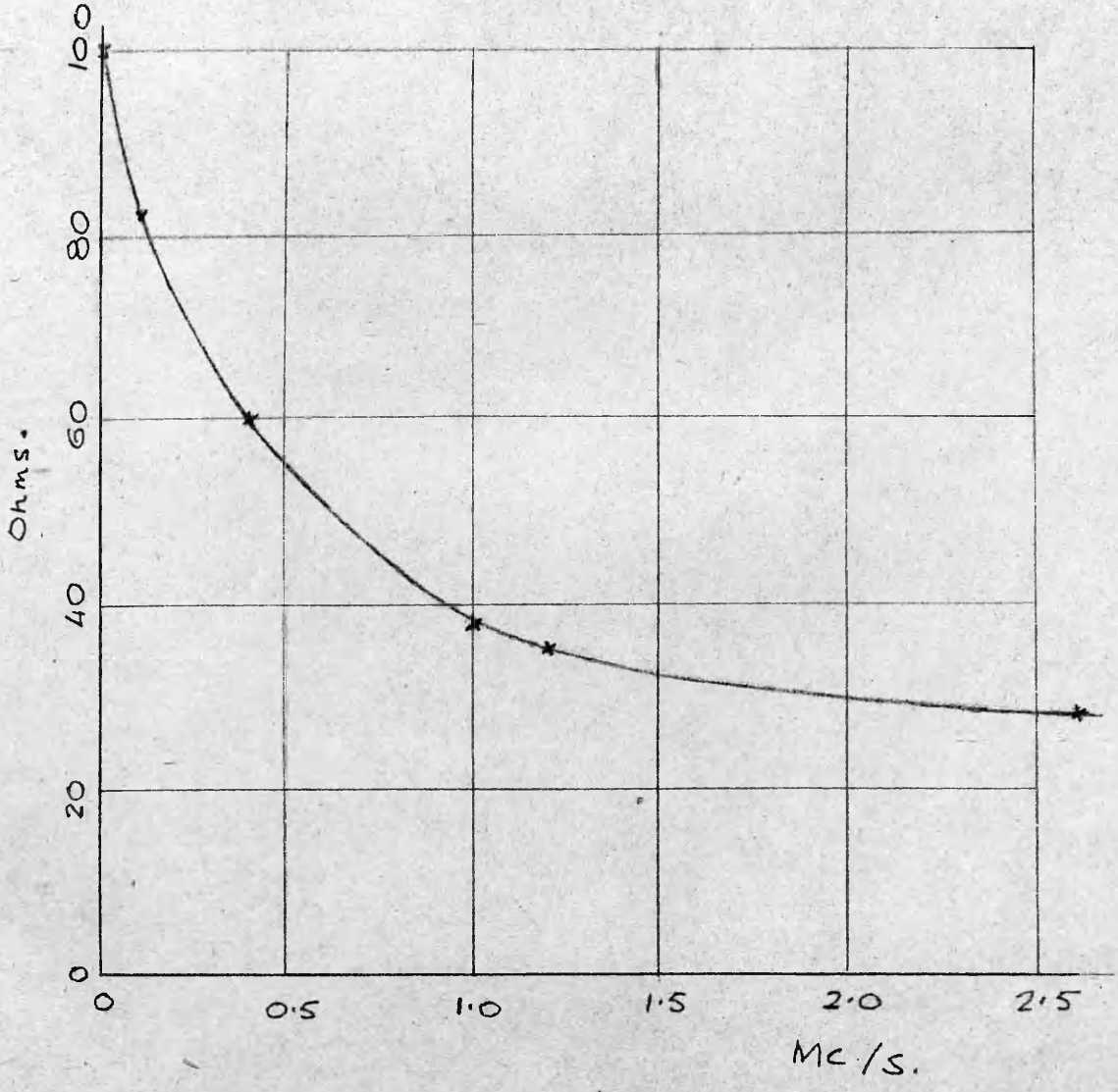

Fig.15. Measured variation of generator winding surge impedance. (Q meter data)

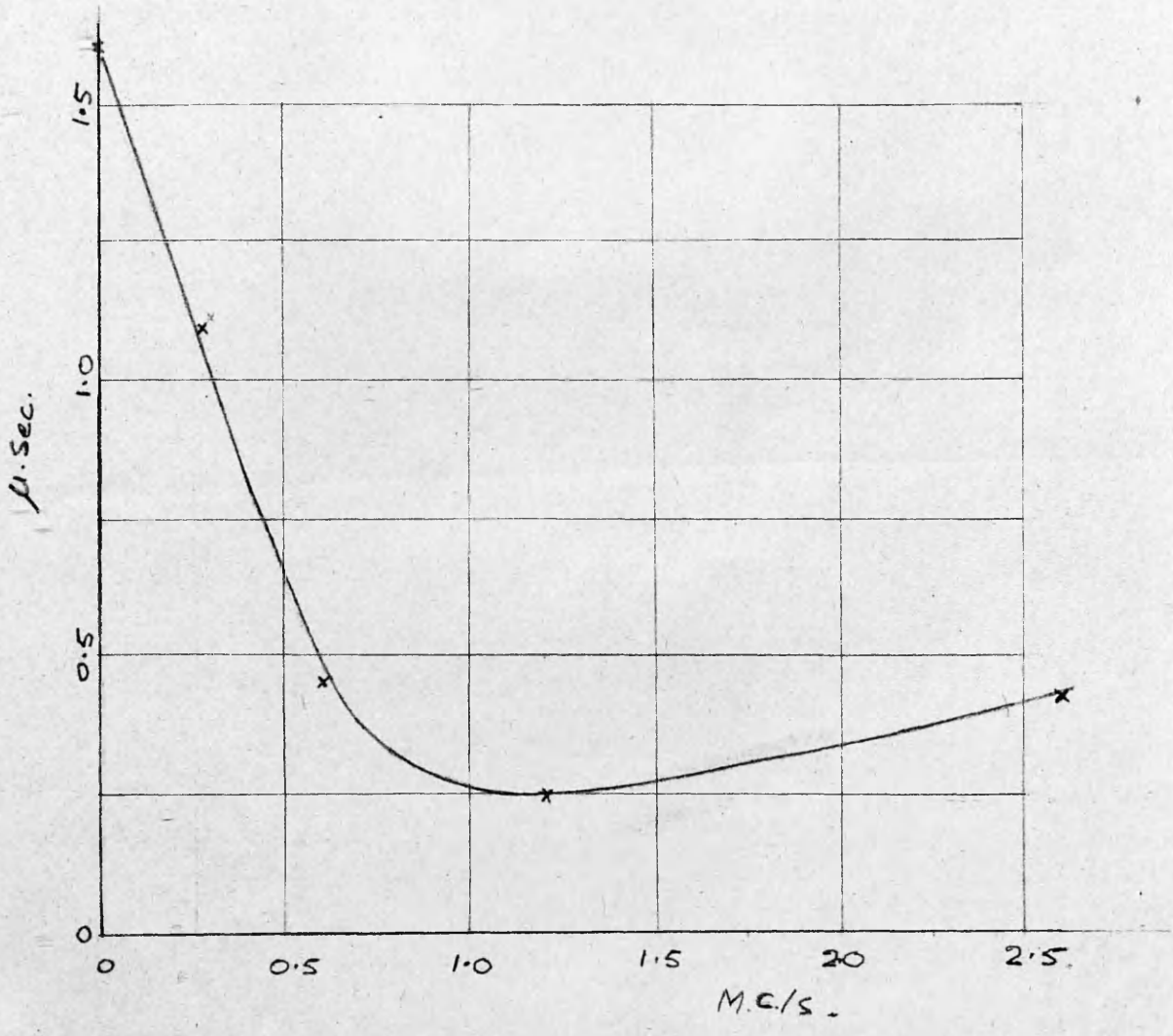

Fig.16. Propagation time along the generator winding. (derived from Q meter data)

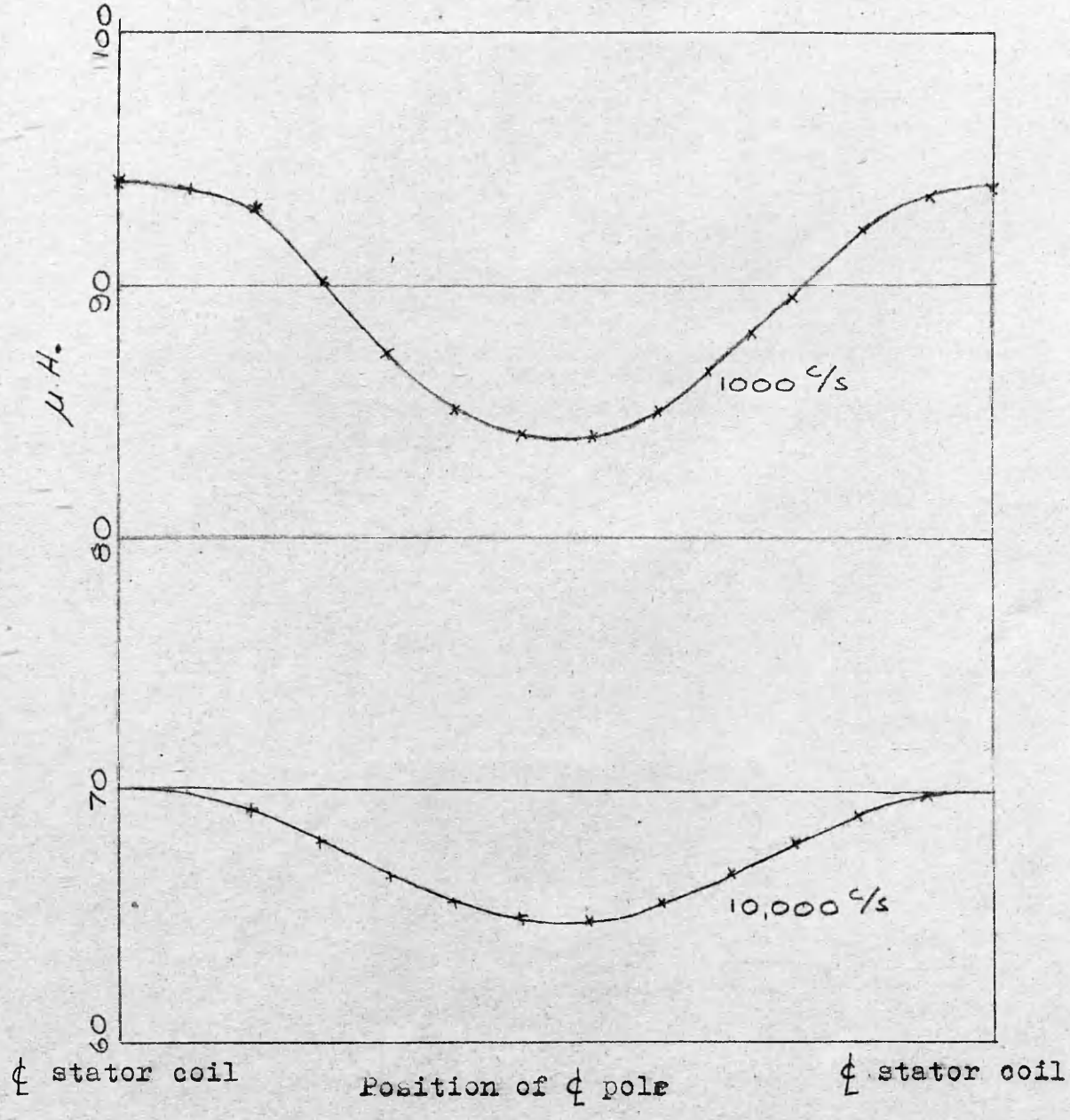

Fig. 17. Variation of winding inductance with rotor position.

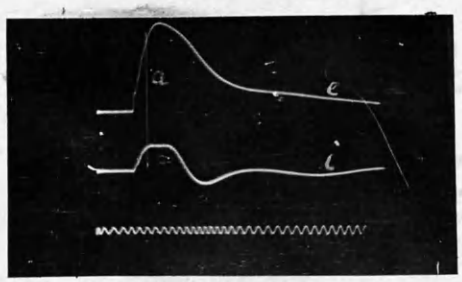

Fig. 18a Transient current response i of generator to voltage impulse e . Surge impedance calculated at point a.

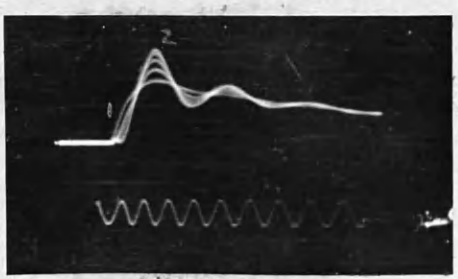

Fig. 18b Voltage response of the open circuited generator winding to an impulse

(i) voltage input

(ii) voltage at the open circuited end of the winding.

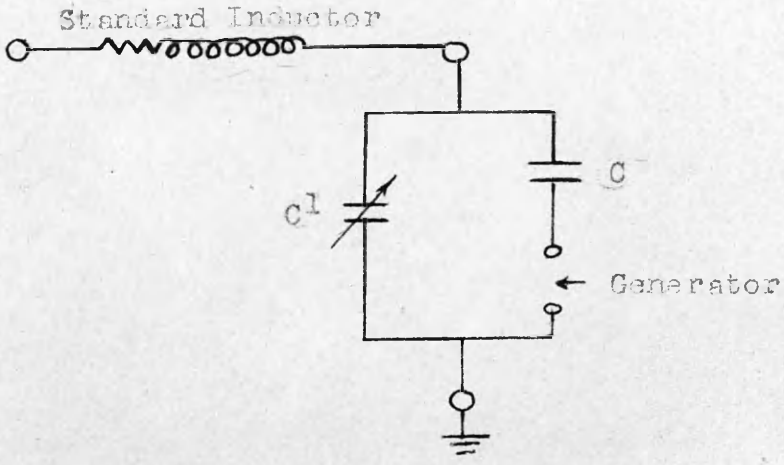

Fig. 19. Circuit for 'Q' meter measurement.

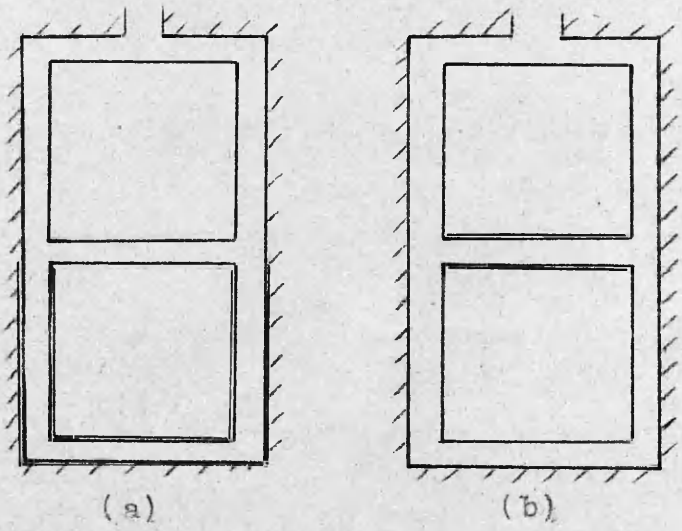

Fig. 20. Apparent current distribution in slot.

(a) Source connected between a conductor and core.

(b) Source connected between two conductors.

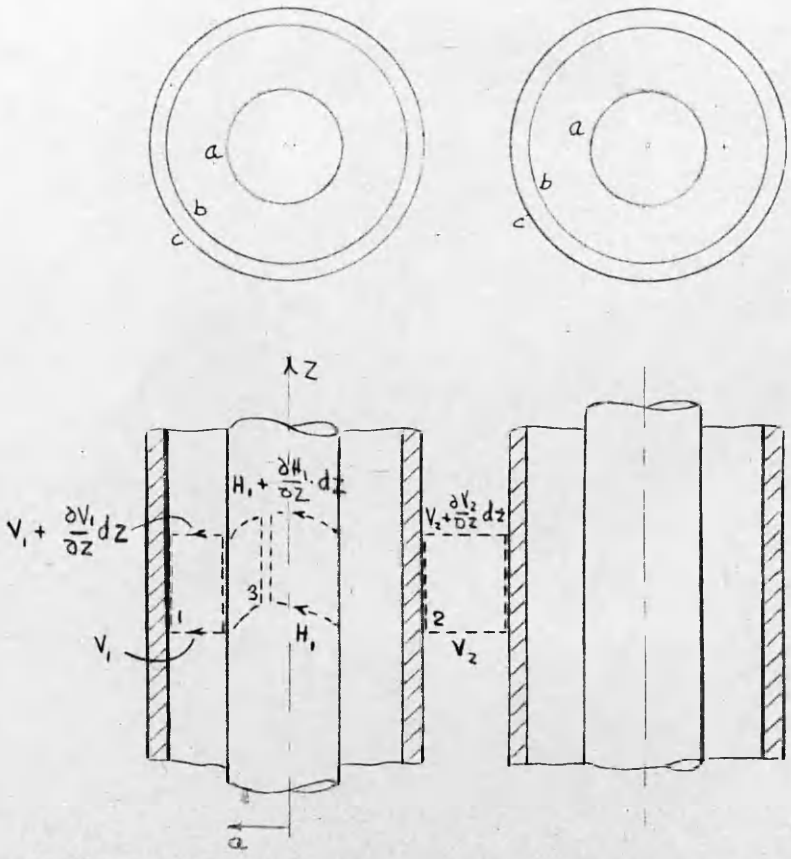

Fig. 21. Cable with individual sheaths.

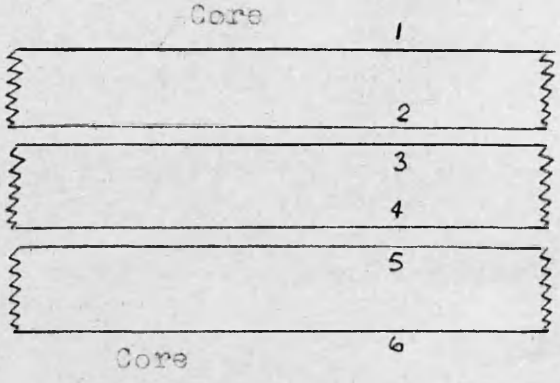

Fig. 22. Equivalent representation of cable.

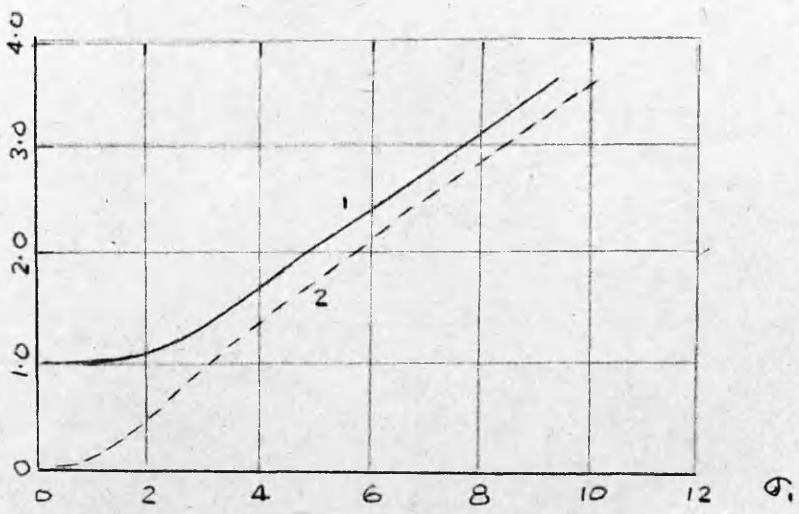

Fig. 23. Skin effect in solid wires.

(1) Ratio of A.C. resistance to D.C.resistance.

(2) Ratio of internal resistance to D.C.resistance.

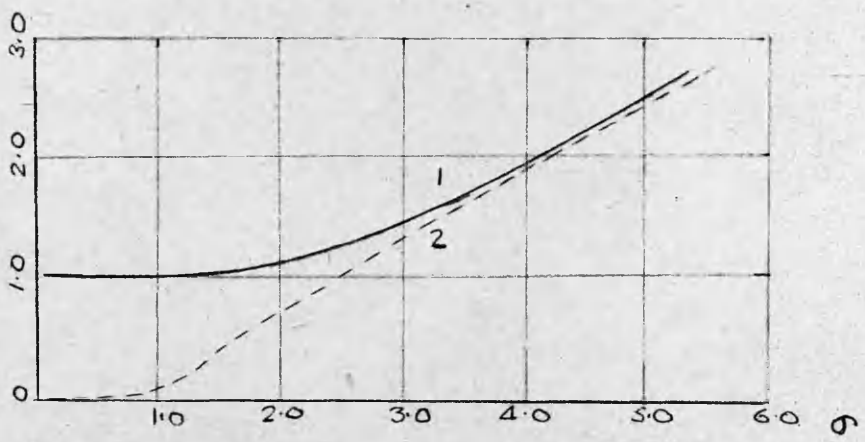

Fig. 24. Skin effect in cylindrical shells.

(1) Ratio of A.C. resistance to D.C.resistance.

(2) Ratio of internal resistance to D.C.resistance.

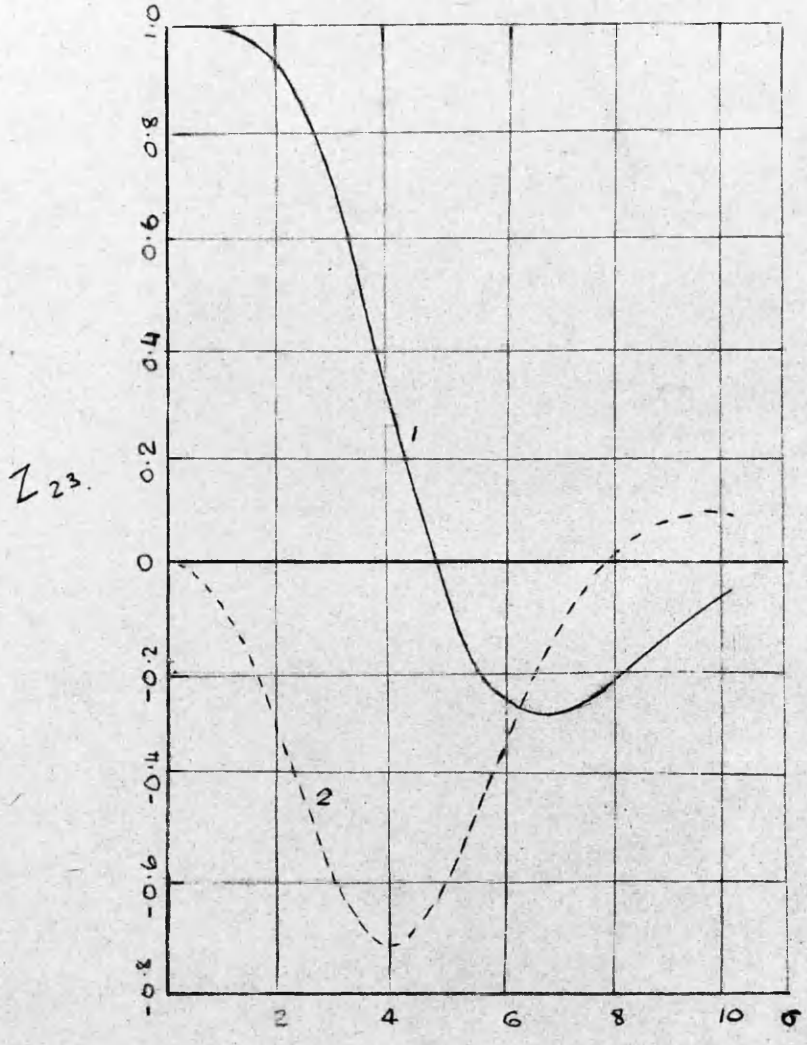

Fig. 25. Ratios of transfer resistance (1), and transfer reactance (2) of a cylindrical shell to its D.C. resistance.

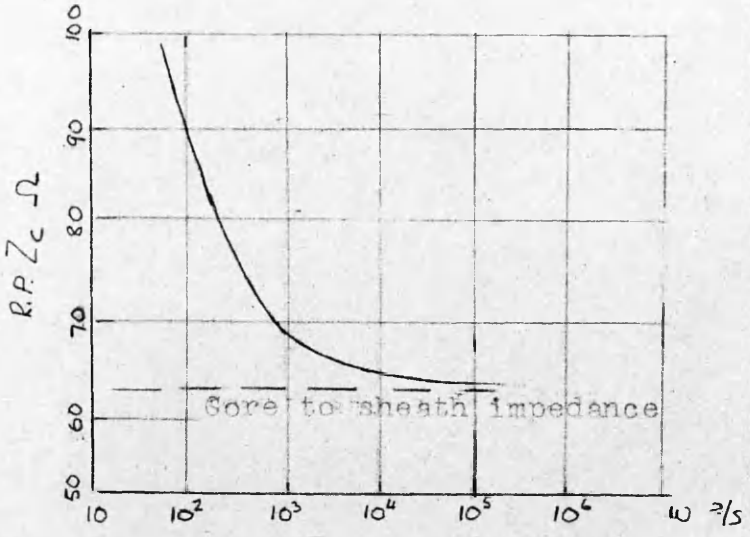

Fig. 26a. Real part of cable surge impedance.

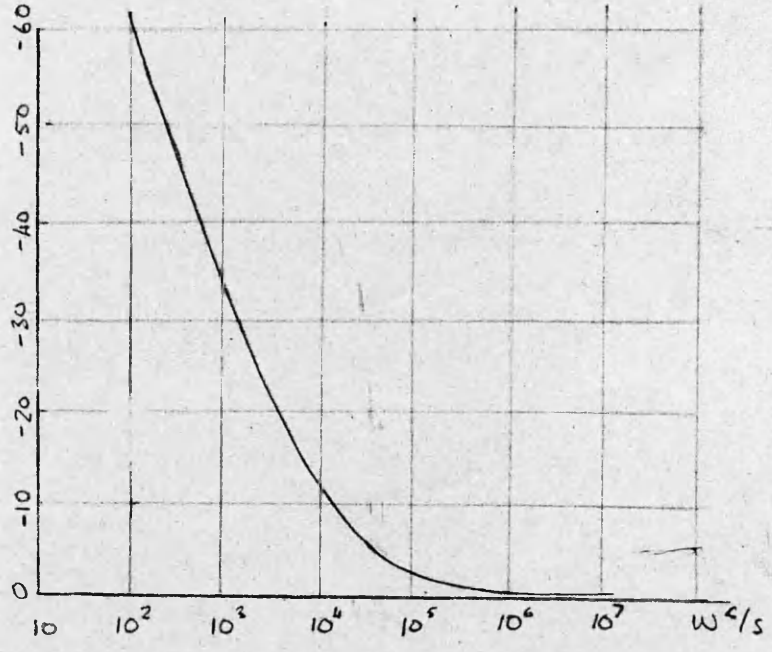

Fig. 26b. Imaginary part of cable surge impedance.

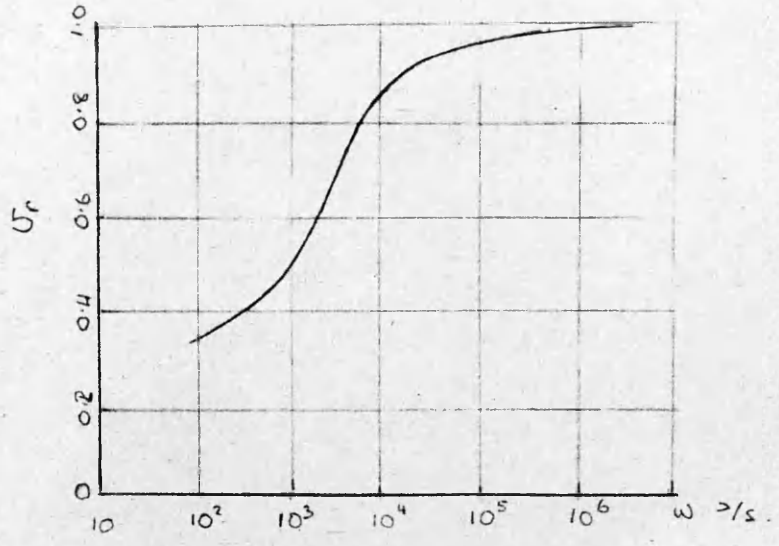

Fig. 27. Relative phase velocity characteristic. of cable.

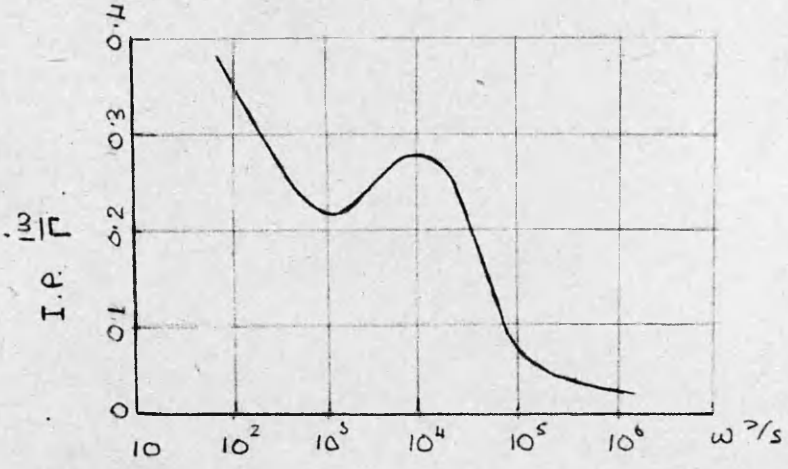

Fig. 28. Attenuation characteristics of cable due only to metal losses.

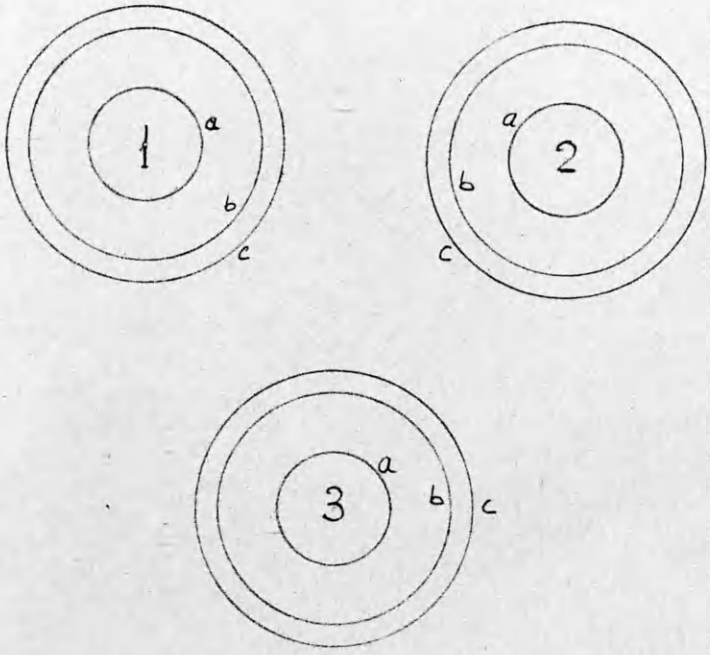

Fig. 29. Three-core coil with individual sheaths.

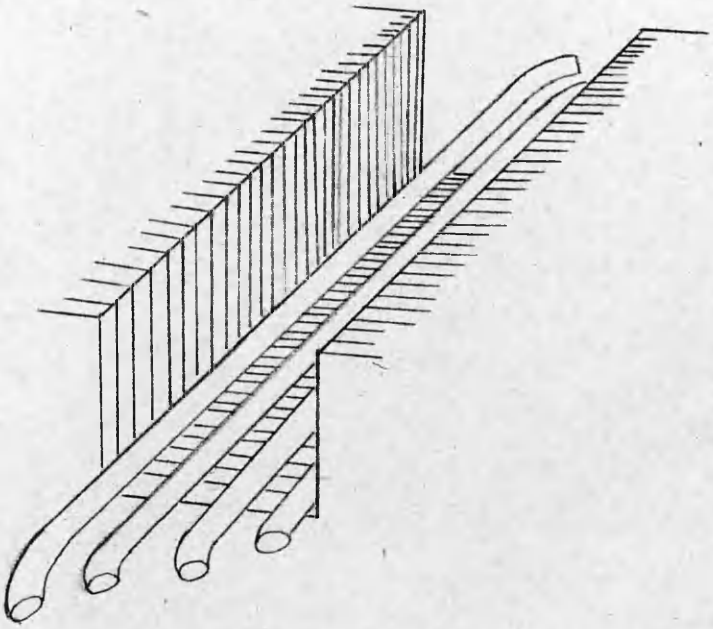

Fig. 30. Generator slot.

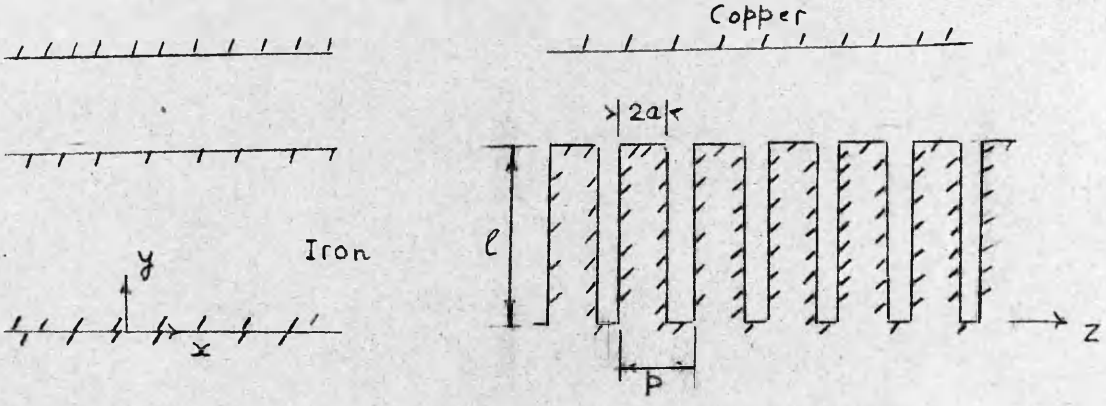

Fig. 31. Theoretical structure of generator.

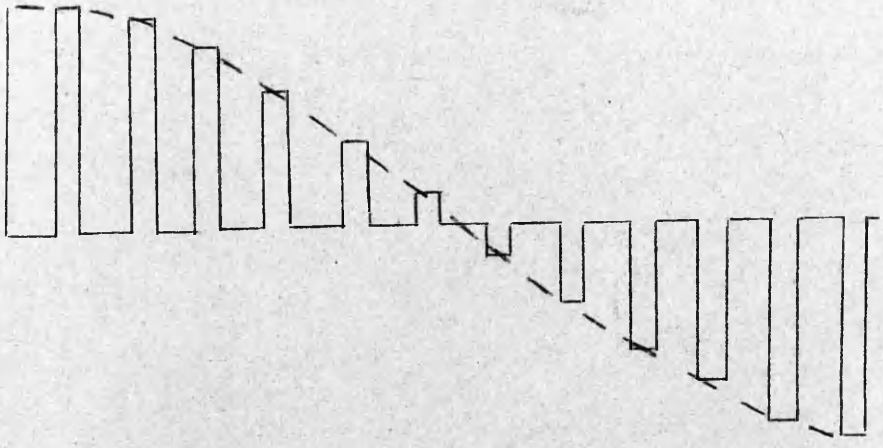

Fig. 32. Electric field at the slot mouths.

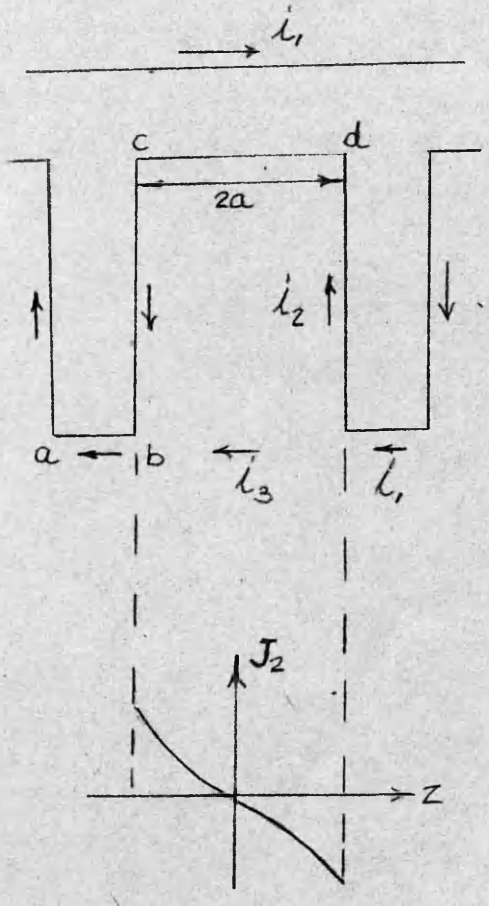

Fig. 33. Current density in the laminations.

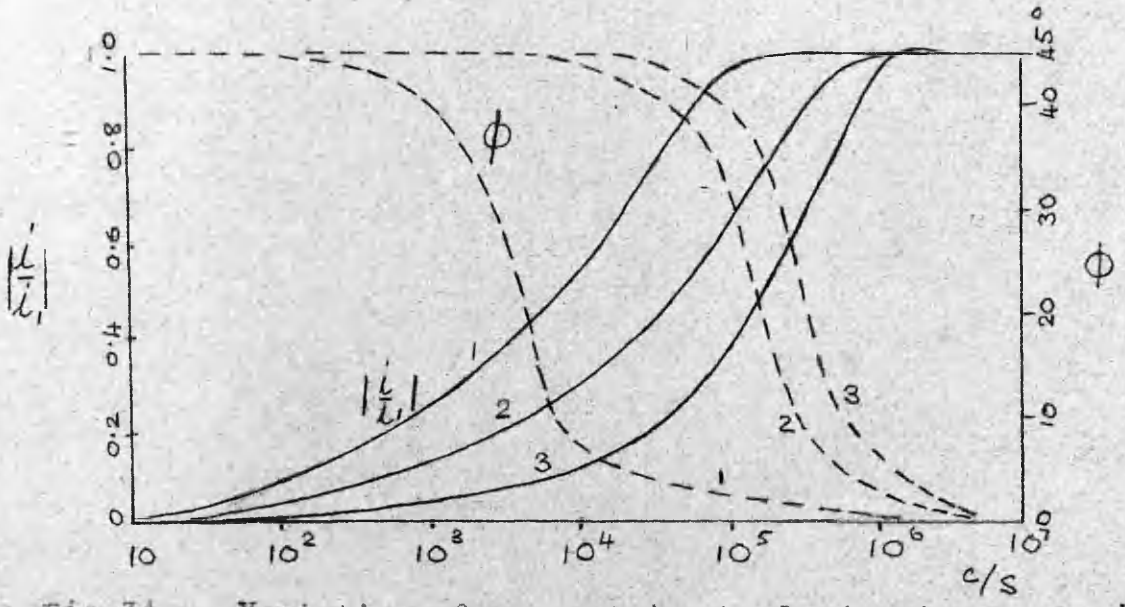

Fig.34. Variation of current in the laminations.

Laminations: (1) u_r = 1000, a = 0.0019cm., = 10^7 v/m.
(2) u_r = 700, a = 0.0019cm., = 10^7 v/m.
(3) u_r = 700, a = 0.00127cm., = 10^7 v/m.

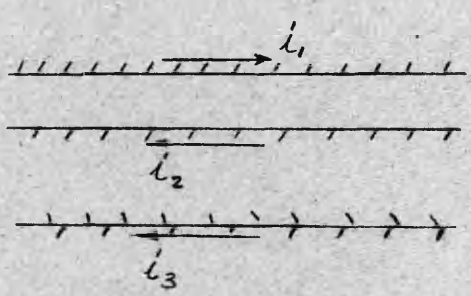

Fig. 35. Current flow in generator.

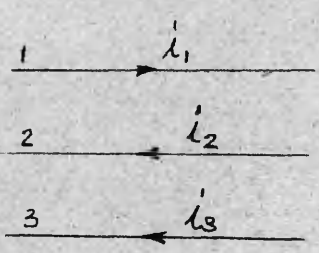

Fig. 36. Three wire transmission line.

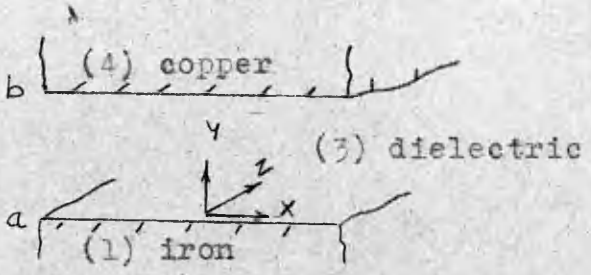

Fig. 37. Wave guide for Z_{12}.

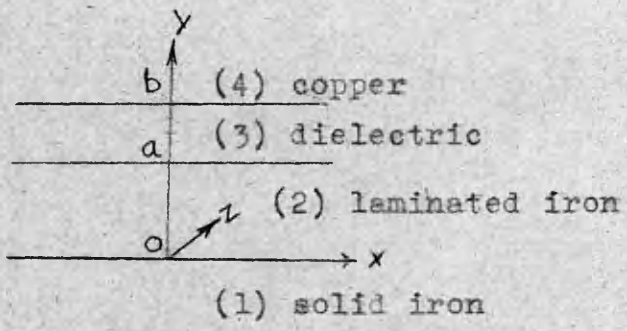

Fig. 38. Wave guide for Z_{13}.

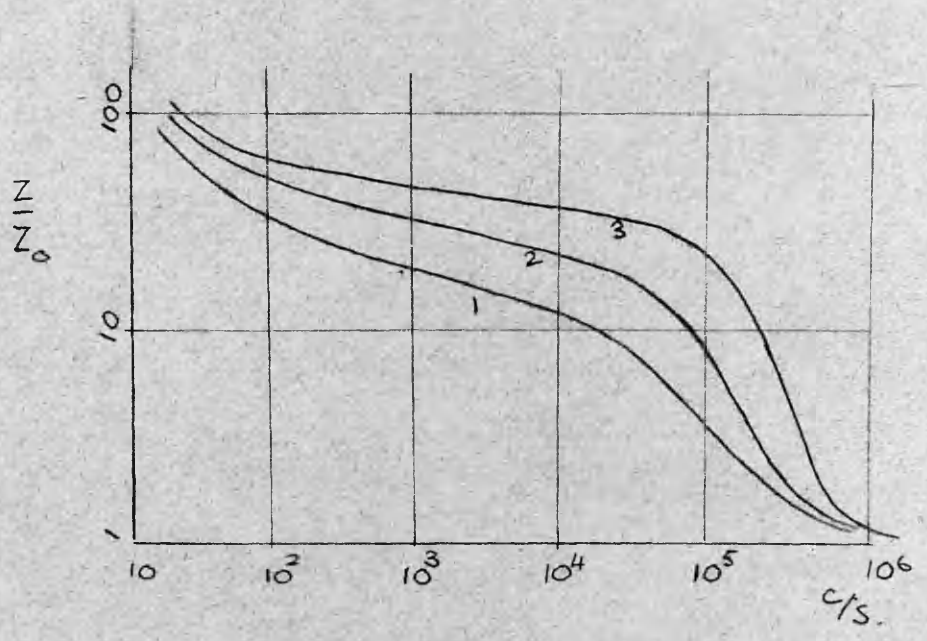

Fig. 39. Variation of surge impedance.

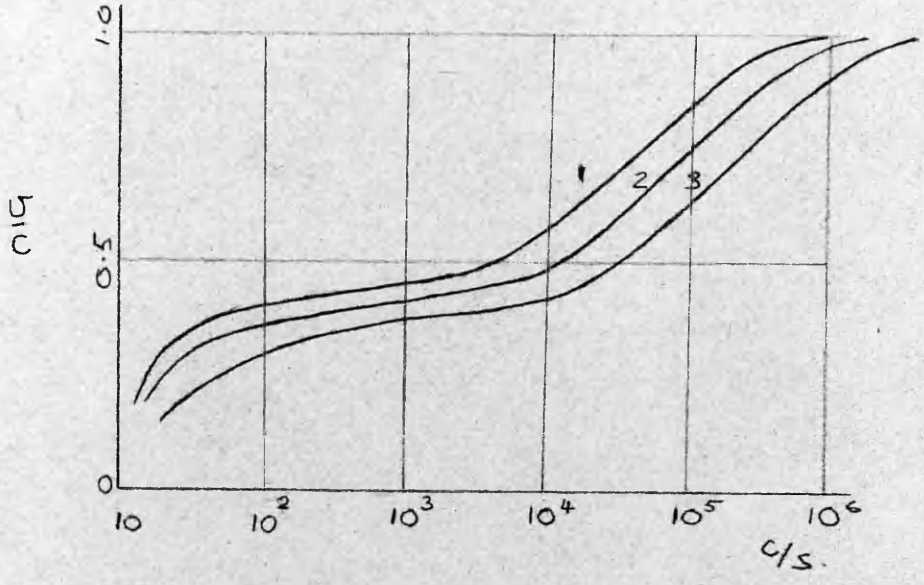

Fig.40.Variation of the phase velocity.

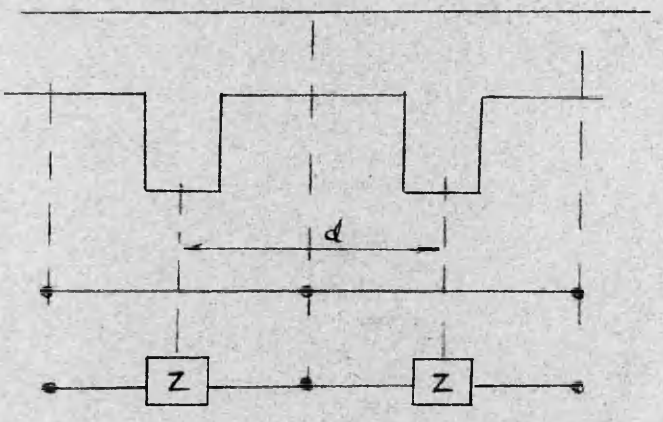

Fig. 41. Periodic guide and its equivalent circuit.

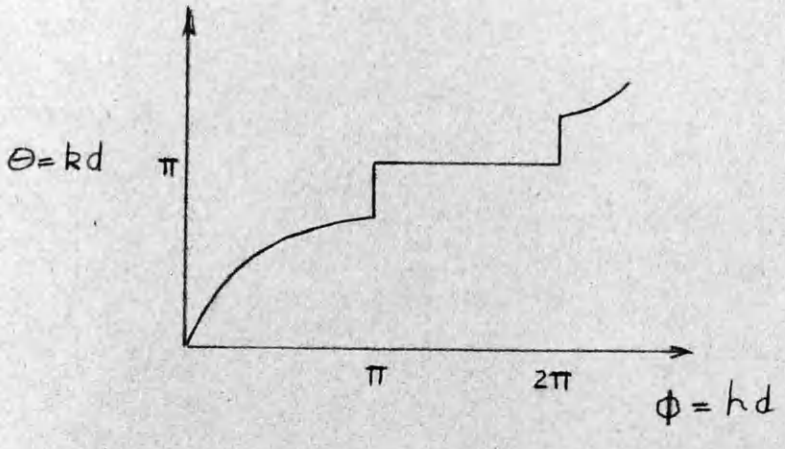

Fig. 42. Frequency characteristic of periodic line.

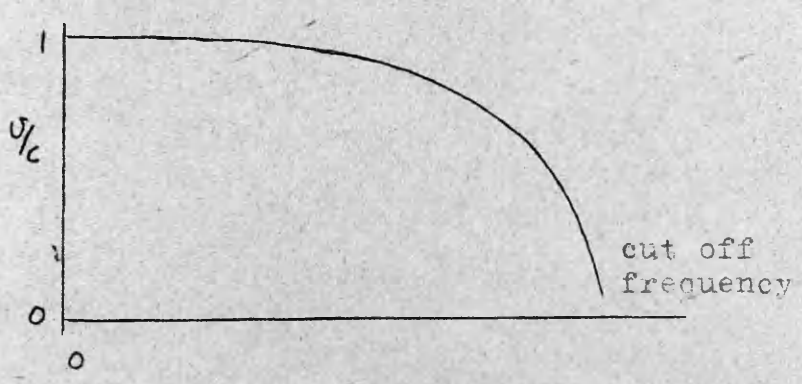

Fig. 43. Phase velocity in the generator slot neglecting losses.

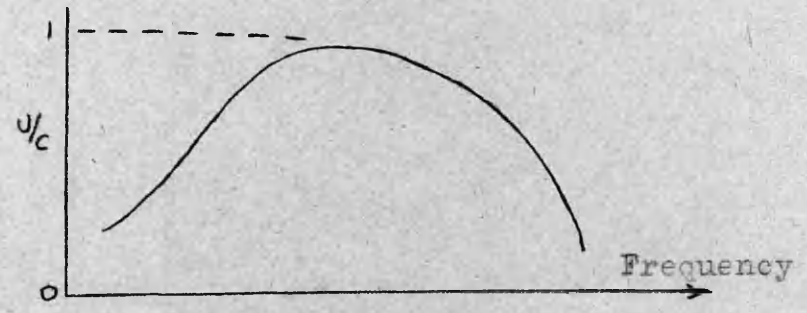

Fig. 44. The complete phase velocity characteristic.

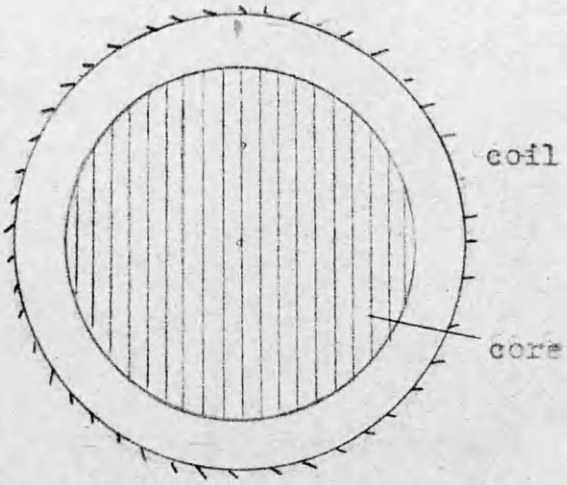

Fig. 45. Simplified cross- section of transformer.

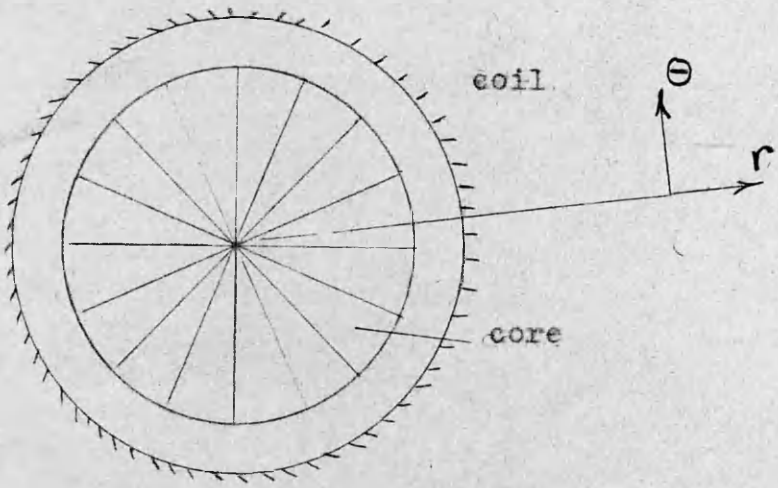

Fig. 46. Ideal transformer core.

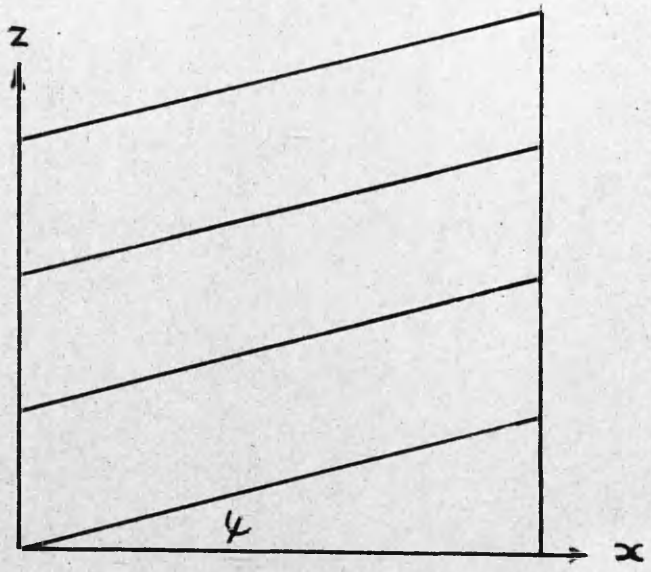

Fig. 47. Coil represented as a sheath conducting in one direction.

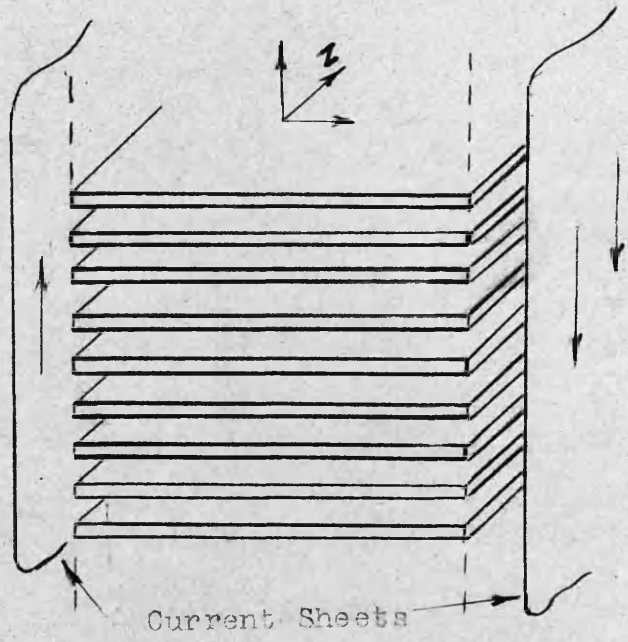

Fig. 48. A stack of laminations between two current sheets.

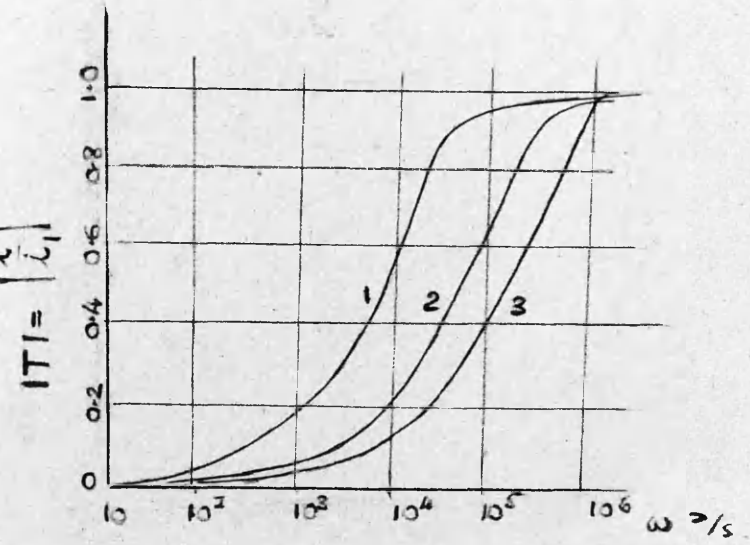

Fig. 49. Modulus of current in lamination

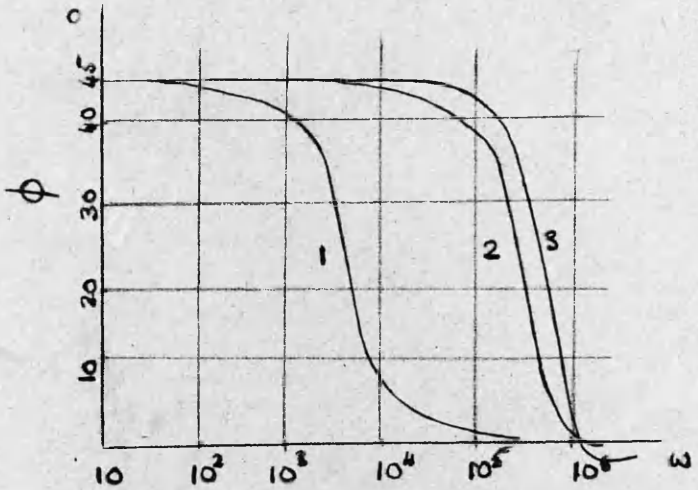

Fig. 50. Relative phase of lamination current.

Laminations: (1) μ_r = 1000, a = 0.019 cm., $\sigma = 10^7$ v/m.

(2) μ_r = 700, a = 0.019 cm., $\sigma = 10^7$ v/m.

(3) μ_r = 700, a = 0.0127 cm., $\sigma = 10^7$ v/m.

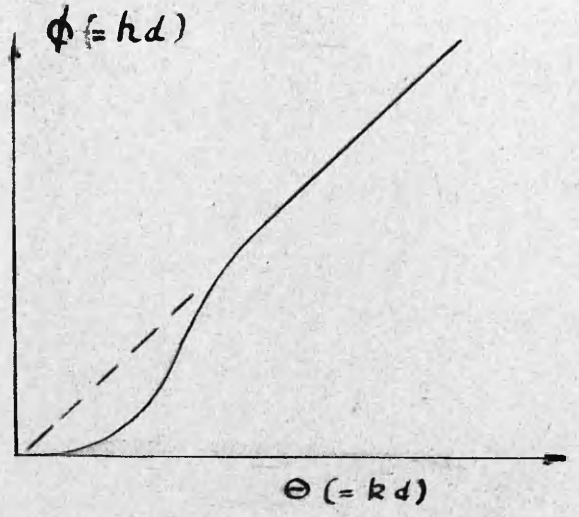

Fig. 51. Frequency characteristic of coil with anisotropic core.

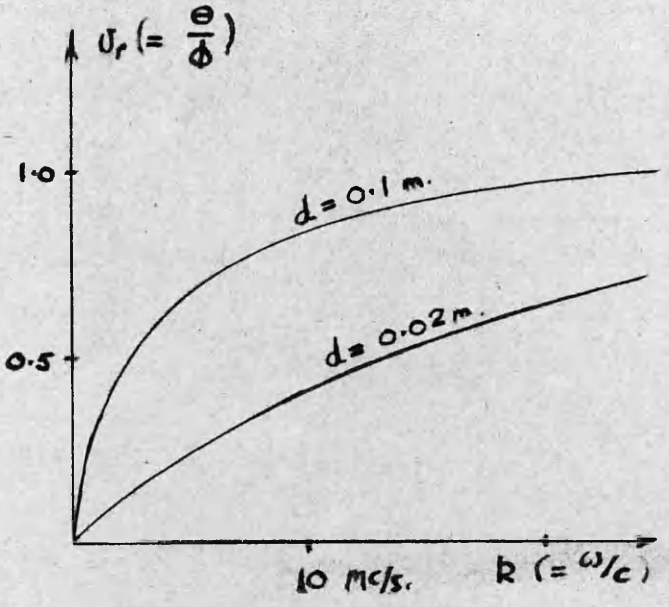

Fig. 52. Phase velocity characteristic of coil with anisotropic core.

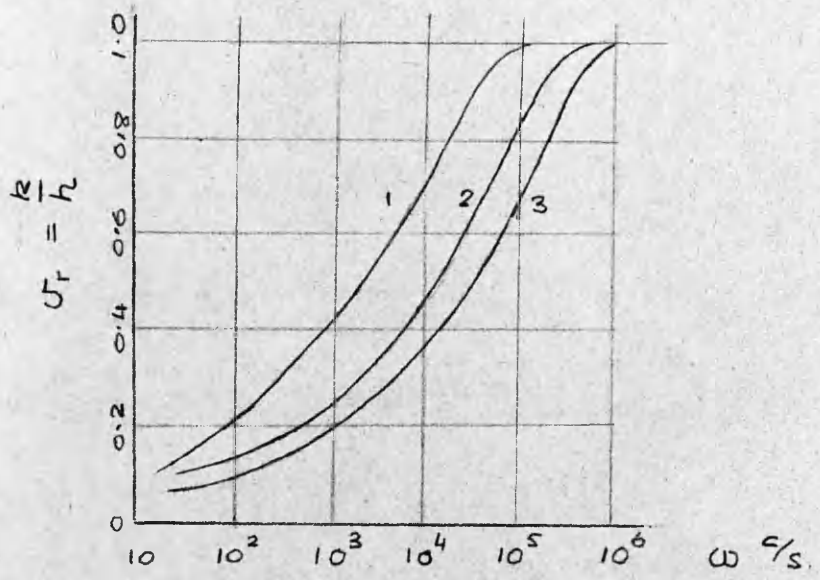

Fig. 53. Relative phase velocity characteristics of coil with laminated core.

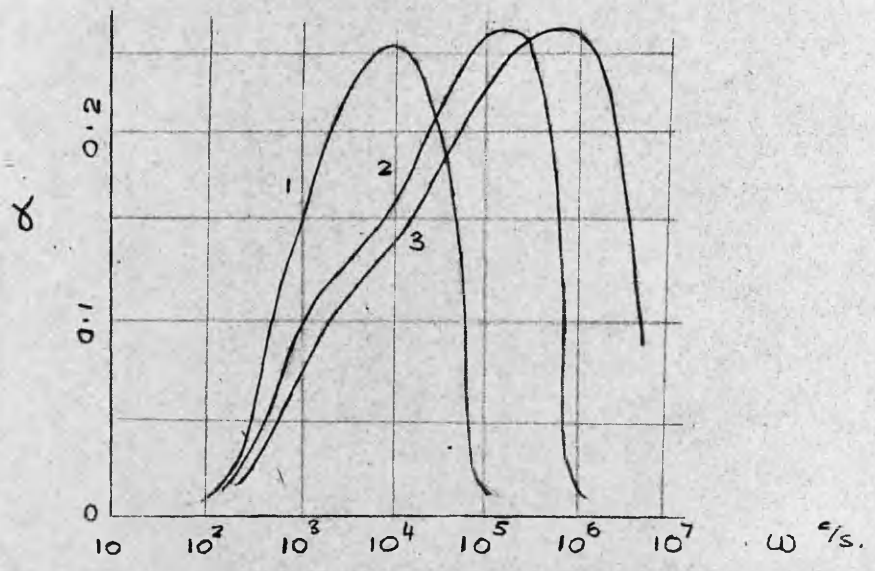

Fig. 54. Attenuation characteristics of coil with laminated core.

Laminations: (1) μ_r = 1000, a = 0.0019cm., $\sigma = 10^7$ v/m.
(2) μ_r = 700, a = 0.0019cm., $\sigma = 10^7$ v/m.
(3) μ_r = 700, a = 0.00127cm., $\sigma = 10^7$ v/m.

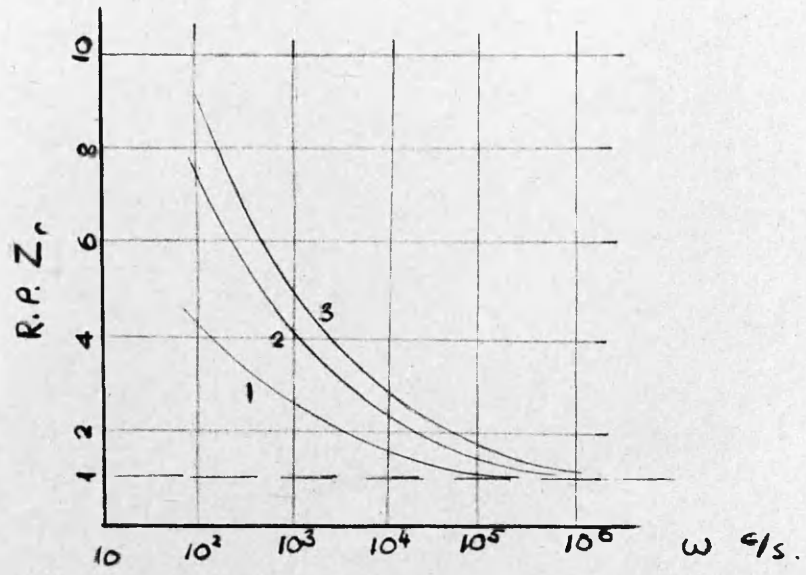

Fig. 55. Surge impedance characteristics of coil with laminated core.

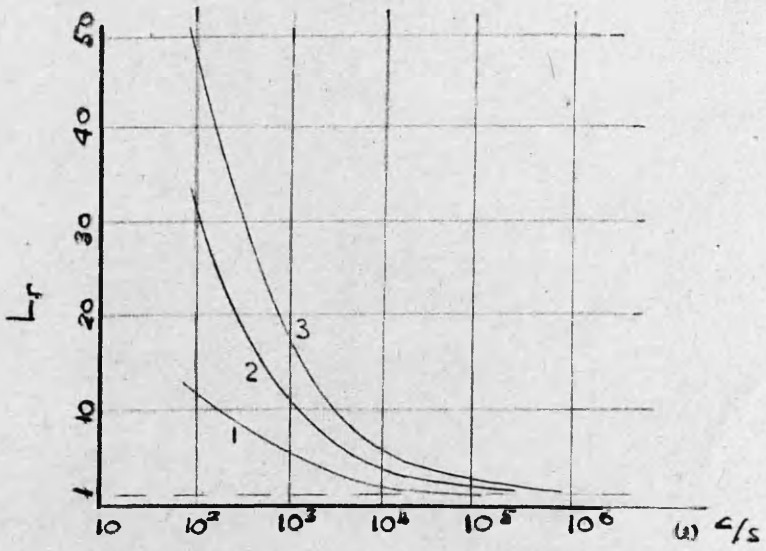

Fig. 56. Inductance characterics of coil with laminated core.

Laminations: (1) μ_r = 1000, a = 0.0019cm., $\sigma = 10^7$ v/m .
(2) μ_r = 700, a = 0.0019cm., $\sigma = 10^7$ v/m .
(3) μ_r = 700, a = 0.00127cm., $\sigma = 10^7$ v/m .

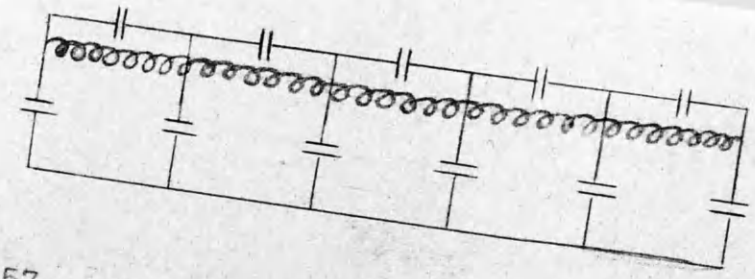

Fig. 57. Equivalent circuit of transformer and generator.

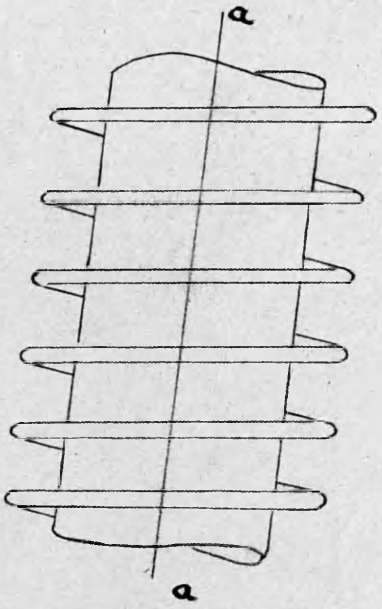

Fig. 58. Single layer transformer coil.

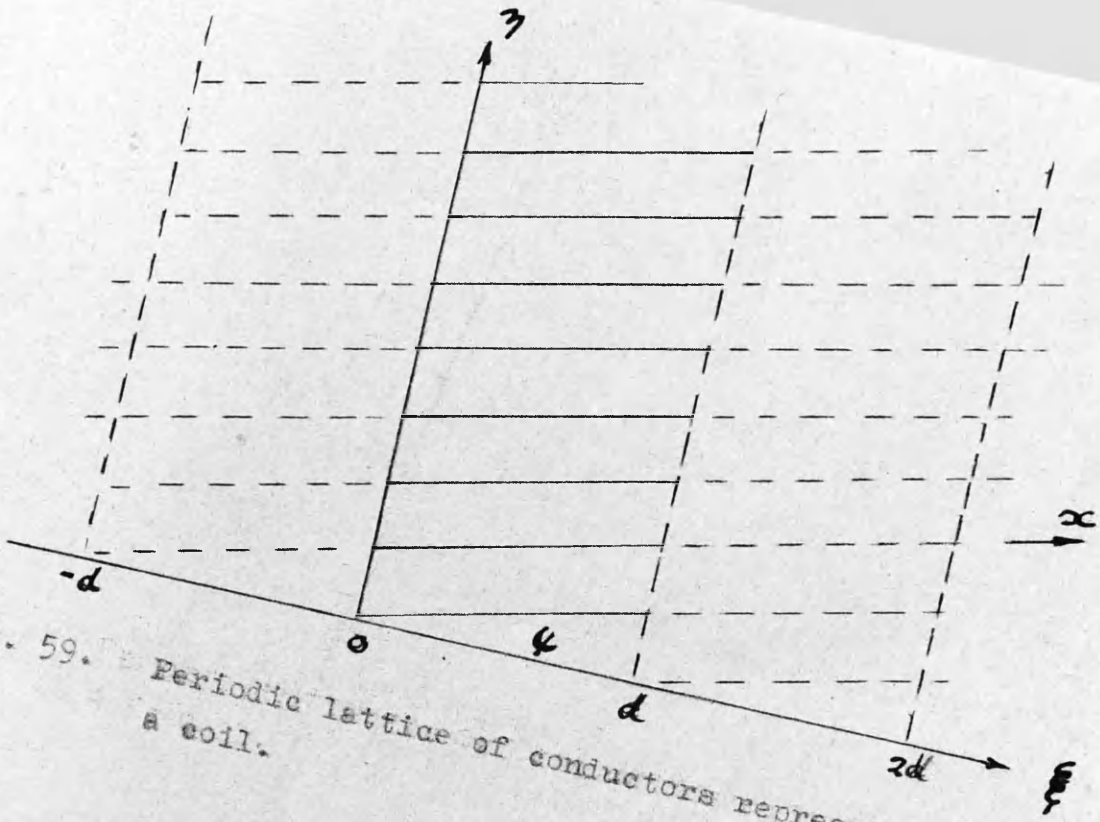

Fig. 59. Periodic lattice of conductors representing a coil.

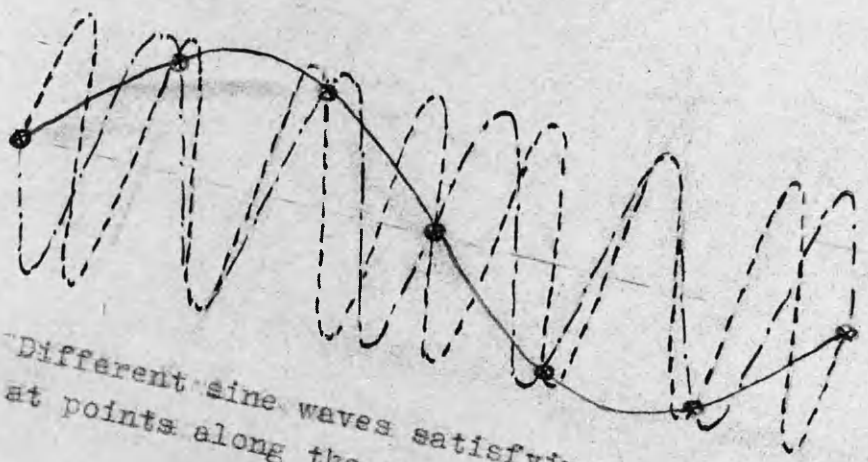

Fig. 60. Different sine waves satisfying the voltages at points along the coil cut by line $\xi = 0$

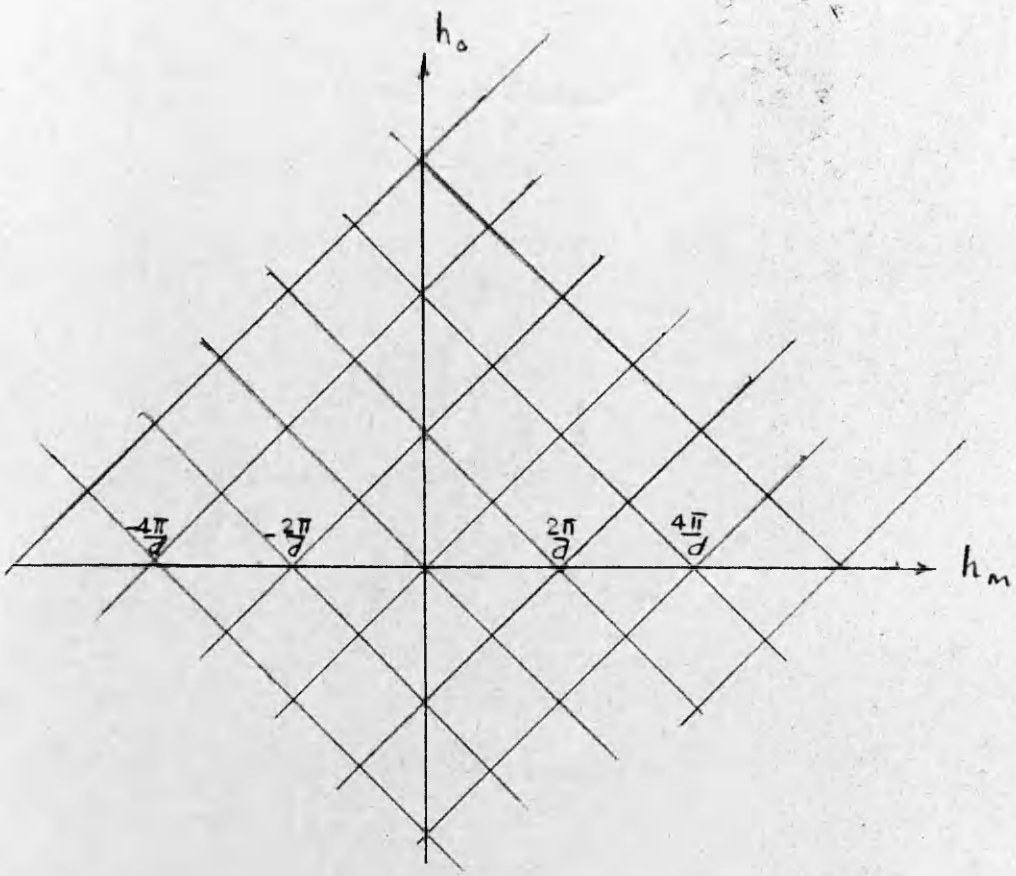

Fig. 61. Frequency characteristic of coil.

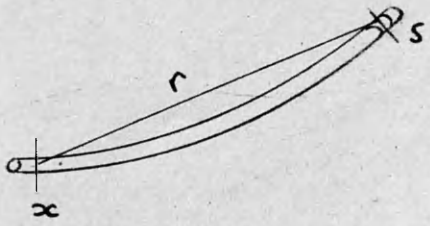

Fig. 62. Definition of retardation distance.

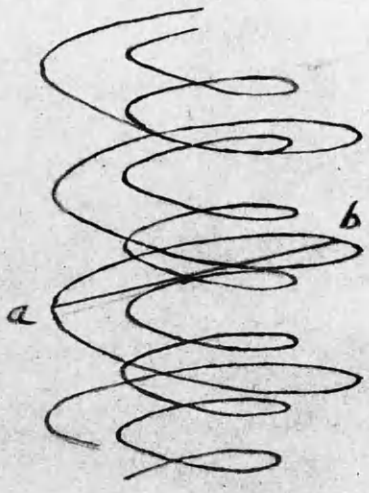

Fig. 63. Double helical coil.

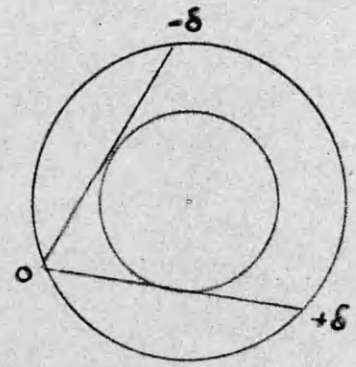

Fig. 64. Cross section of a transformer coil and core indicating the range of interaction of the currents.

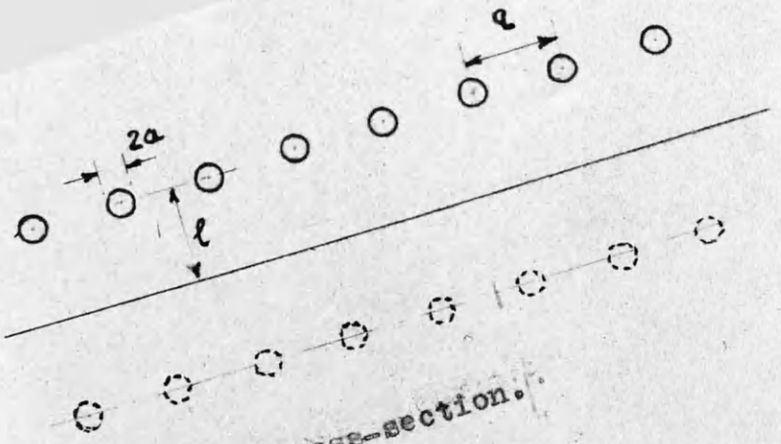

Fig.65. Coil cross-section.

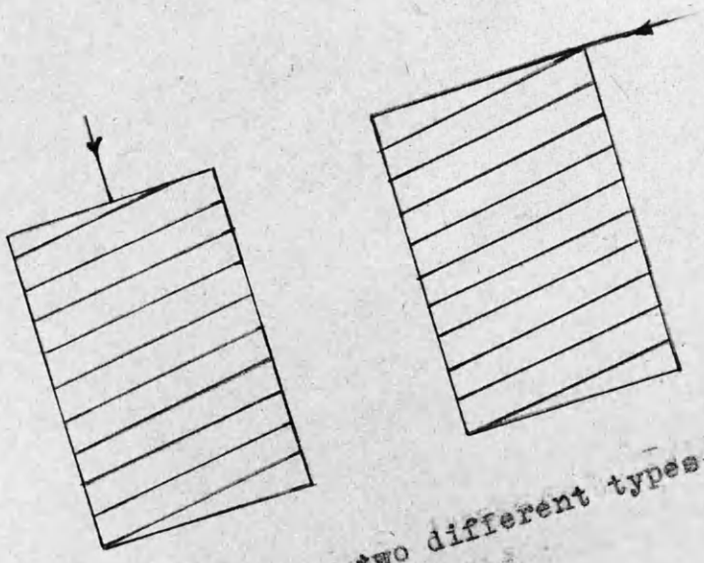

Fig. 66. Indicating two different types of connection to coils.

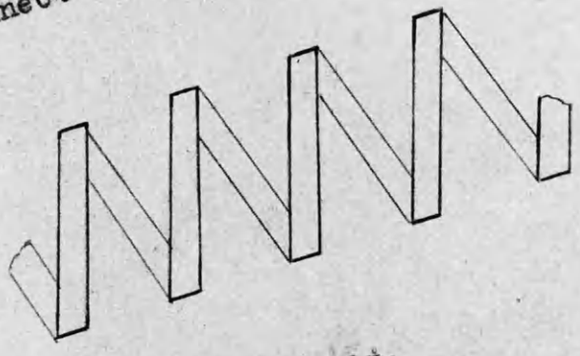

Fig. 67. Tape helix.

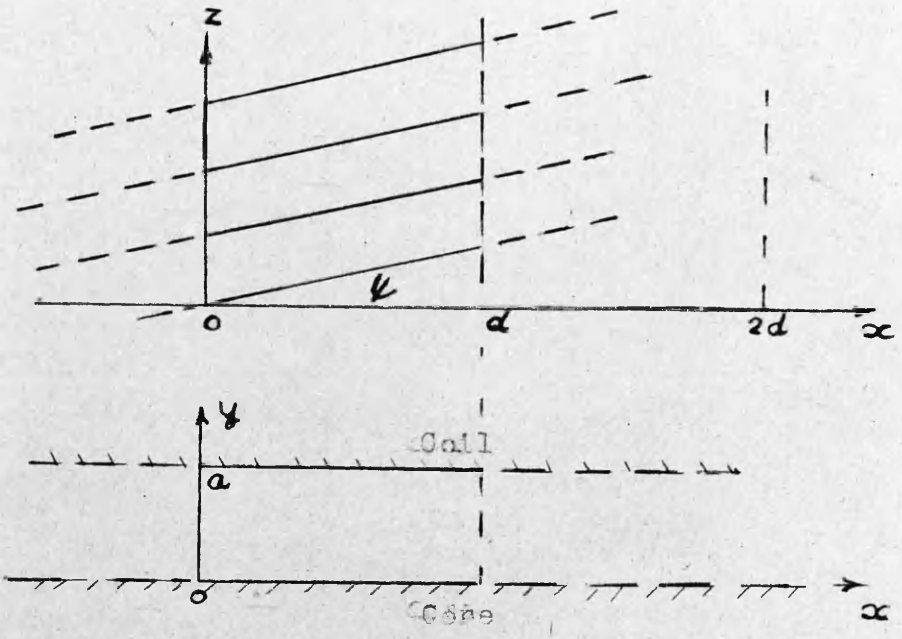

Fig. 68. Equivalent coil structure.

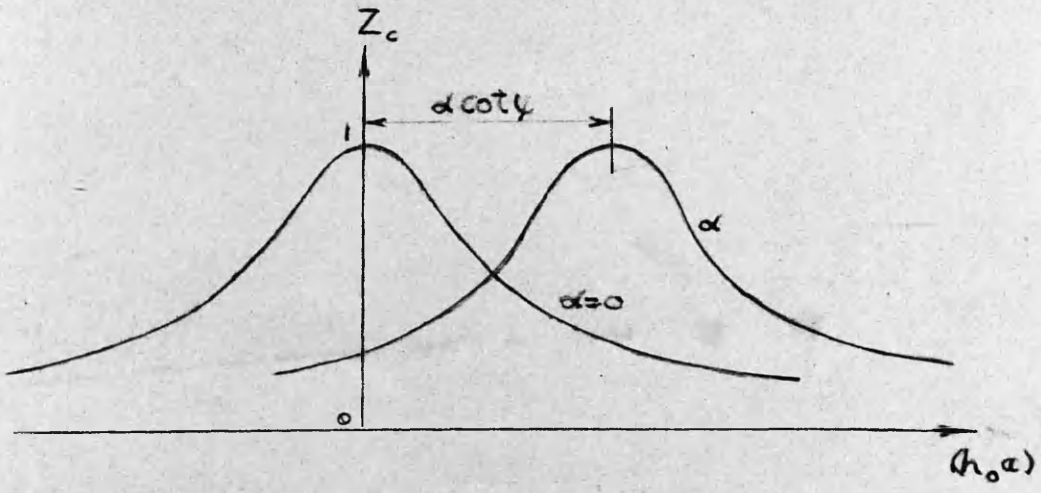

Fig. 69. Variation of surge impedance of coil for natural helix modes.

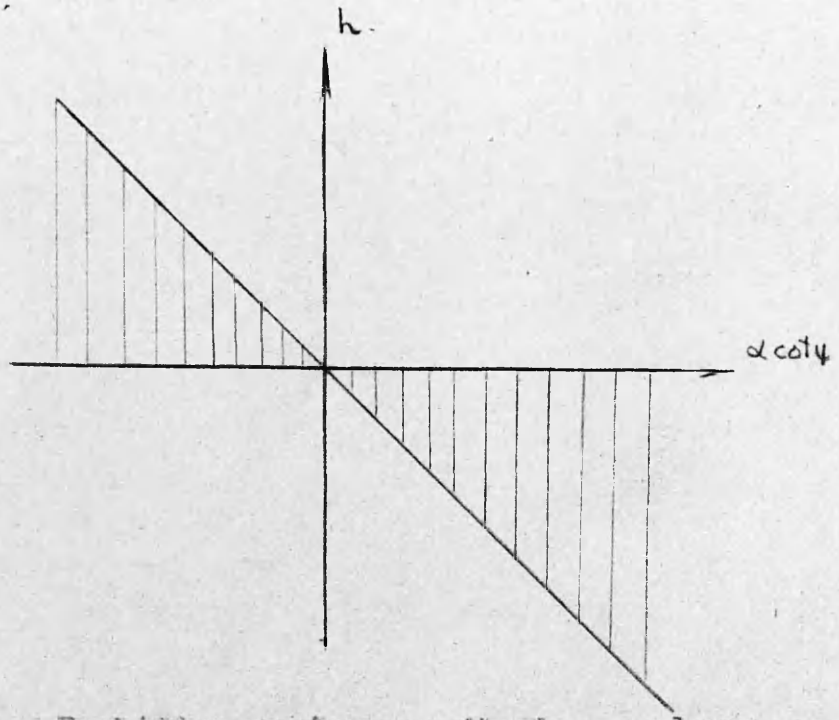

Fig. 70. Forbidden regions on the h - plane. for propagation along a semi-infinite coil.

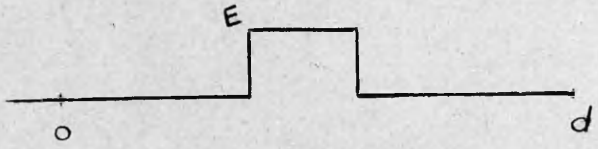

Fig. 71. Voltage source at Z = 0.

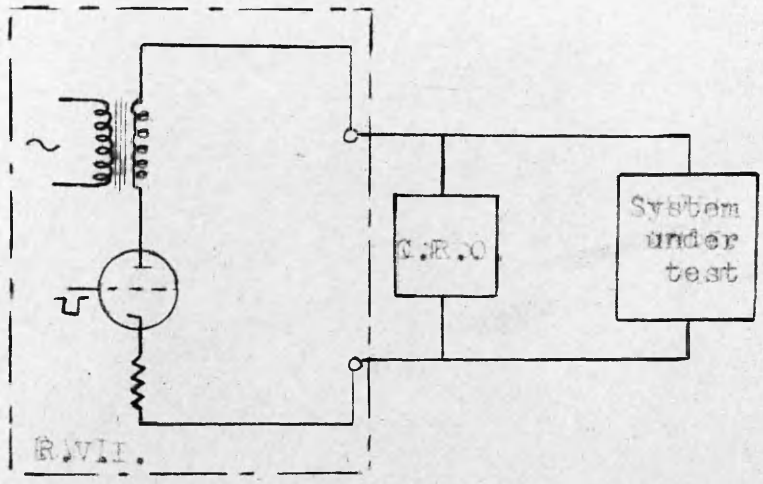

Fig. 72. R.V.I. Injection Circuit.

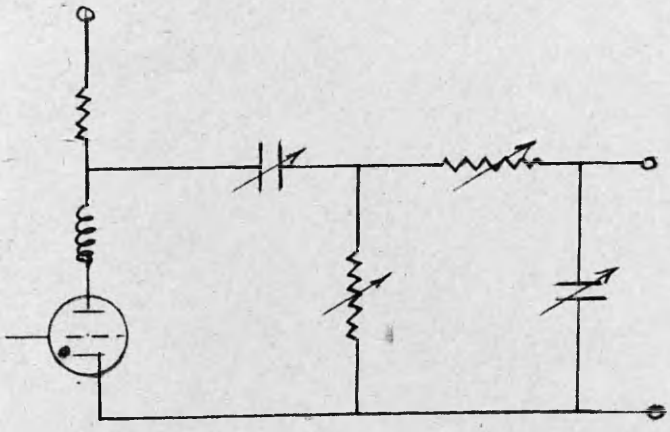

Fig. 73. Basic Circuit of R.S.G.

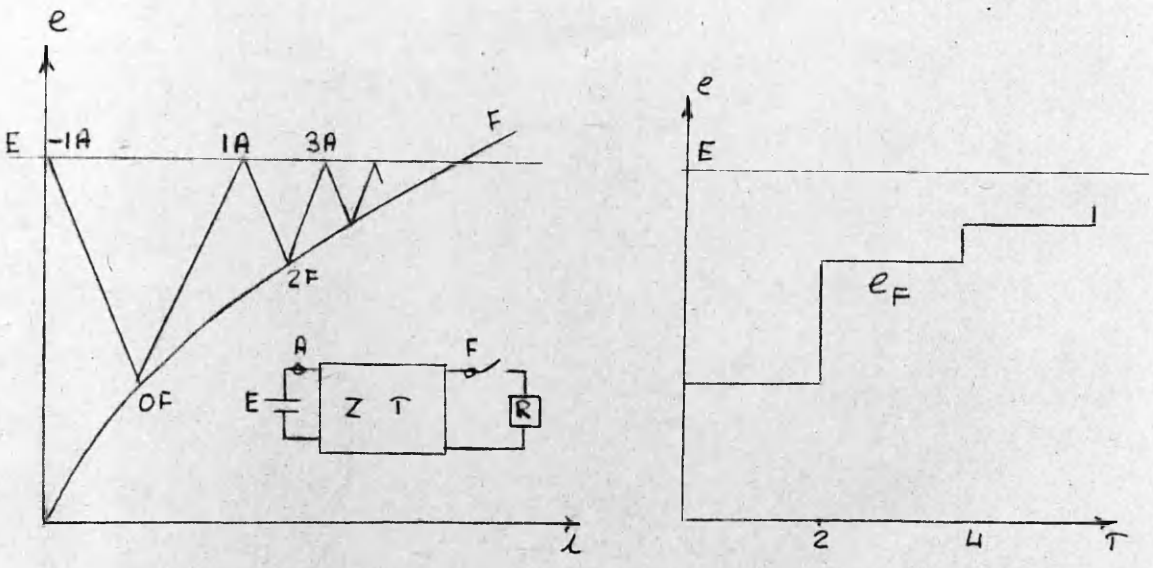

Fig. 74. Transient conditions on a line terminated by a non-linear resistance.

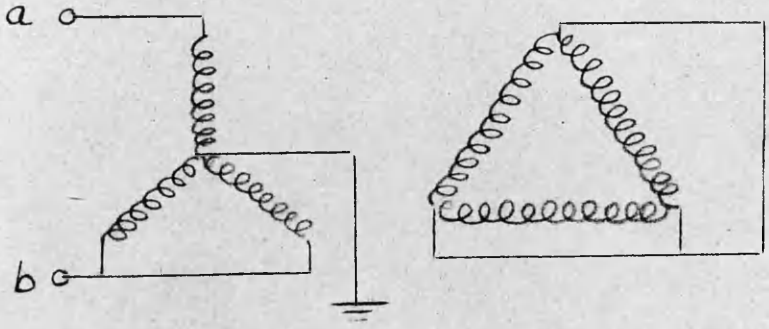

Fig. 75. Transformer connections.

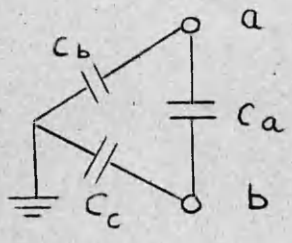

Fig. 76. Instrument terminal capacitances.

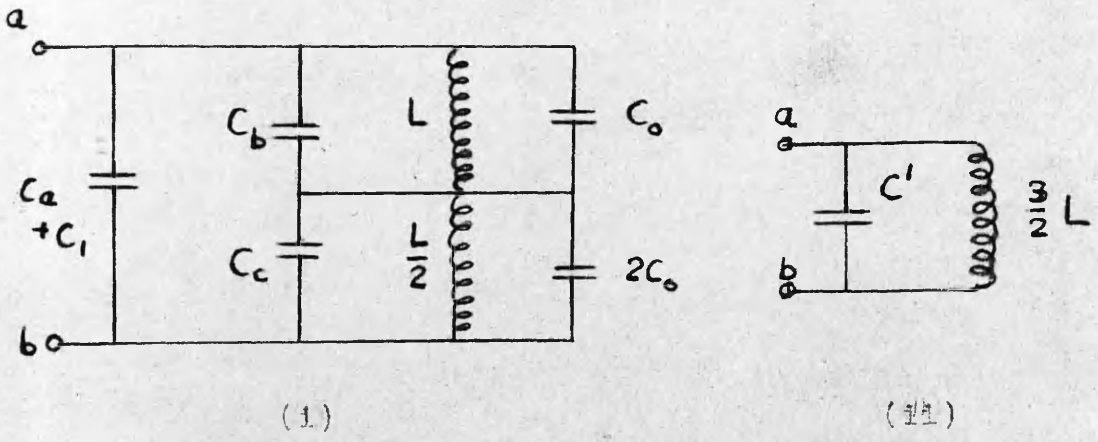

Fig. 77. Equivalent circuit of transformer and instrument.

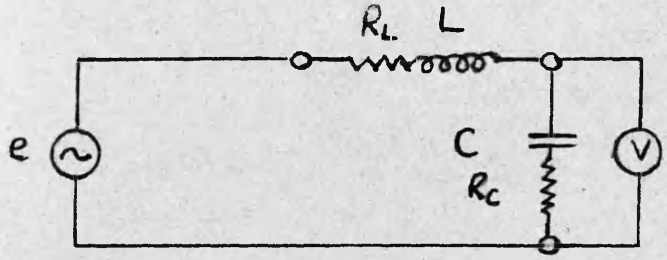

Fig. 78. 'Q' meter circuit.

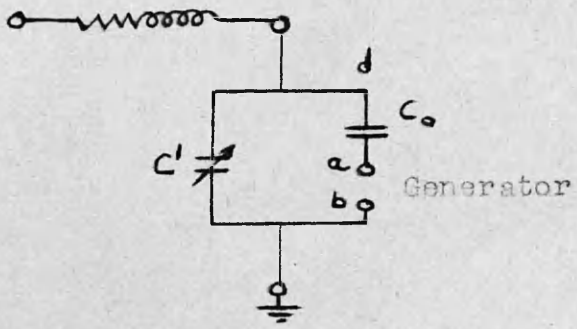

Fig. 79. Circuit for measurement of generator impedance.

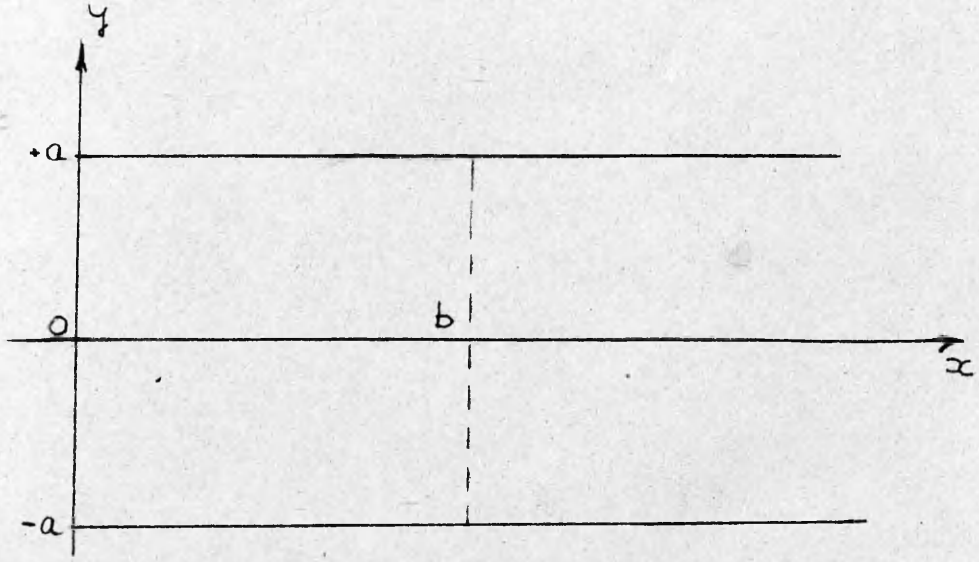

Fig. 80. Generator lamination.

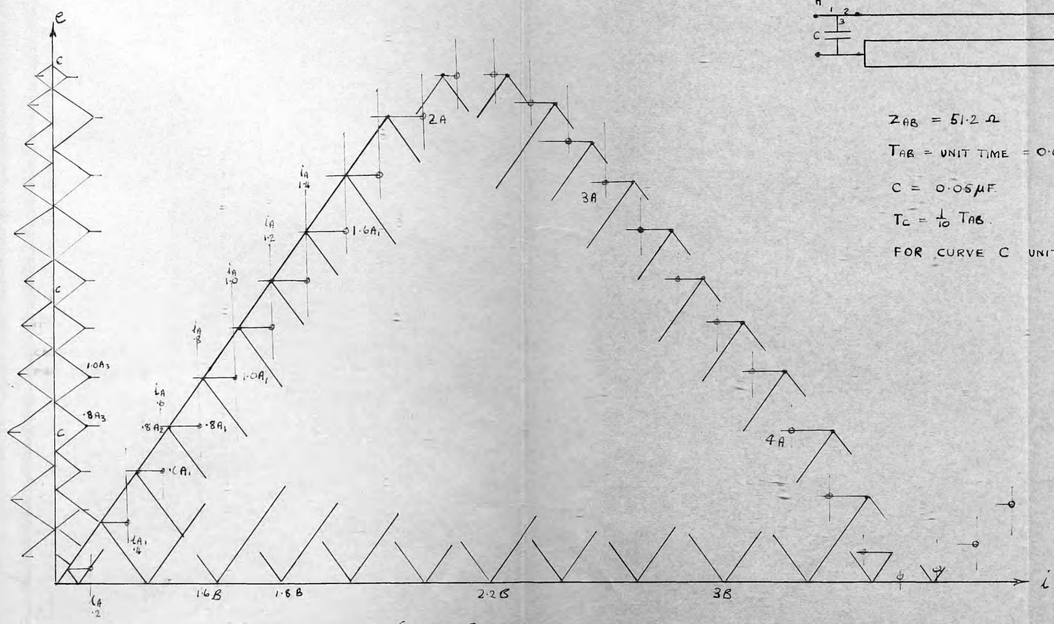

SURGE DIAGRAM

$Z_{AB} = 51{\cdot}2\ \Omega$

T_{AB} = UNIT TIME = 0·0265 m.s.

$C = 0{\cdot}05\mu F$

$T_C = \frac{1}{10} T_{AB}$.

FOR CURVE C UNIT TIME = 1·15 T_{AB}.

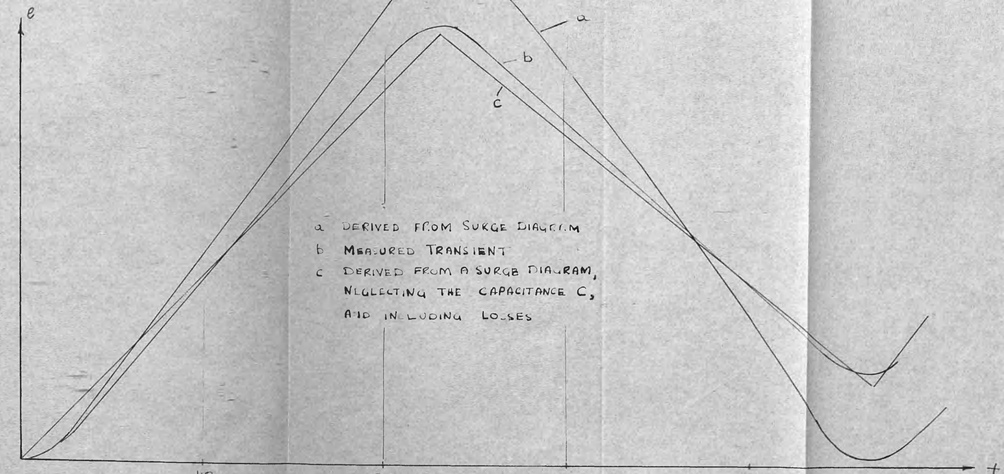

a DERIVED FROM SURGE DIAGRAM

b MEASURED TRANSIENT

c DERIVED FROM A SURGE DIAGRAM, NEGLECTING THE CAPACITANCE C, AND INCLUDING LOSSES

UNITS OF T_{AB}

VOLTAGE AT A

RESPONSE OF A LOSSLESS CABLE TO A SINUSOIDAL CURRENT INPUT

FIG. 81

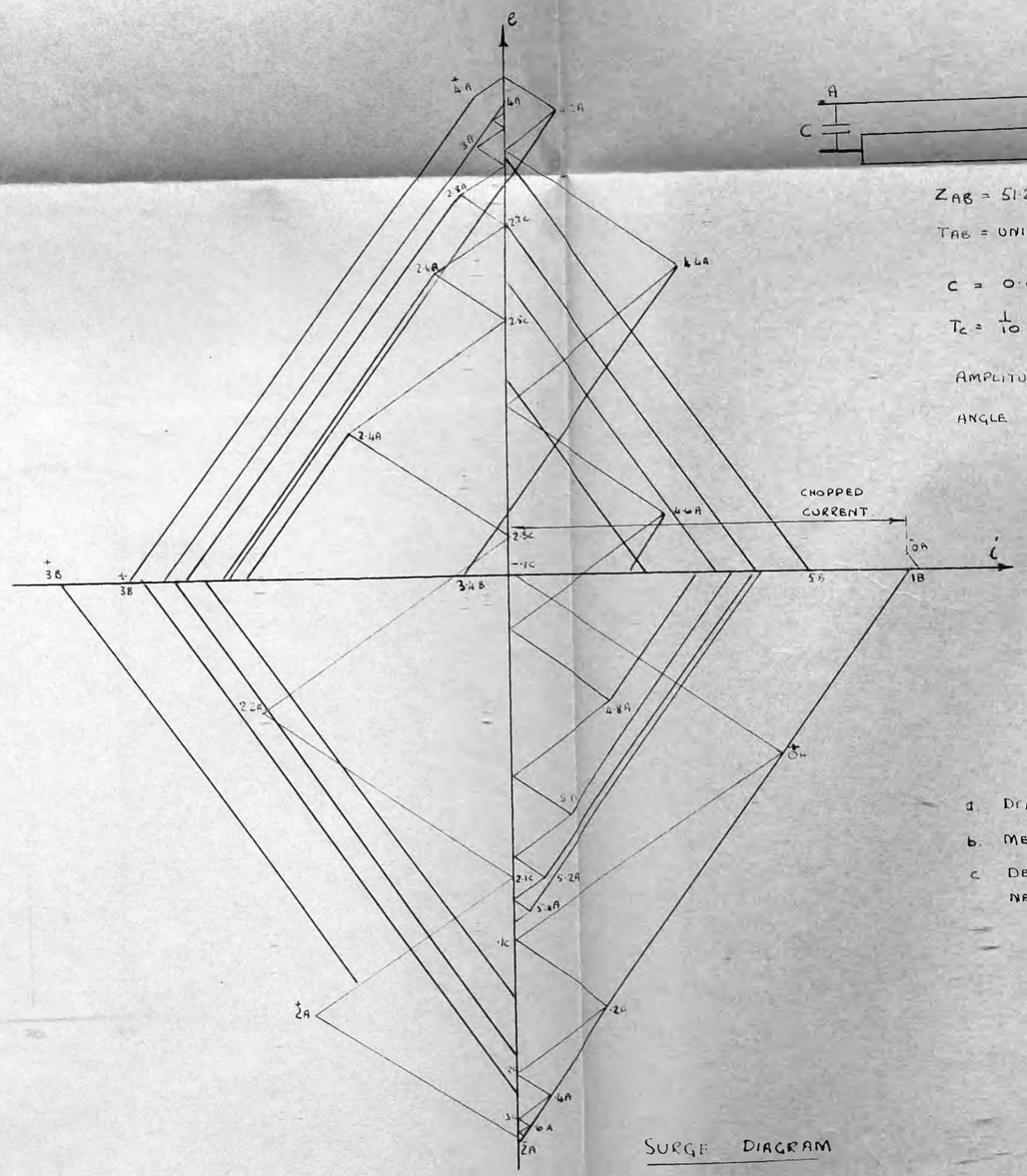

SURGE DIAGRAM

Z_{AB} = 51.2Ω

T_{AB} = UNIT TIME = 0.025 m.s.

C = 0.05 μF.

$T_C = \frac{1}{10} T_{AB}$

AMPLITUDE FACTOR = 1.87

ANGLE OF CHOP = 39°

a. DERIVED FROM SURGE DIAGRAM.

b. MEASURED TRANSIENT

c. DERIVED FROM A SURGE DIAGRAM NEGLECTING THE CAPACITANCE C.

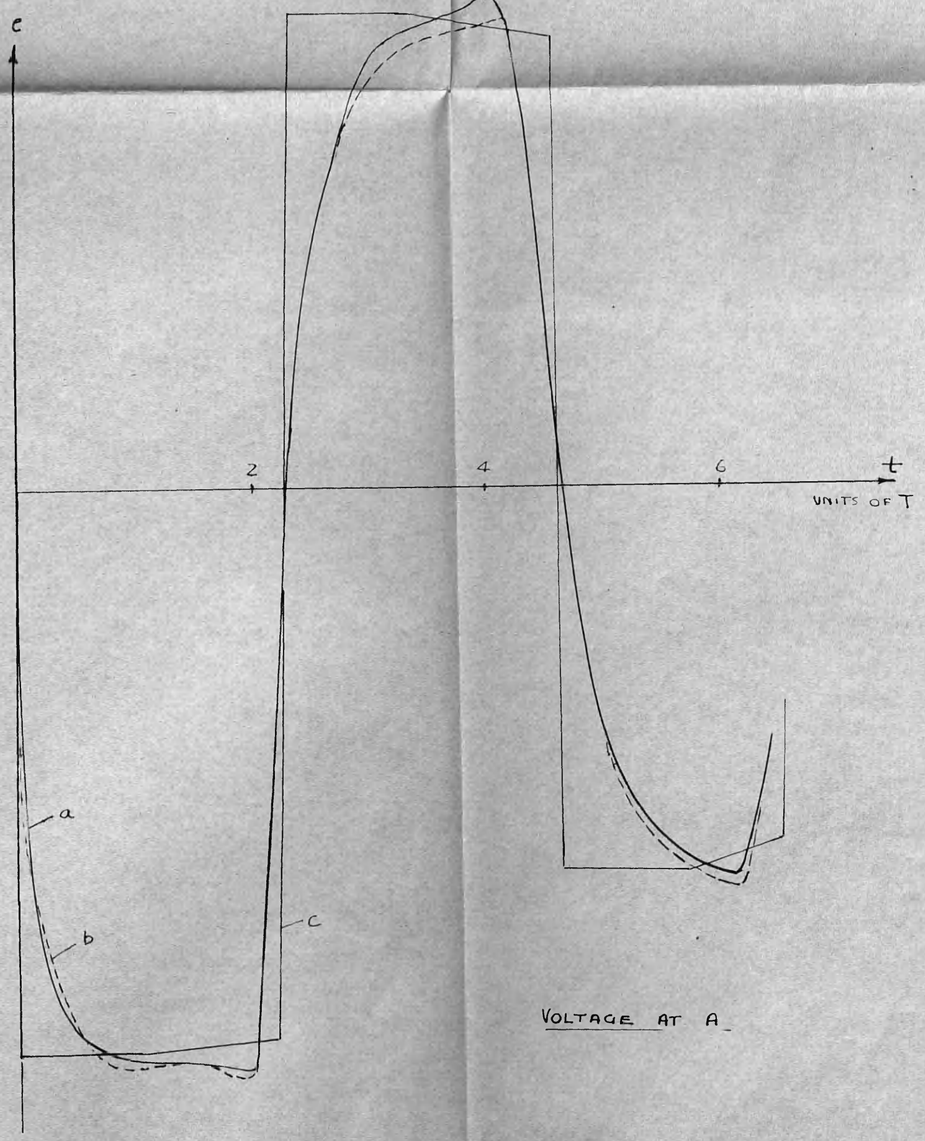

VOLTAGE AT A

RESPONSE OF A CABLE TO A CHOPPED HALF SINE WAVE OF CURRENT - LOSSES ARE ACCOUNTED FOR

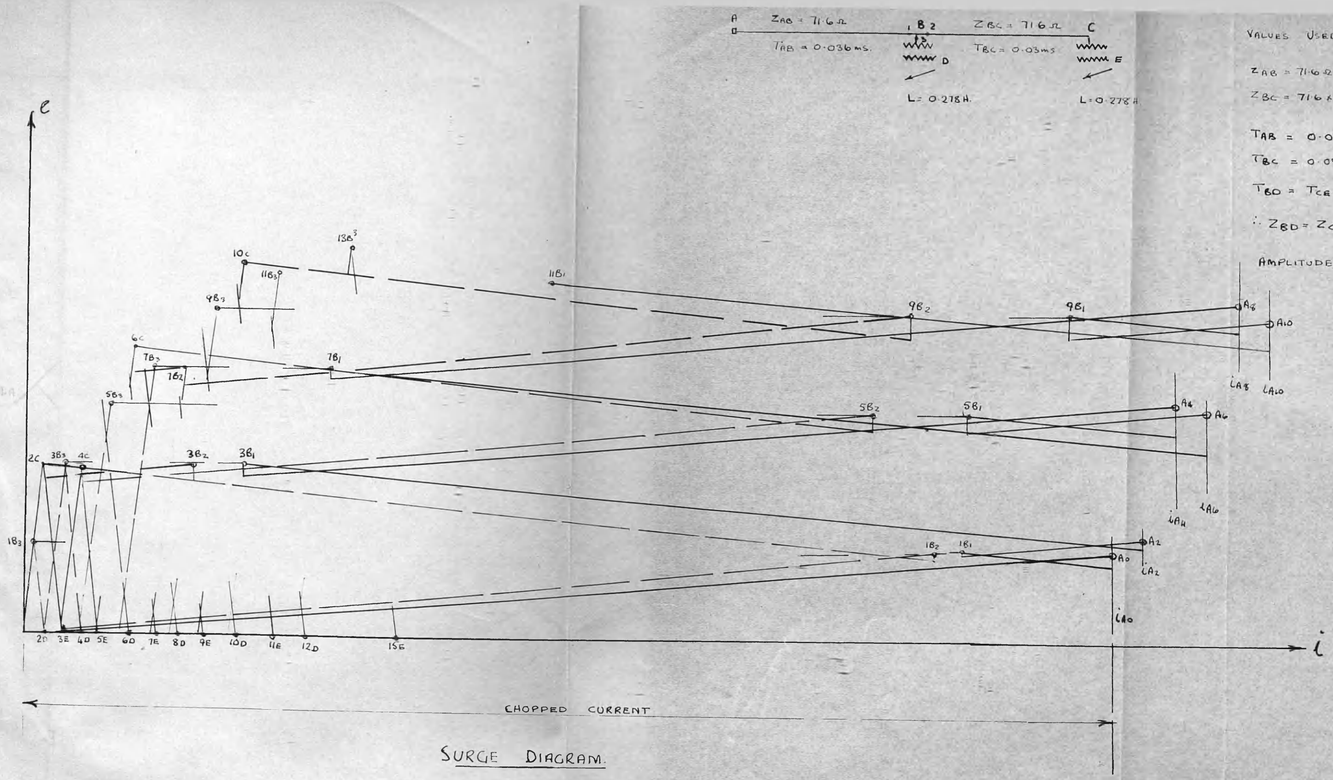

SURGE DIAGRAM.

VALUES USED IN DIAGRAM

$Z_{AB} = 716\,\Omega$

$Z_{BC} = 716 \times \frac{\cdot 036}{\cdot 030} = 86\,\Omega$

$T_{AB} = 0{\cdot}036\,mS. = T$

$T_{BC} = 0{\cdot}036\,mS.$

$T_{BD} = T_{CE} = 0{\cdot}036\,mS.$

$\therefore Z_{BD} = Z_{CE} = \frac{0{\cdot}278}{0{\cdot}036 \times 10^{-3}} = 7{\cdot}62 \times 10^{3}\,\Omega.$

AMPLITUDE FACTOR 1·88

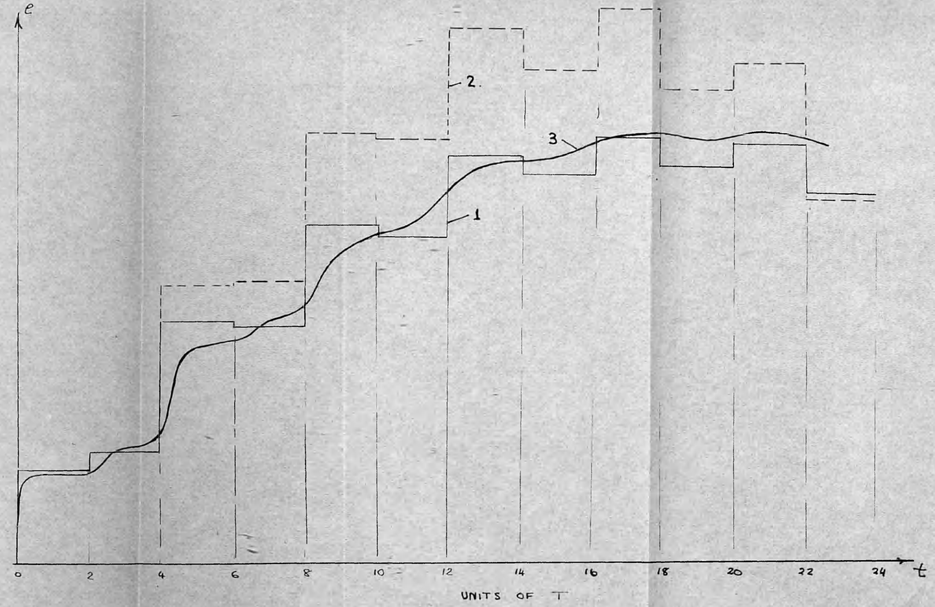

VOLTAGE AT A

1 OBTAINED FROM SURGE DIAGRAM

2. OBTAINED FROM E SURGE DIAGRAM AND IGNORING LOSSES

3. MEASURED VOLTAGE

RECOVERY VOLTAGE AT C.B. A WHEN A PHASE TO PHASE SHORT OCCURS ON THE SECONDARIES OF BOTH TRANSFORMERS,

AND THE CURRENT IS EXTINGUISHED AT 37° BEFORE CURRENT ZERO.

FIG. 88

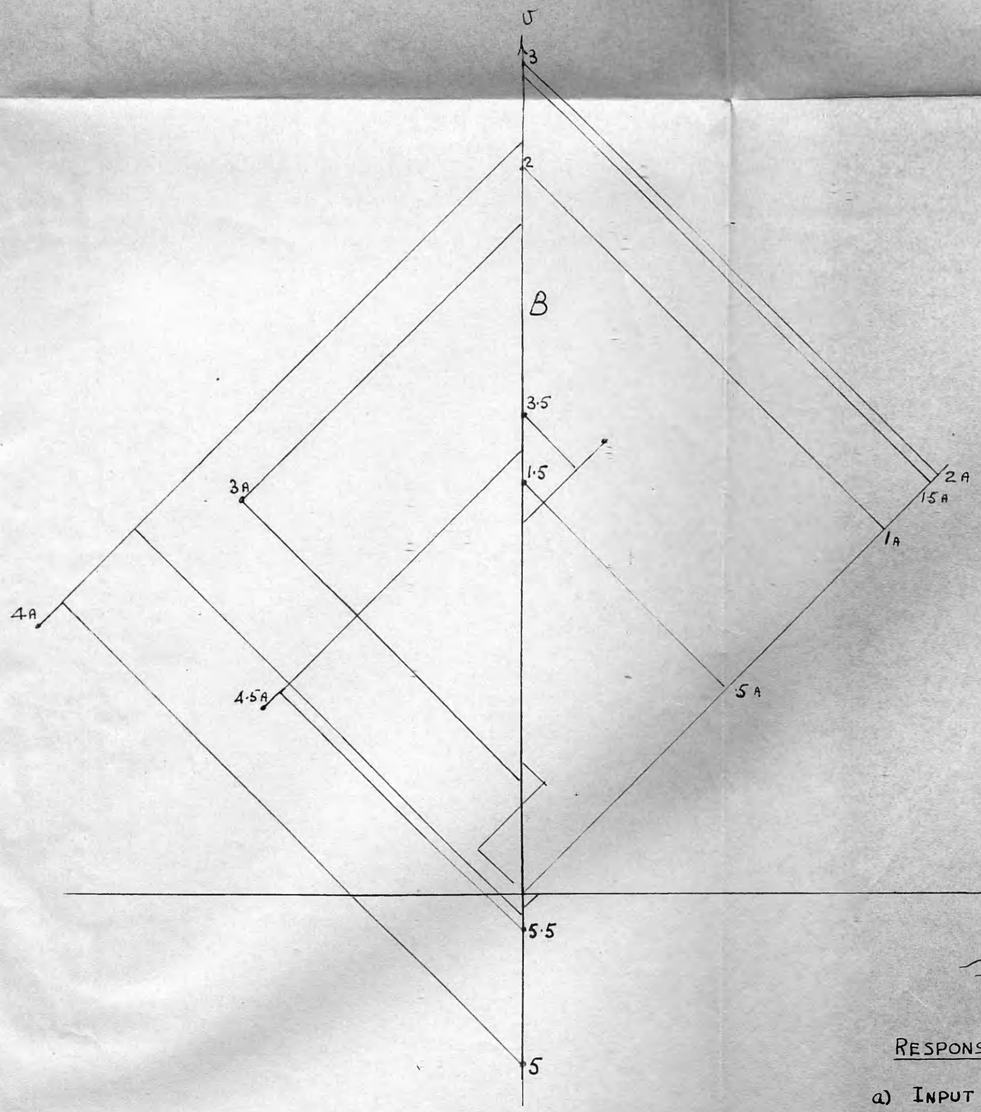

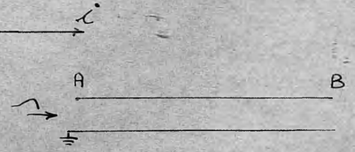

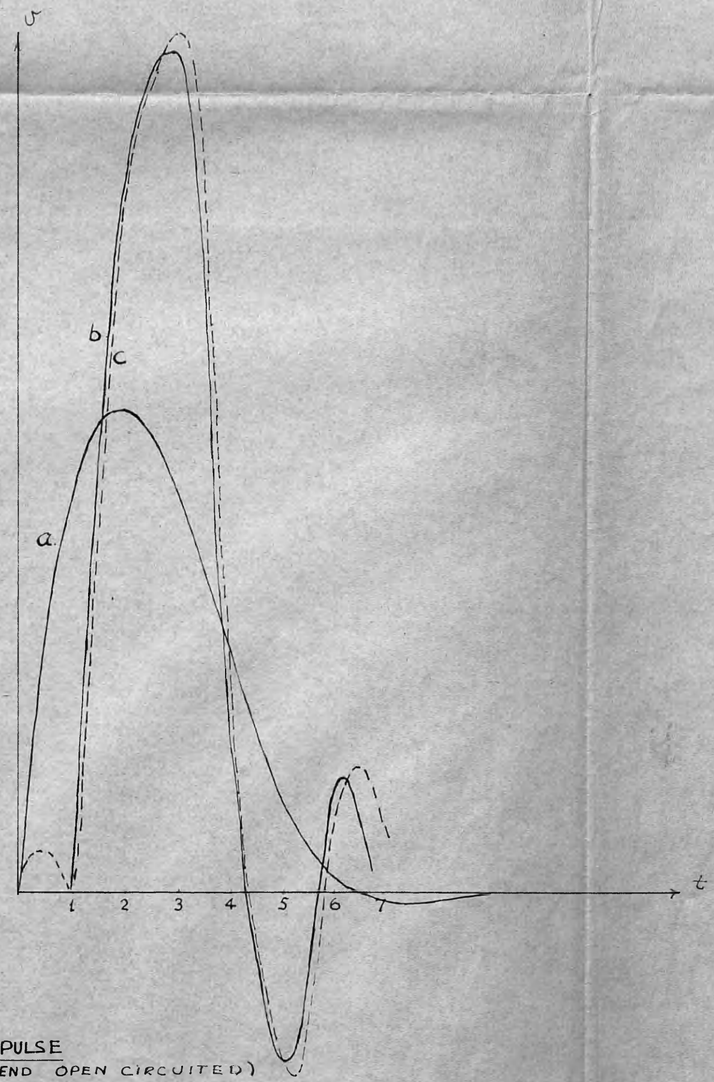

RESPONSE OF GENERATOR WINDING TO IMPULSE

(END OPEN CIRCUITED)

a) INPUT AT END A.

b) VOLTAGE AT B FOUND USING BERGERON'S GRAPHICAL METHOD, AND CONSIDERING THE WINDING AS A TRANSMISSION LINE (THE DAMPING FACTOR USED IN THE DIAGRAM WAS DERIVED FROM THE MEASURED VOLTAGE TRANSIENT.)

c) VOLTAGE AT B OBTAINED EXPERIMENTALLY.